CHAPTER 10: THE BIG PICTURE: COSMOCHEMISTRY

10.1 INTRODUCTION

In the previous nine chapters we acquired a full set of geochemical tools. In this and subsequent chapters, we will apply these tools to understanding the Earth. Certainly any full understanding of the Earth includes an understanding of its origin and its relationship to its neighboring celestial bodies. That is our focus in this chapter.

The question of the origin of the Earth is closely tied to that of the composition of the Earth, and certainly the latter is central to geochemistry. Indeed, one of the primary objectives of early geochemists was to determine the abundance of the elements in the Earth. It is natural to wonder what accounts for these abundances and to ask whether the elemental abundances in the Earth are the same as the abundances elsewhere in the solar system and in the universe. We might also ask why the Earth consists mainly of magnesium, silicon, oxygen, and iron? Why not titanium, fluorine and gold? Upon posing these questions, the realm of geochemistry melds smoothly into the realms of cosmochemistryand cosmology. Cosmochemistry has as its objective an understanding of the distribution and abundance of elements in the Solar System, and, to a lesser degree, the cosmos (the latter is relegated to secondary stature because the data on objects outside the Solar System are much less complete).

The composition of the Earth is unique: there is undoubtedly no other celestial body that has exactly the same composition of the Earth. Nevertheless, the composition of the Earth is similar to that of the other terrestrial planets: Mercury, Venus, Mars, and the Moon. The Earth also shares a common geochemical heritage with the remainder of the Solar System, and all bodies in the Solar System probably have the same relative abundances of some elements, and the same isotopic compositions of most elements. What we know of the composition of the remainder of the universe suggests that it has a composition that is grossly similar to our Solar System: it is dominated by hydrogen and helium, with lesser amounts of carbon, oxygen, magnesium, silicon and iron, but there are local differences, particularly in the abundances of elements heavier than hydrogen and helium.

The unique composition of the Earth is product of three sets of processes. These include those processes responsible for the creation of elements, that is, nucleosynthetic processes, the creation of the Solar System, and finally the formation of the Earth itself. We will begin by considering nucleosynthesis. Meteorites are the principal record of formation of the Solar System and of the planetary bodies within it, so we devote considerable space to understanding these objects. Perhaps ever since he acquired the capacity to contemplate the abstract, man has wondered about how and when the Earth formed. The answer to the question can be provided by applying the tools of geochemistry to meteorites. We close the chapter by attempting to construct a history of Solar System and planetary formation from the meteorite record.

10.2 IN THE BEGINNING...NUCLEOSYNTHESIS

10.2.1 Astronomical Background

Nucleosynthesis is the process of creation of the elements. While we could simply take for granted the existence of the elements, such an approach is somehow intellectually unsatisfactory. The origin of the elements is both a geochemical and astronomical question, perhaps even more a cosmological one. Our understanding of nucleosynthesis comes from a combination of observations of the abundances of the elements (and their isotopes) in meteorites and from observations on stars and related objects. Thus to understand how the elements formed we need to understand a few astronomical observations and concepts. The universe began about 14 Ga ago with the Big Bang; since then the universe has been expanding, cooling, and evolving. This hypothesis follows from two observations: the relationship between red-shift and distance and the cosmic background radiation, particularly the former.

Stars shine because of exothermic nuclear reactions occurring in their cores. The energy released by these processes creates a tendency for thermal expansion that, in general, exactly balances the tendency

for gravitational collapse. Surface temperatures are very much cooler than temperatures in stellar cores. For example, the Sun, which is an average star in almost every respect, has a surface temperature of 5700 K and a core temperature thought to be 14,000,000 K.

Stars are classified based on their color (and spectral absorption lines), which is in turn related to their surface temperature. From hot to cold, the classification is: O, B, F, G, K, M, with subclasses designated by numbers, e.g., F5. (The mnemonic is '*O Be a Fine Girl, Kiss Me!*'). The Sun is class G. Stars are also divided into Populations. Population I stars are second or later generation stars and have greater heavy element contents than Population II stars. Population I stars are generally located in the main disk of the galaxy, whereas the old first generation stars of Population II occur mainly in globular clusters that circle the main disk.

On a plot of luminosity versus wavelength of their principal emissions (i.e., color), called a Hertzsprung-Russell diagram (Figure 10.01), most stars (about 90%) fall along an array defining an inverse correlation, called the "Main Sequence" between these two properties. Since wavelength is inversely related to the fourth power of temperature, this correlation means simply that hot stars give off more energy (are more luminous) than cooler stars. Mass and radius are also simply related to temperature for these so-called main sequence stars: hot stars are big, small cool stars are small. Thus O and B stars are large, luminous and hot; K and M stars are small, faint, and cool. The relationship between mass, luminosity, and temperature is nonlinear, however. For example, an O star that is 30 times as massive as the Sun will have a surface temperature 7 times as hot and a luminosity 100,000 times greater. Stars on the main sequence produce energy by 'hydrogen burning', fusion of hydrogen to produce helium. Since the rate at which these reactions occur depends on temperature and density, hot, massive stars release more energy than smaller ones. As a result they exhaust the hydrogen in their cores much more rapidly. Thus there is an inverse relationship between the lifetime of a star, or at least the time it spends on the main sequence, and its mass. The most massive stars, up to 100 solar masses, have life expectancies of only about 10^6 years, whereas small stars, as small as 0.01 solar masses, remain on the main sequence more than 10^{10} years.

The two most important exceptions to the main sequence stars, the red giants and the white dwarfs, represent stars that have burned all the H fuel in the cores and have moved on in the evolutionary sequence. H in the core is not replenished because the density difference prevents convection between the core and outer layers, which are still H-rich. The interior part of the core collapses under gravity. With enough collapse, the layer immediately above the He core will begin to "burn" H again, which again stabilizes the star. The core, however, continues to collapse until temperature and pressure are great enough for He burning to begin. At the same time, and for reasons not fully understood, the exterior expands and cools, resulting in a *red giant*, a star that is over-luminous relative

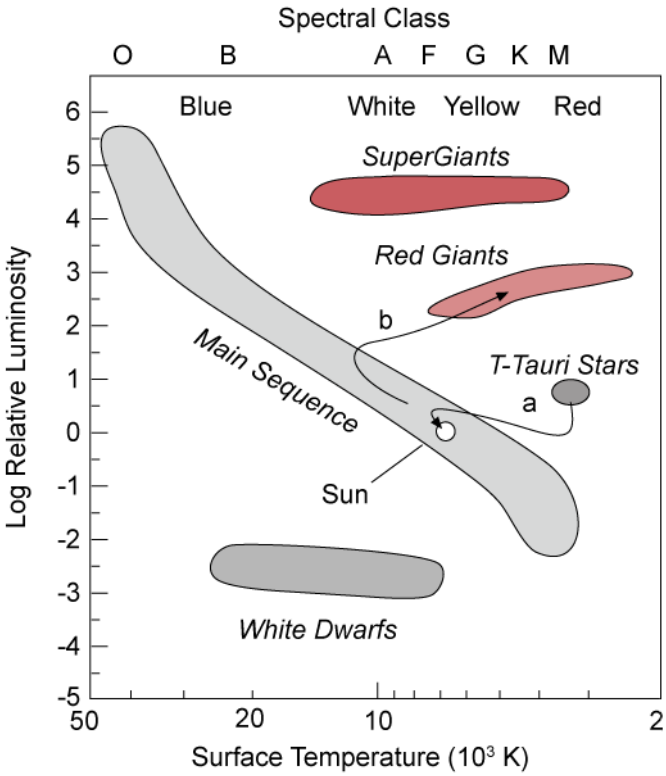

Figure 10.01. The Hertzsprung-Russell diagram of the relationship between luminosity and surface temperature. Arrows show evolutionary path for a star the size of the Sun in pre- (a) and post- (b) main sequence phases.

to main sequence stars of the same color. When the Sun reaches this phase, in perhaps another 5 Ga, it will expand to the Earth's orbit. A star will remain in the red giant phase for something like 10^6–10^8 years. During this time, radiation pressure results in a greatly enhanced solar wind, of the order of 10^{-6} to 10^{-7}, or even 10^{-4}, solar masses per year (the Sun's solar wind is 10^{-14} solar masses per year, so that in its entire lifetime the Sun will blow off 1/10,000 of its mass through the solar wind).

The fate of stars after the red giant phase (when the He in the core is exhausted) depends on their mass. Nuclear reactions in small stars cease and they simply contract, their exteriors heating up as they do so, to become *white dwarfs*. The energy released is that produced by previous nuclear reactions and gravitational potential energy. This is the likely fate of the Sun. White Dwarfs are underluminous relative to stars of similar color on the main sequence. They can be thought of as little more than glowing ashes. Unless they blow off sufficient mass during the red giant phase, large stars die explosively, in supernovae. (Novae are entirely different events that occur in binary systems when mass from a main sequence star is pulled by gravity onto a white dwarf companion.) Supernovae are incredibly energetic events. The energy released by a supernova can exceed that released by an entire galaxy (which, it will be recalled, consists of on the order of 10^9 stars) for days or weeks!

10.2.2 The Polygenetic Hypothesis of Burbidge, Burbidge, Fowler and Hoyle

Our understanding of nucleosynthesis comes from three sets of observations: (1) the abundance of isotopes and elements in the cosmos, (2) experiments on nuclear reactions that determine what reactions are possible (or probable) under given conditions, and (3) inferences about possible sites of nucleosynthesis and about the conditions that prevail in those sites. The abundances of the element in primitive meteorites are by far our most important source of information of elemental abundances. Some additional information can be obtained from spectral observations of stars. The abundances of the elements in the Solar System are shown in Figure 10.2. Any successful theory of nuclear synthesis must explain this abundance pattern. Thus the chemical and isotopic composition of meteorites is a matter of keen interest, not only to geochemists, but to astronomers and physicists as well.

The cosmology outlined above provides two possibilities for formation of the elements: (1) they were formed in the Big Bang itself, or (2) they were subsequently produced. One key piece of evidence comes from looking back into the history of the cosmos. Astronomy is a bit like geology in that just as

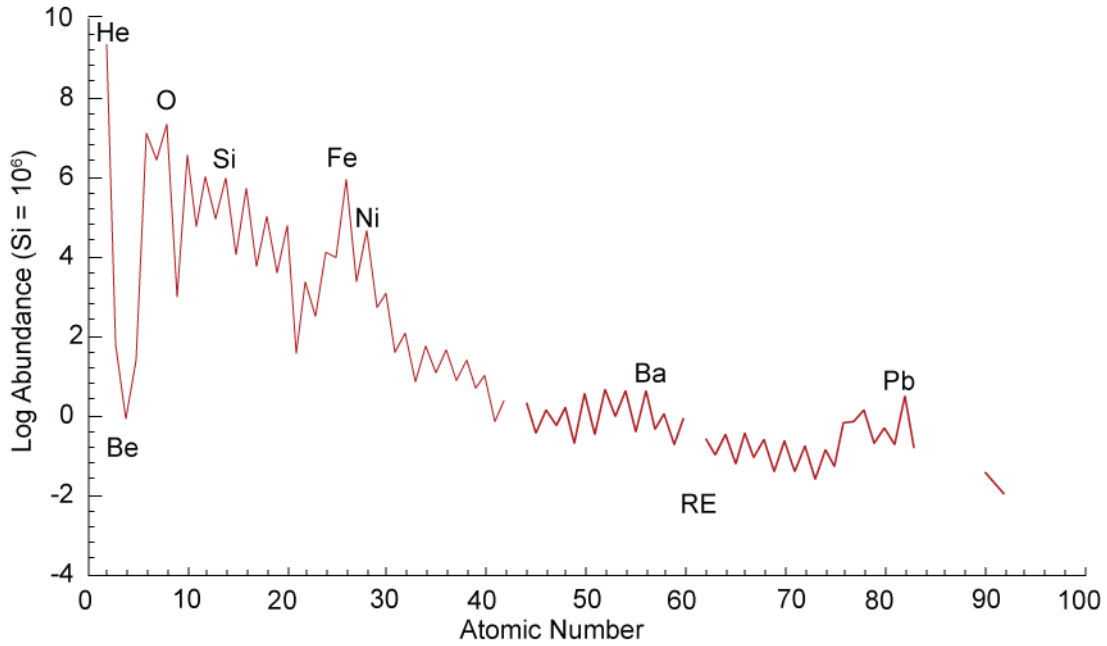

Figure 10.02. Solar system abundance of the elements relative to silicon as a function of atomic number.

we learn about the evolution of the Earth by examining old rocks, we can learn about the evolution of the cosmos by looking at old stars. The old stars of Population II are considerably poorer in heavy elements than are young stars. In particular, Population II stars have a Fe/H ratio typically a factor of 100 lower than the Sun. This suggests that much of the heavy element inventory of the galaxy has been produced since these stars formed more than 10 Ga ago. There are also significant variations in the Fe/H ratio between galaxies. In particular, dwarf spheroidal galaxies appear to be deficient in Fe, and sometimes in C, N, and O, relative to our own galaxy. Other galaxies show distinct radial compositional variations. For example, the O/H ratio in the interstellar gas of the disk of the spiral galaxy M81 falls by an order of magnitude with distance from the center. Finally, one sees a systematic decrease in the Fe/H ratio of white dwarfs (the remnants of small to medium size stars) with increasing age. On the other hand, old stars seem to have about the same He/H ratio as young stars. Indeed ^{4}He seems to have an abundance of 25±2% everywhere in the universe.

Thus the observational evidence suggests that (1) H and He are everywhere uniform, implying their creation and fixing of the He/H ratio in the Big Bang, and (2) elements heavier than Li were created by subsequent processes. The production of these heavier elements seems to have occurred steadily through time, but the efficiency of the process varies between galaxies and even within galaxies.

Early attempts (~1930–1950) to understand nucleosynthesis focused on single mechanisms. Failure to find a single mechanism that could explain the observed abundance of nuclides, even under varying conditions, led to the present view that relies on a number of mechanisms operating in different environments and at different times for creation of the elements in their observed abundances. This view, which has been called the polygenetic hypothesis, was first proposed by Burbidge, Burbidge, Fowler and Hoyle (1957). The abundance of trace elements and their isotopic compositions in meteorites were perhaps the most critical observations in development of the theory. An objection to the polygenetic hypothesis was the apparent uniformity of the isotopic composition of the elements, but variations in the isotopic composition have now been demonstrated for a few elements in some meteorites. The isotopic compositions of other elements, such as oxygen and the rare gases, vary between classes of almost all meteorites. Furthermore, there are significant variations in isotopic composition of some elements, such as carbon, among stars. These observations provide strong support for this theory.

To briefly summarize it, the polygenetic hypothesis proposes four phases of nucleosynthesis. *Cosmological nucleosynthesis* occurred shortly after the universe began and is responsible for the cosmic inventory of H and He, and some of the Li. Even though helium is the main product of nucleosynthesis in the interiors of main sequence stars, not enough helium has been produced in this manner to significantly change its cosmic abundance. The lighter elements, up to and including Si and a fraction of the heavier elements, but excluding Li and Be, may be synthesized in the interiors of larger stars during the final stages of their evolution (*stellar nucleosynthesis*). The synthesis of the remaining elements occurs as large stars exhaust the nuclear fuel in their interiors and explode in nature's grandest spectacle, the supernova (*explosive nucleosynthesis*). Finally, Li and Be are continually produced in interstellar space by interaction of cosmic rays with matter (*galactic nucleosynthesis*).

10.2.3 Cosmological Nucleosynthesis

Immediately after the Big Bang, the universe was too hot for any matter to exist. But within a microsecond or so, it had cooled to 10^{11} K so that matter began to condense. At first electrons, positrons, and neutrinos dominated, but as the universe cooled and expanded, protons and neutrons became more abundant. These existed in an equilibrium dictated by the following reactions:

$$^1H + e^- \rightleftarrows n + \nu \quad \text{and} \quad n + e^+ \rightleftarrows {}^1H + \bar{\nu}\,^\dagger$$

At first, neutrons and protons existed in equal numbers. But as temperatures cooled through 10^{10} K, the reactions above progressively favored protons. These reactions are possible only at these extreme temperatures so that in less than two seconds they ceased, freezing in 6 to 1 ratio of protons to neutrons.

† The ν (nu) is the symbol for a neutrino; the bar indicates the anti-particle, an anti-neutrino in this case.

CHAPTER 10: COSMOCHEMISTRY

A somewhat worrisome question is why matter is exists at all. Symmetry would seem to require production of equal number of protons and anti-protons that would have annihilated themselves by:

$$p + \bar{p} \rightarrow 2\gamma^*$$

The current theory is that the hyperweak force was responsible for an imbalance favoring matter over anti-matter. The same theory predicts a half-life of the proton of 10^{32} yrs, a prediction not yet verified.

It took another 100 seconds for the universe to cool to 10^9 K, which is cool enough for ^{2}H to form:

$$^1H + {}^1n \rightarrow {}^2H + \gamma$$

At about the same time, the following reactions could also occur:

$$^2H + {}^1n \rightarrow {}^3H + \gamma; \; ^2H + {}^1H \rightarrow {}^3H + \gamma$$

$$^2H + {}^1H \rightarrow {}^3He + \beta^+ + \gamma; \; ^3He + n \rightarrow {}^4He + \gamma$$

and $$^2H + {}^2H \rightarrow {}^3He + n; \; ^3He + {}^4He \rightarrow {}^7Be + \gamma; \; ^7Be + e^- \rightarrow {}^7Li + \gamma$$

Formation of elements heavier than Li, however, was inhibited by the instability of nuclei of masses 5 and 8. Figure 3 illustrates the compositional evolution of the early cosmos. Two factors bring this process to a halt: (1) falling temperatures and (2) the decay of free neutrons: outside the nucleus, neutrons have a half-life of only 10 minutes, so nucleosynthetic reactions that consume neutrons eventually cease. Within 20 minutes or so, the universe cooled below 3×10^8 K and nuclear reactions were no longer possible. Thus, the Big Bang created H, He and Li (^{7}Li/H = 10^{-9}). Some 700,000 years later, the universe had cooled to about 3000 K, cool enough for electrons to be bound to nuclei, forming atoms. With this *recombination*, the universe became transparent, i.e., radiation could freely propagate through it. The faint radiation known as the cosmic background radiation provides a snapshot of the universe at that time.

The first seconds and minutes of the cosmos are surprisingly well understood, in part because the conditions that prevailed can be reproduced, at least on a micro scale, in high energy accelerators/colliders. Experiments in these accelerators provide tests and calibrations of cosmological theory. The ratio of hydrogen, helium, and lithium created by these reactions depends on density and temperature and, in part because of the decay of free neutrons; it is also function of the rate at which these falls as the cosmos expands. An indication of the success of cosmological theory is that predicts the H and He abundances, and their isotopic composition, in the cosmos. On the other hand, the very earliest history of the cosmos, the first femtosecond or so, is less well understood because the conditions that prevailed are too energetic to be reproduced in accelerators.

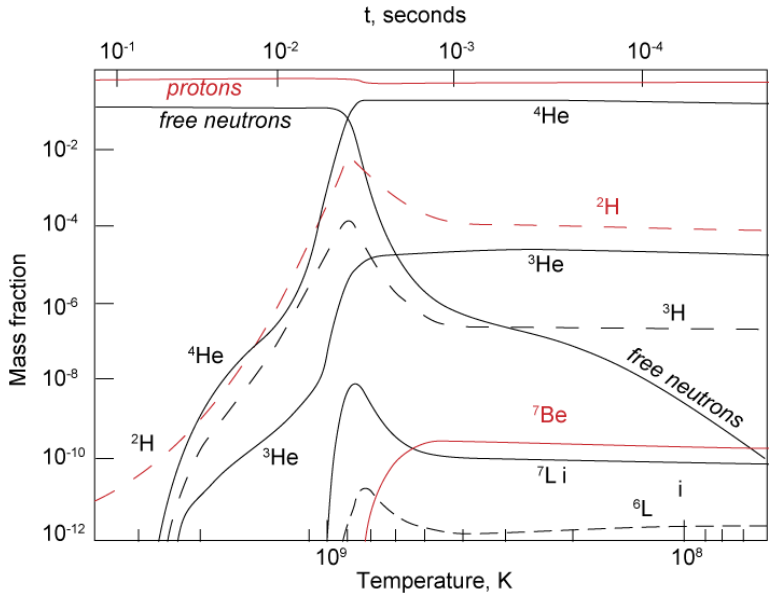

Figure 10.03 Compositional evolution during cosmological nucleosynthesis. ^{7}Be and ^{3}H are unstable and decay to ^{7}Li and ^{3}He with half-lives of 53 days (4.6 x 10^6 s) and 12.3 years (4 x 10^8 s) respectively. After Ned Wright's Cosmology Tutorial (http://www.astro.ucla.edu/~wright/cosmolog.htm).

* γ (gamma) is used here to indicate energy in the form of a gamma ray.

10.2.4 Nucleosynthesis in Stellar Interiors

10.2.4.1 Hydrogen, Helium, and Carbon Burning Stars

For quite some time after the Big Bang, the universe was a more or less homogeneous, hot gas. "Less" turns out to be critical. Inevitably (according to fluid dynamics), inhomogeneities in the gas developed, and indeed, very slight inhomogeneities are observed in the cosmic background radiation. These inhomogeneities enlarged in a sort of runaway process of gravitational attraction and collapse. Thus were formed protogalaxies, perhaps 0.5 Ga after the Big Bang. Instabilities within the protogalaxies collapsed into stars. Once this collapse proceeded to the point where density reaches 6 g/cm and temperature reaches 10 to 20 million K, nucleosynthesis began in the interior of stars by *hydrogen burning*, or the *pp process*, which involves reactions such as:

$$^1H + {}^1H \rightarrow {}^2H + \beta^+ + \nu; \quad {}^2H + {}^1H \rightarrow {}^3He + \gamma \quad \text{and} \quad {}^3He + {}^3He \rightarrow {}^4He + 2{}^1H + \gamma$$

There are also other reaction chains that produce ^{4}He that involve Li, Be, and B, either as primary fuel or as intermediate reaction products. Later, when some carbon had already been produced by the first generation of stars and supernovae, second and subsequent generation stars with masses greater than about 1.1 solar masses produced He by another process as well, the *CNO cycle*:

$$^{12}C(p,\gamma)\ ^{13}N(\beta^+,\gamma)\ ^{13}C(p,\gamma)\ ^{14}N(p,\gamma)\ ^{15}O(\beta^+,\nu)\ ^{15}N(p,\alpha)\ ^{12}C^{\ddagger}$$

In this process carbon acts as a sort of nuclear catalyst: it is neither produced nor consumed. The net effect is consumption of 4 protons and two positrons to produce a neutrino, some energy and a ^{4}He nucleus. The $^{14}N(p,\gamma)\ ^{15}O$ is the slowest in this reaction chain, so there tends to be a net production of ^{14}N as a result. Also, though both ^{12}C and ^{13}C are consumed in this reaction, ^{12}C is consumed more rapidly, so this reaction chain should increase the $^{13}C/^{12}C$ ratio.

The heat produced by these reactions counterbalances gravitational collapse and these reactions proceed in main sequence stars (Figure 10.1) until the hydrogen in the stellar core is consumed. How quickly this happens depends, as we noted earlier, on the mass of the star.

Once the H is exhausted in the stellar core, fusion ceases, and the balance between gravitational collapse and thermal expansion is broken. The interior of the star thus collapses, raising the star's temperature. The exterior expands and fusion begins in the shells surrounding the core, which now consists of He. This is the *red giant* phase. If the star is massive enough for temperatures to reach 10^8 K and density to reach 10^4 g/cc in the He core (stars with masses greater than about 0.8 solar masses), *He burning* can occur:

$$^4He + {}^4He \rightarrow {}^8Be + \gamma \qquad \text{and} \qquad {}^8Be + {}^4He \rightarrow {}^{12}C + \gamma$$

The catch in this reaction is that the half-life of ^{8}Be is only 10^{-16} sec, so 3 He nuclei must collide essentially simultaneously, hence densities must be very high. He burning also produces O, and lesser amounts of ^{20}Ne and ^{24}Mg, in the red giant phase, but Li, Be, and B are skipped: they are not synthesized in these phases of stellar evolution. These nuclei are unstable at the temperatures of stellar cores. Rather than being produced, they are consumed in stars.

There is a division of evolutionary paths once helium in the stellar core is consumed. Densities and temperatures necessary to initiate further nuclear reactions cannot be achieved by low-mass stars, such as the Sun, (because the gravitational force is not sufficient to overcome coulomb repulsion of electrons) so their evolution ends after the Red Giant phase, the star becoming a white dwarf. Massive stars, those greater than about 4 $M_\odot$[¶], however, undergo further collapse and the initiation of *carbon and oxygen burning* when temperatures reach 600 million K and densities 5×10^5 g/cc. However, stars with intermediate masses, between 4 and 11 $M_\odot$, can be entirely disrupted by the initiation of carbon burning.

[‡] Here we are using a notation commonly used in nuclear physics. The notation:

$$^{12}C(p,\gamma)^{13}N$$

is equivalent to:

$$^{12}C + p \rightarrow {}^{13}N + \gamma$$

[¶] The symbol ⊙ is the astronomical symbol for the Sun. $M_\odot$ therefore indicates the mass of the Sun.

For stars more massive 11 $M_\odot$, about 1% of all stars, evolution now proceeds at an exponentially increasing pace (Figure 10.4) with reactions of the type:

$$^{12}C + {}^{12}C \rightarrow {}^{20}Ne + {}^{4}He + \gamma$$

$$^{16}O + {}^{16}O \rightarrow {}^{28}Si + {}^{4}He + \gamma$$

and $$^{12}C + {}^{16}O \rightarrow {}^{24}Mg + {}^{4}He + \gamma$$

Also, ^{14}N created during the hydrogen-burning phase of second generation stars can be converted to ^{22}Ne. A number of other less abundant nuclei, including Na, Al, P, S and K are also synthesized at this time, and in the subsequent process, *Ne burning*.

During the final stages of evolution of massive stars, a significant fraction of the energy released is carried off by neutrinos created by electron-positron annihilations in the core of the star. If the star is sufficiently oxygen-poor that its outer shells are reasonably transparent, the outer shell of the red giant may collapse during last few 10^4 years of evolution to form a *blue giant*.

10.2.4.2 The e-process

Eventually, a new core consisting mainly of ^{28}Si is produced. At temperatures near 10^9 K and densities above 10^7 g/cc a process known as *silicon burning*, or the *e-process*, (for equilibrium) begins, and lasts for a week or less, again depending on the mass of the star. The process of silicon burning is really a variety of reactions that can be summarized as the photonuclear rearrangement of a gas originally consisting of ^{28}Si nuclei into one which via intervening beta decays consists mainly of ^{56}Ni, which then decays, with a half life of 6 days, to ^{56}Fe, the most stable of all nuclei. At 10^9 K, thermal photons have energies near 1 MeV; absorbing such photons overcomes the energy barriers between nuclei, allowing the system to evolve towards a minimum energy state by making the most stable nuclei. This is analogous to the rapid approach to chemical equilibrium that occurs once temperatures become high enough to overcome kinetic barriers.

The e-process includes reactions such as:

$$^{28}Si + \gamma \rightleftarrows {}^{24}Ne + {}^{4}He$$

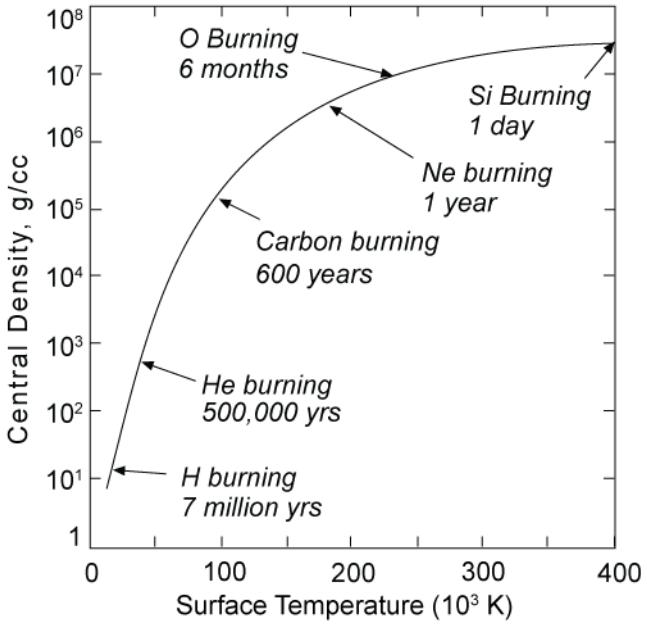

Figure 10.04. Evolutionary path of the core of star of 25 solar masses (after Bethe and Brown, 1985). Note that the period spent in each phase depends on the mass of the star: massive stars evolve more rapidly.

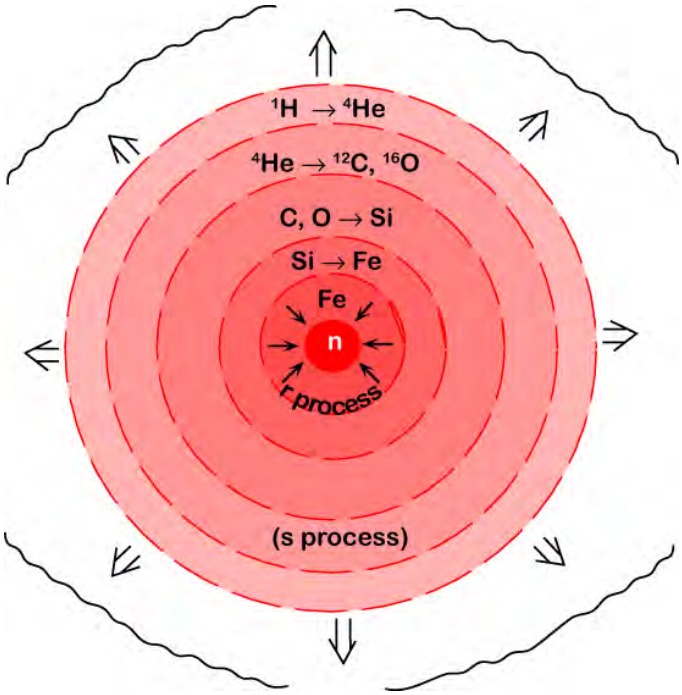

Figure 10.05. Schematic diagram of stellar structure at the onset of the supernova stage. Nuclear burning processes are illustrated for each stage.

$$^{28}Si + {}^{4}He \rightleftarrows {}^{32}S + \gamma$$
$$^{32}S + {}^{4}He \rightleftarrows {}^{36}Ar + \gamma$$

While these reactions can proceed in either direction, there is a tendency for the build up of heavier nuclei with masses 32, 36, 40, 44, 48, 52 and 56. Partly as a result of the e-process, these nuclei are unusually abundant in nature. In addition, because a variety of nuclei are produced during C and Si burning phases, other reactions are possible, synthesizing a number of minor nuclei.

The star is now a cosmic onion of sorts, consisting of a series of shells of successively heavier nuclei and a core of Fe (Figure 10.5). Though temperature increases toward the interior of the star, the structure is stabilized with respective to convection and mixing because each shell is denser than the one overlying it.

Fe-group elements may also be synthesized by the e-process in Type I supernovae*. Type I supernovae occur when white dwarfs of intermediate mass (3-10 solar masses) stars in binary systems accrete material from their companion. When their cores reach the so-called Chandrasekhar limit, C burning is initiated and the star explodes.

10.2.4.3 The s-process

In second and later generation stars containing heavy elements, yet another nucleosynthetic process can operate. This is the slow neutron capture or *s-process*. It is so called because the rate of capture of neutrons is slow compared to the *r-process*, which we will discuss below. It operates mainly in the red giant phase (as evidenced by the existence of ^{99}Tc and enhanced abundances of several s-process nuclides in red giants) where neutrons are produced by reactions such as:

$$^{13}C + {}^{4}He \rightarrow {}^{16}O + n$$
$$^{22}Ne + {}^{4}He \rightarrow {}^{25}Mg + n$$
$$^{17}O + {}^{4}He \rightarrow {}^{20}Ne + n$$

(but even H burning produces neutrons, so that the s-process operates to some degree even in main sequence stars). These neutrons are captured by nuclei to produce successively heavier elements. The principle difference between the *s* and *r* process, discussed below, is the rate of capture relative to the decay of unstable isotopes. In the *s* process, a nucleus may only capture a neutron every thousand years or so. If the newly produced

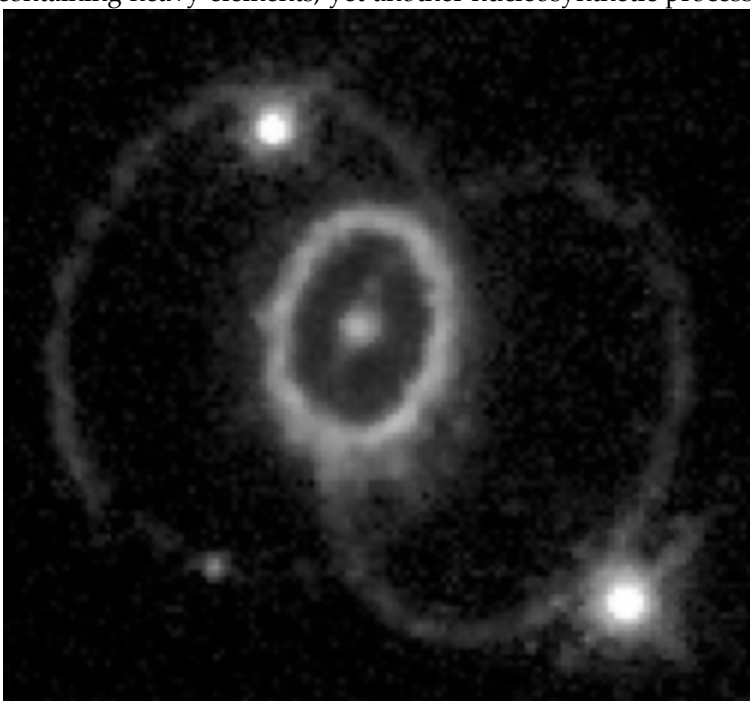

Figure 10.06. Rings of glowing gas surrounding the site of the supernova explosion named Supernova 1987A photographed by the wide field planetary camera on the Hubble Space Telescope in 1994. The nature of the rings is uncertain, but they may be probably debris of the supernova illuminated by high-energy beams of radiation or particles originating from the supernova remnant in the center.

*Astronomers recognize two kinds of supernovae: Type I and Type II. A Type I supernova occurs when a white dwarf in a binary system accretes mass from its sister star. Its mass reaches the point where carbon burning initiates and the star is explosively disrupted. The explosions of massive stars that we are considering are the Type II supernovae.

nucleus is not stable, it will decay before another neutron is captured. As a result, the s-process path closely follows the valley of stability on the chart of the nuclides and nuclear instabilities cannot be bridged.

10.2.5 Explosive Nucleosynthesis

The e-process stops at mass 56. In Chapter 8 we noted that ^{56}Fe had the highest binding energy per nucleon, i.e., it is the most stable nucleus. Thus fusion can release energy only up to mass 56; beyond this the reactions become endothermic, i.e., they consume energy. Once the stellar core has been largely converted to Fe, a critical phase is reached: the balance between thermal expansion and gravitational collapse is broken. The stage is now set for the catastrophic death of the star: a supernova explosion, the ultimate fate of stars with masses greater than about 8 solar masses. The energy released in the supernova is astounding. In its first 10 seconds, the 1987A supernova (Figure 10.06) released more energy than the entire visible universe, 100 times more energy than the Sun will release in its entire 10 billion year lifetime.

When the mass of the iron core reaches 1.4 solar masses (the Chandrasekhar mass), further gravitational collapse cannot be resisted even by coulomb repulsion. The supernova begins with the collapse of this stellar core, which would have a radius of several thousand km (similar to the Earth's radius) before collapse, to a radius of 100 km or so. The collapse occurs in a few tenths of a second. When matter in the center of the core is compressed beyond the density of nuclear matter (3×10^{14} g/cc), it rebounds, sending a massive shock wave back out. As the shock wave travels outward through the core, the temperature increase resulting from the compression produces a breakdown of nuclei by photodisintegration, e.g.:

$$^{56}\text{Fe} + \gamma \rightarrow 13\ ^{4}\text{He} + 4\ ^{1}\text{n};$$

$$^{4}\text{He} + \gamma \rightarrow 2\ ^{1}\text{H} + 2\ ^{1}\text{n}$$

Thus much of what took millions of years to produce is undone in an instant. However, photodisinte-

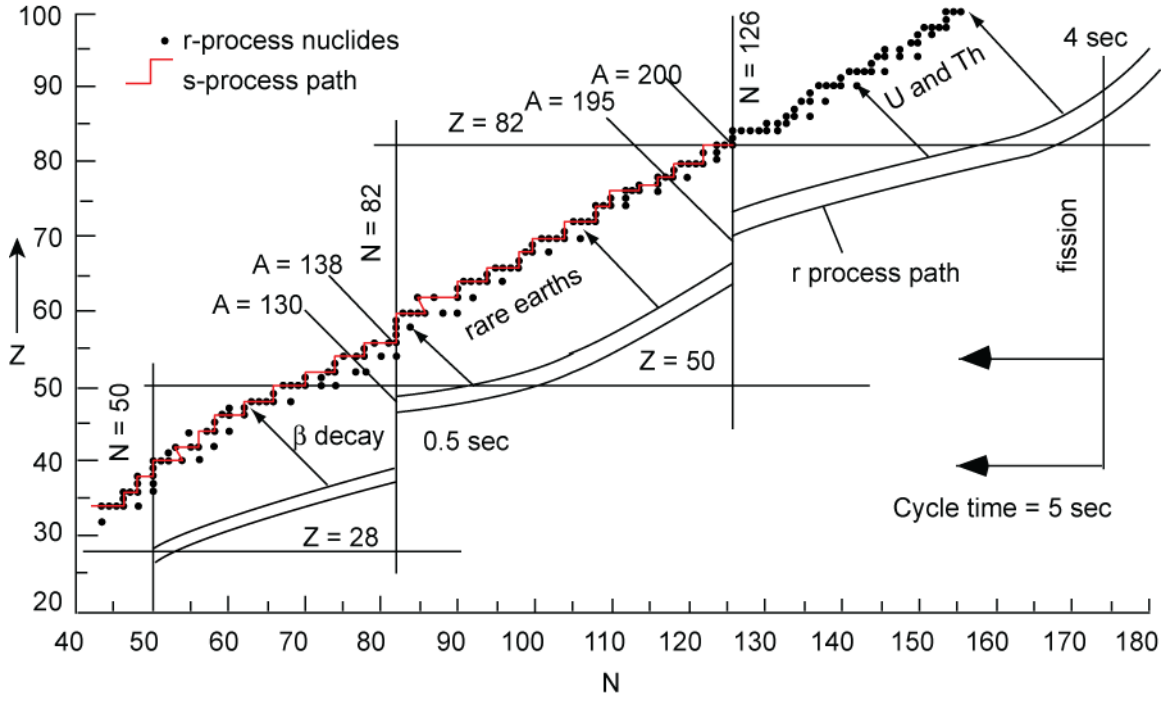

Figure 10.07. Diagram of the r-process path on a Z vs. N diagram. Dashed region is r-process path; solid line through stable isotopes shows the s-process path.

gration produces a large number of free neutrons (and protons), which leads to another important nucleosynthetic process, the *r-process*.

Another important effect is the creation of huge numbers of neutrinos by positron-electron annihilations, these particles having "condensed" as pairs from gamma rays. The energy carried away by neutrinos leaving the supernova exceeds the kinetic energy of the explosion by a factor of several hundred, and exceeds the visible radiation by a factor of some 30,000. The neutrinos leave the core at nearly the speed of light. Though neutrinos interact with matter very weakly, the density of the core is such that their departure is delayed slightly. Nevertheless, they travel faster than the shock wave and are delayed less than electromagnetic radiation. Thus neutrinos from the 1987A supernova arrived at Earth (some 160,000 years after the event) a few hours before the supernova became visible.

When the shock wave reaches the surface of the core, the outer part of the star is blown apart in an explosion of unimaginable violence. But amidst the destruction new nucleosynthetic processes occur. As the shock wave passes through outer layers, it may 'reignite' them, producing explosive Ne, O and C burning. These processes produce isotopes of S, Cl, Ar, Ca, Ti, and Cr, and some Fe.

10.2.5.1 The r-process

The neutrons produced by photodisintegration in the core are captured by those nuclei that manage to survive this hell. Because the abundance of neutrons is exceedingly high, nuclei capture them at a rapid rate; so rapid that even an unstable nucleus will capture a neutron before it has an opportunity to decay. The result is a build up of neutron-rich unstable nuclei. Eventually the nuclei capture enough neutrons that they are not stable even for a small fraction of a second. At that point, they β^- decay to new nuclides, which are more stable and capable of capturing more neutrons. This is the *r-process* (rapid neutron capture), and is the principle mechanism for building up the heavier nuclei. It reaches a limit when nuclei beyond A ≈ 90 are reached. These heavy nuclei fission into several lighter fragments. The r-process is thought to have a duration of 1 to 100 sec during the peak of the supernova explosion. Figure 10.70 illustrates this process.

The r-process produces broad peaks in elemental abundance around the neutron magic numbers

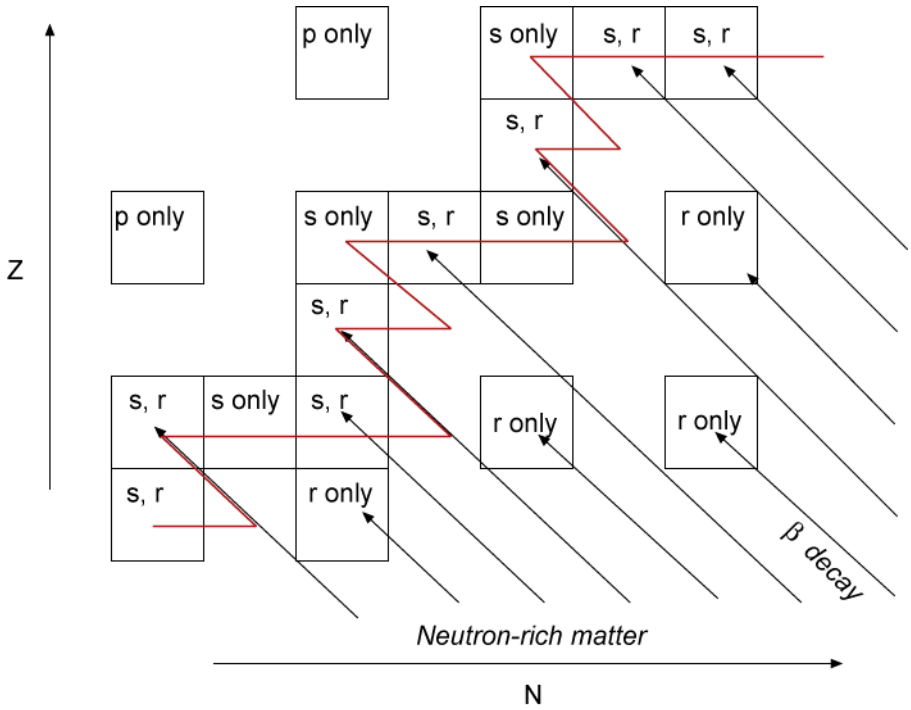

Figure 10.08. Z vs. N diagram showing production of isotopes by the r- s- and p-processes. Squares are stable nuclei; wavy lines are beta-decay path of neutron-rich isotopes produced by the r-process; solid line through stable isotopes shows the s-process path.

(50, 82, 126, corresponding to the elements Sr & Zr, Ba, and Pb). This results because nuclei with magic numbers of neutrons are particularly stable, and have very low cross sections for capture of neutrons, and because nuclei just short of magic numbers have particularly high capture cross sections. Thus the magic number nuclei are both created more rapidly and destroyed more slowly than other nuclei. When they decay, the sharp abundance peak at the magic number becomes smeared out.

10.2.5.2 The p-process

The r-process tends to form the heavier (neutron-rich) isotopes of a given element. Proton capture, or the *p-process*, also occurs in supernovae and is responsible for the lightest isotopes of a given element. The probability of proton capture is much less than that of neutron capture. You can easily imagine the reason for this: to be captured, the proton must have sufficient energy to overcome the coulomb repulsion and approach to within 10^{-14} cm of the nucleus where the strong force dominates over the electromagnetic one. In contrast even low energy neutrons can be captured by nuclei since the neutron is uncharged and there is no coulomb repulsion. The production of nuclei by the p-process is much smaller than by neutron capture processes, and is significant only for those nuclides than cannot be produced in other ways. These tend to be the lightest isotopes of an element. Because of the improbability of proton capture, these light, p-process-only isotopes tend to be the least abundant.

Figure 10.08 illustrates how these three processes, the s-, r-, and p-process, create different nuclei. Notice the shielding effect. If an isotope with z protons and n neutrons has a stable isobar with n+x neutrons and p-x protons, this isotope is shielded from production by the r-process because β-decay will cease when that stable isobar is reached. The most abundant isotopes of an element tend to be those created by all processes; the least abundant are those created by only one, particularly by only the p-process. The exact abundance of an isotope depends on a number of factors, including its neutron-capture cross section*, and the neutron capture cross section and stability of neighboring nuclei.

Let's return to the exploding star. In the inner part of the stellar core, the reactions we just discussed do not take place. Instead, the core collapses to the point where all electrons are welded to protons to form a ball of neutrons: a neutron star. This inner core is hot: 100 billion Kelvin. And like a ballerina pulling in her arms, it conserves angular momentum by spinning faster as it collapses. The neutron star inside the expanding supernova shell of 1987A may be spinning at 2000 revolutions per second. Neutron stars emits radiation in beacon-like fashion: a *pulsar*. The collapse of cores of the most massive stars, however, may not stop at all. They collapse to a diameter of zero and their density becomes infinite. Such an object is called a singularity. Its gravitational attraction is so great even light cannot escape, creating a *black hole*.

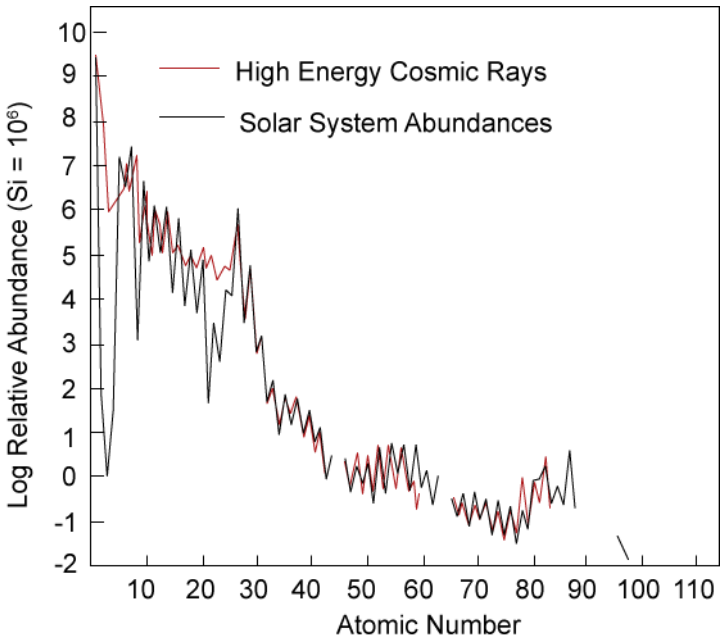

Figure 10.09. Comparison of relative abundances in cosmic rays and the solar system.

* In a given flux of neutrons, some nuclides will be more likely to capture and bind a neutron that others, just as some atoms will be more likely to capture and bind an electron than others. The neutron capture cross section of a nuclide is a measure of the affinity of that nuclide for neutrons, i.e., a measure of the probability of that nuclide capturing a neutron in a given neutron flux.

10.2.6 Nucleosynthesis in Interstellar Space

Except for production of ^{7}Li in the Big Bang, Li, Be, and B are not produced in any of the above situations. One clue to the creation of these elements is their abundance in galactic cosmic rays: they are over abundant by a factor of 10^{6}, as is illustrated in Figure 10.09. They are believed to be formed by interactions of cosmic rays with interstellar gas and dust, primarily reactions of ^{1}H and ^{4}He with carbon, nitrogen and oxygen nuclei. These reactions occur at high energies (higher than the Big Bang and stellar interiors), but at low temperatures where the Li, B and Be can survive.

10.2.5 Summary

Figure 10.10 is a part of the Z vs. N plot showing the abundance of the isotopes of elements 68 through 73. It is a useful region of the chart of the nuclides for illustrating how the various nucleosynthetic processes have combined to produce the observed abundances. First, we notice that even numbered elements tend to have more stable nuclei than odd numbered ones — a result of the greater stability of nuclides with even Z. We also notice that nuclides having a neutron-rich isobar (recall that isobars have the same value of A, but a different combination of N and Z) are underabundant, for example ^{170}Yb and ^{176}Lu. This under-abundance results from these nuclides being 'shielded' from production by β^- decay of r-process neutron-rich nuclides. In these two examples, ^{170}Er and ^{176}Yb would be the ultimate product of neutron-rich unstable nuclides of mass number 170 and 176 produced during the r-process. Also notice that ^{168}Yb, ^{174}Hf and ^{180}Ta are very rare. These nuclides are shielded from the r-process and are also off the s-process path. They are produced only by the p-process. Finally, those nuclides that can be produced by both the s- and the r-process tend to be the most abundant; for example, ^{176}Yb is about half as abundant as ^{174}Yb because the former is produced by the r-process only while the latter can be produced by both the s- and the r-process. ^{176}Yb cannot be produced by the s-process because during the s-process, the flux of neutrons is sufficiently low that any ^{175}Yb produced decays to

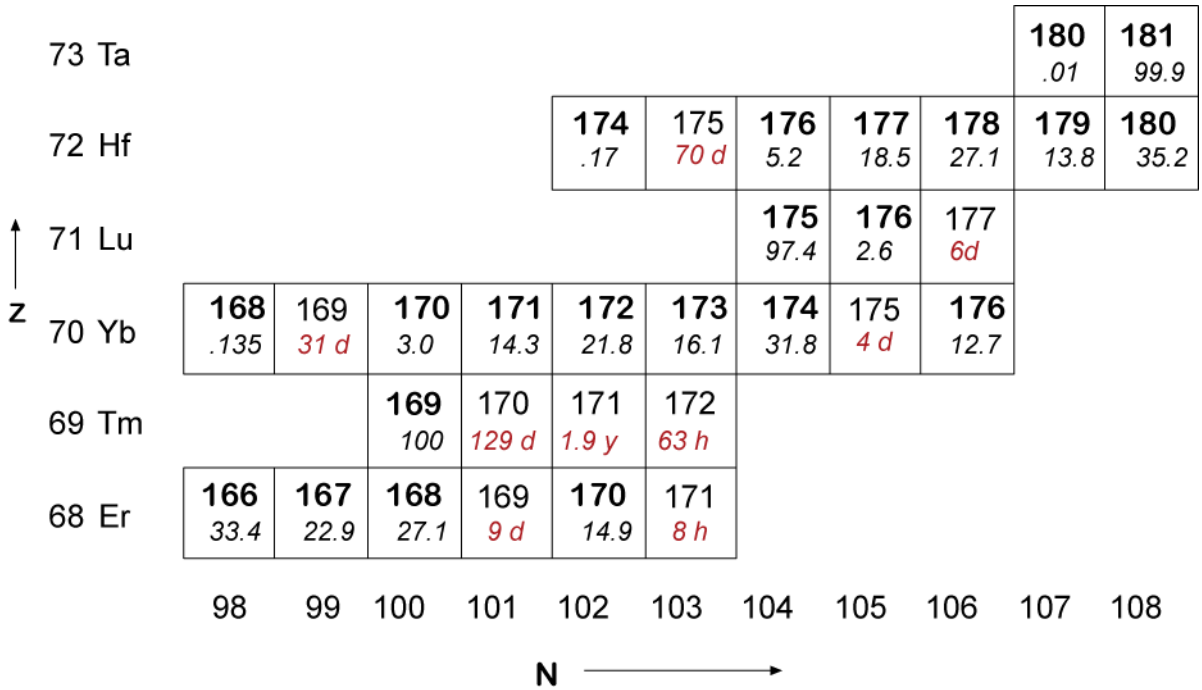

Figure 10.10. View of part of Chart of the Nuclides. Mass numbers of stable nuclides are shown in bold, their isotopic abundance is shown in italics as percent. Mass numbers of short-lived nuclides are shown in plain text with their half-lives also given.

^{175}Lu before it can capture a neutron and become a stable ^{176}Yb.

The heavy element yield of stellar and explosive nucleosynthesis will vary tremendously with the mass of the star. A star of 60 solar masses will convert some 40% of its mass to heavy elements. The bulk of this is apparently ejected into the interstellar medium. Stars too small to become supernovae will convert relatively small fractions of their mass to heavy elements, and only a very small fraction of this will be ejected. One the whole, stars in the mass range of 20-30 solar masses probably produce the bulk of the heavy elements in the galaxy. While such stars, which are already quite large compared to the mean stellar mass, convert a smaller fraction of their mass to heavy elements than truly massive stars, they are much more abundant than the very massive stars.

Novae may also make a significant contribution to the cosmic inventory of a few relatively light elements such as ^{19}F and ^{7}Li, as well as the rarer isotopes of C, N, and O. Novae occur when mass is accreted to a white dwarf from a companion red giant. If the material is mainly hydrogen and accretion is relatively slow, H burning may be ignited on the surface of the white dwarf, resulting in an explosion that ejects a relatively small fraction of the mass of the star.

10.3 METEORITES: ESSENTIAL CLUES TO THE BEGINNING

In subsequent sections we want to consider the formation of the Earth and its earliest history. The Earth is a dynamic body; its rock formations are continually being recycled into new ones. As a result, old rocks are rare. The oldest rocks are 4.0 Ga; some zircon grains as old as 4.4 Ga have been found in coarse-grained, metamorphosed sediments. The geological record ends there: there is no trace of the earliest history of the Earth in terrestrial rocks. So to unravel Earth's early history, we have to turn to other bodies in the Solar System. So far, we have samples only of the Moon and meteorites, and a few analyses of the surface of Venus and Mars†. The Moon provides some clues to the early history of planets; but meteorites provide the best clues as to the formation of planets and the Solar System. We now turn our attention to them.

Meteorites are traditionally classified according to their composition, mineralogy, and texture. The first order division is between *Stones* and *Irons*. You can pretty well guess what this means: stones are composed mainly of silicates while irons are mainly metal. An intermediate class is the *Stony Irons*, a mixture of silicate and metal. Stones are subdivided into *chondrites* and *achondrites* depending on whether they contain *chondrules*, which are small spherical particles that were once molten and can constitute up to 80 % of the mass of chondrites (though the average is closer to perhaps 40%).

Another way of classifying meteorites is to divide them into *primitive* and *differentiated*. Chondrites constitute the primitive meteorites, while the achondrites, irons, and stony-irons constitute the differentiated meteorites. *The chemical and physical properties of chondrites are primarily a result of processes that occurred in the solar nebula*, the cloud of gas and dust from which the solar system formed. On the other hand, *the chemical and physical properties of differentiated meteorites are largely the result of igneous processes occurring on meteorite parent bodies, namely as-*

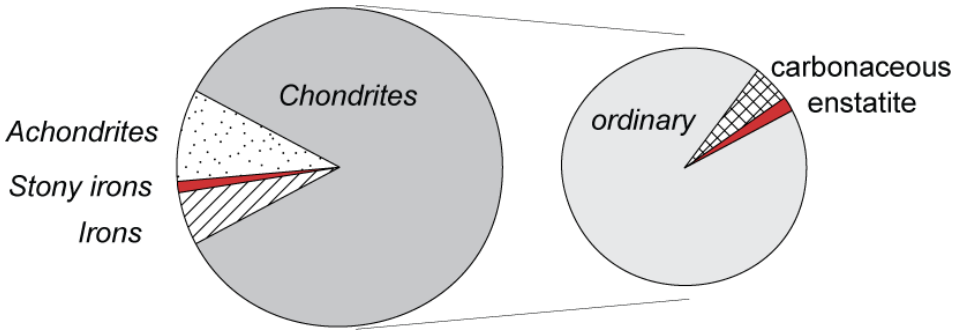

Figure 10.11. Relative abundance of major types of meteorites falls. Smaller pie chart on the right shows relative proportion of different chondrite classes.

† As we shall see, a few meteorites probably come from Mars, providing additional information on the composition of that planet.

teroids. Primitive meteorites contain clues about early solar system formation whereas differentiated meteorites contain clues about early planetary differentiation.

Figure 10.12. *Leoville* (CV3) carbonaceous chondrite. Many of the chondrules have been deformed into elongate spheroids. This meteorite also contains CAI's. NASA photo.

Meteorites are also divided into *Falls* and *Finds*. Falls are meteorites recovered after observation of a fireball whose trajectory can be associated an impact site. Finds are meteorites found but not observed falling. Some Finds have been on the surface of the Earth for considerable time and consequently can be weathered. Thus the compositional information they provide is less reliable than that of falls. An exception of sorts to this is the Antarctic meteorites. Meteorites have been found in surprising numbers in the last 30 years or so in areas of low snowfall in Antarctica where ice is eroded by evaporation and wind. Meteorites are concentrated in such areas by glaciers. Because of storage in the Antarctic deep freeze, they are little weathered.

Figure 10.11 illustrates the relative abundance of the various meteorite types among Falls. Stones, and ordinary chondrites in particular, predominate among Falls. Irons are over-represented among Finds because they are more likely to be recognized as meteorites, and because they are more likely to be preserved. Even among the Falls, irons may be over-represented for these reasons. There are over 17,000 meteorites in collections around the world, most of which now come from Antarctic collecting programs and similar scientific collecting programs in the deserts of Africa and Australia.

10.3.1 Chondrites: The Most Primitive Objects

Chondrites consist of varying proportions of the following: chondrules, refractory calcium-aluminum inclusions (generally called CAI's), amoeboid olivine aggregates (AOA's) and a fine-grained, mixture of minerals and amorphous material called the matrix – we'll discuss these components in more detail below. An example is shown in Figure 10.12. The mineralogical, textural, and compositional (including isotopic composition) features of these components indicate that they formed while dispersed in the solar nebula and were subsequently aggregated to form the meteorite parent bodies. These components were subsequently processed in the parent bodies through aqueous alteration or thermal metamorphism. In addition, many are highly brecciated as a result of collisions and impacts on the surface of the parent bodies. Nevertheless, all chondrites classes have concentrations of *condensable* elements, that is, all elements except H, C, N, O, and the noble gases, that are within a factor of 2 of solar concentrations. This contrasts strongly with the composition of differentiated meteorites, terrestrial materials, lunar materials, etc., all of which differ strongly from the solar composition. Since the Sun comprises more than 99% of the mass of the solar system, its composition is effectively identical to the composition of the solar system, and to the solar nebula from which the solar system formed. *The importance of chondrites is thus clear: they represent samples of the cloud of gas and dust from which all bodies in the solar system formed.* To the degree they have not been obscured by subsequent processing in asteroidal bodies, details of their compositions, their mineralogy, and their textures provide insights into the conditions and processes in the solar nebula that led to the solar system we observe and inhabit today.

10.3.1.1 Chondrite Classes and Their Compositions

Table 10.01 summarizes the general characteristics of the various chondrite groups. There are three main classes: *Carbonaceous (C)*, *Ordinary*, and *Enstatite (E)* chondrites. The ordinary and E chondrites are further subdivided based on their iron and nickel content and the degree of oxidation of the iron. The *ordinary chondrites*, which as Figure 10.11 shows are by far the most common, are composed primarily of olivine, orthopyroxene and lesser amounts of Ni-Fe alloy. They are subdivided into classes H (High iron or bronzite), L (Low iron or hypersthene), and LL. The name LL reflects low total iron and low metallic iron. H chondrites contain 25-31% total iron, of which 15-19% is reduced, metallic iron. L chondrites contain 20-25% iron, of which 4-10% is metallic. LL chondrites contain about the same total iron as L chondrites, but only 1-3% is metallic. The enstatite chondrites are highly reduced, with virtually all the iron is present as metal. Reduction of iron increases the $Si/(Fe^{2+}+Mg)$ ratio in silicates and results in enstatite, rather than olivine, being the dominant mineral in these objects, hence the name of the class. The E-chondrites can be further subdivided into EH (high iron) and EL (low iron) classes. Besides enstatite, metal and sulfides, enstatite chondrites contain a number of other exotic minerals, such as phosphides, carbides and a oxynitride of Si, that indicate they formed under highly reducing conditions.

The amount of Fe and the degree of oxidation are two of the features that differentiate the various chondrite classes. This is illustrated in Figure 10.13. The diagonal lines are lines of constant total iron content. H and C chondrites have similar total iron contents, but their oxidation state differs (carbonaceous chondrites are more oxidized). L and LL chondrites have lower total iron contents (and variable oxidation state). E chondrites are highly reduced, and may have high (EH) or low (EL) total iron. The variation in Fe content extends to other siderophile elements as well, reflecting general fractionation between siderophile and lithophile elements in the solar nebula.

Table 10.01. Characteristics of Chondrite Groups

	Principal ferromagnesian silicate	R.I.'s (vol. %)	Fe/(Fe+Mg) of silicate (mole %)	Metal (vol %)	Mean Mg/Si (molar)	Mean Al/Si (mole %)	Mean Ca/Si (mole %)	$\delta^{18}O$ ‰	$\delta^{17}O$ ‰	Chondrules Size (mm)	Chondrules Volume (%)
Carbonaceous											
CI	serpentine	<0.01	45	<0.01	1.05	8.6	6.2	16.4	8.8	—	—
CM	serpentine	5	43	0.1	1.05	9.7	6.8	12.2	4.0	0.3	20
CO	olivine	13	- 23	1 – 5	1.05	9.3	6.8	-1.1	-5.1	0.2	40
CV	olivine	10	6 – 14	0 – 5	1.07	11.6	8.4	0	-4.0	1.0	45
CK	olivine	4	29-33	<0.01	1.08	10.2	7.6	-0.8	-4.6	0.8	15
CR	chlorite	0.5	37-40	5-8	1.05	8.2	5.6	6.3	2.3	0.7	50-60
CH	olivine	0.1	2.5	23	1.06	8.3	6.0	1.5	-0.7	0.02-0.09	70
CB	olivine	<0.1	3.5	60-70	1.08	11.1	7.2	1.7	-1.4	0.5-5	30-40
Ordinary											
H	olivine	0.01-0.2	17	15 – 19	0.96	6.8	4.9	4.1	2.9	0.3	65-75
L	olivine	<0.1	22	4 – 9	0.93	6.6	4.7	4.6	3.5	0.7	65-75
LL	olivine	<0.1	27	0.3 – 3	0.94	6.5	4.7	4.9	3.9	0.9	65-75
Enstatite											
EH	enstatite	<0.1	0.05	8	0.73	5.0	3.6	5.6	3.0	0.2	60-80
EL	enstatite	<0.1	0.05	15	0.87	5.8	3.8	5.3	2.7	0.6	60-80
Other											
R	olivine	<0.1	38	<0.3	0.77	6.4	4.1	4.5	5.2	0.4	>40
K	enstatite	<0.1	2-4	6-10	0.95	6.9	5.0	2.7	-1.3	0.6	27

Table 10.02. Abundances of the Elements

Element		Solar System Photosphere*	Concentration in *Orgueil* (CI)†	σ (%)	Element		Solar Photosphere*	Concentration in *Orgueil* (CI)†	σ (%)
1	H	1×10^{12}	2.02%	10	44	Ru	69.2	0.683	3
2	He	9.77×10^{10}	56.0 nL/g		45	Rh	13.2	0.14	3
3	Li	1.26×10^{1}	1.49	10	46	Pd	49.0	0.556	10
4	Be	2.51×10^{1}	0.0249	10	47	Ag	8.71	0.197	10
5	B	5.01×10^{2}	0.69	13	48	Cd	58.9	0.68	10
6	C	2.45×10^{8}	3.22%	10	49	In	6.61	0.078	10
7	N	8.51×10^{7}	3180	10	50	Sn	1×10^{2}	1.68	10
8	O	4.90×10^{8}	46.4%	10	51	Sb	10	0.133	10
9	F	3.63×10^{4}	58.2	15	52	Te	1.72×10^{2}	2.27	10
10	Ne	1.00×10^{8}	203 pL/g		53	I	32.4	0.433	20
11	Na	2.14×10^{6}	4982	5	54	Xe	1.45×10^{2}	8.6pL/g	
12	Mg	3.47×10^{7}	9.61%	3	55	Cs	13.2	0.188	5
13	Al	2.95×10^{6}	8490	3	56	Ba	1.35×10^{2}	2.41	10
14	Si	3.47×10^{7}	10.68%	3	57	La	14.8	0.245	5
15	P	2.82×10^{5}	926	7	58	Ce	38.0	0.639	5
16	S	2.14×10^{7}	5.41%	5	59	Pr	5.13	0.0964	10
17	Cl	3.16×10^{5}	698	15	60	Nd	31.6	0.474	5
18	Ar	2.51×10^{6}	751 pL/g		62	Sm	10.2	0.154	5
19	K	1.32×10^{5}	544	5	63	Eu	3.24	0.058	5
20	Ca	2.29×10^{6}	9320	3	64	Gd	13.2	0.204	5
21	Sc	1.48×10^{3}	5.90	3	65	Tb	0.79	0.0375	10
22	Ti	1.05×10^{5}	458	4	66	Dy	13.8	0.256	10
23	V	1.00×10^{4}	54.3	5	67	Ho	1.82	0.0567	10
24	Cr	4.68×10^{5}	2646	3	68	Er	8.51	0.166	5
25	Mn	2.45×10^{5}	1933	3	69	Tm	1.0	0.0256	10
26	Fe	2.82×10^{7}	18.43 %	3	70	Yb	12.0	0.165	5
27	Co	8.32×10^{4}	506	3	71	Lu	1.15	0.0254	10
28	Ni	1.78×10^{6}	1.077 %	3	72	Hf	7.59	0.107	5
29	Cu	1.62×10^{4}	131	10	73	Ta	0.74	0.0142	6
30	Zn	3.89×10^{4}	323	10	74	W	4.79	0.0903	4
31	Ga	7.59×10^{2}	9.71	5	75	Re	1.86	0.0395	4
32	Ge	1.57×10^{3}	32.6	10	76	Os	28.2	0.506	2
33	As	2.34×10^{2}	1.81	5	77	Ir	22.4	0.48	4
34	Se	2.24×10^{3}	21.4	5	78	Pt	63.1	0.982	4
35	Br	4.27×10^{2}	3.50	10	79	Au	10.2	0.148	4
36	Kr	2.0×10^{3}	8.7pL/g		80	Hg	12.3	0.31	20
37	Rb	3.98×10^{2}	2.32	5	81	Tl	7.9	0.143	10
38	Sr	9.33×10^{2}	7.26	5	82	Pb	1.0×10^{2}	2.53	10
39	Y	1.74×10^{2}	1.56	3	83	Bi	5.31	0.111	15
40	Zr	3.98×10^{2}	3.86	2	90	Th	1.20	0.0298	10
41	Nb	26.3	0.247	3	92	U	3.39×10^{-1}	0.0078	10
42	Mo	83.2	0.928	5					

σ is the estimated uncertainty in the concentrations in CI chondrites.
* Atoms relative to H = 10^{12}
† concentrations in ppm unless otherwise indicated. Modified from Palme and Jones (2005).

As there name implies, *carbonaceous chondrites* differ from other chondrite classes in being rich in carbon compounds, including a variety of organic compounds, most notably amino acids (indeed, 70

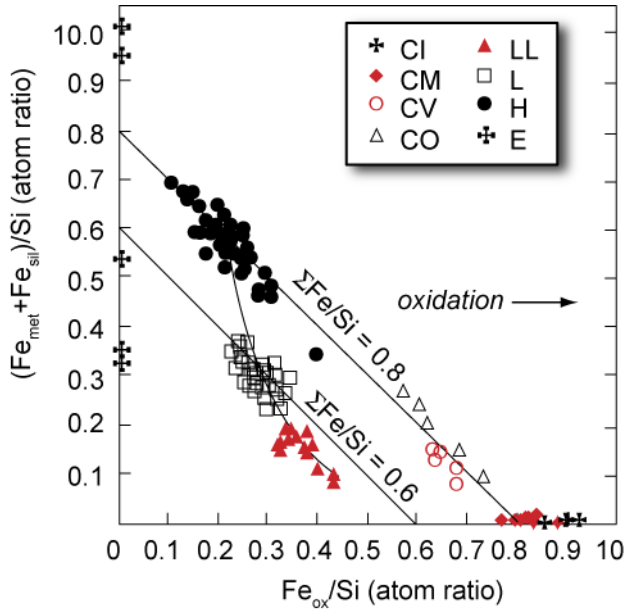

Figure 10.13. Ratio of reduced and oxidized iron to Si in chondrites. Carbonaceous and H group chondrites have approximately equal ΣFe/Si ratios; L and LL groups are iron depleted. After Wasson (1974).

in the CI chondrite *Orgueil* and the solar photosphere. These compositions are also compared in Figure 10.14. As maybe seen, the CI chondrites composition matches that of the Sun remarkably well for all but H, O, C, N, and the rare gases*. CI chondrites thus seem to be collections of bulk nebular dust that escaped high temperature processing, and attendant chemical fractionations, that affected material in other chondrites.

Because it matches the composition of the Sun so well, the composition of CI chondrites is taken to represent that composition of the solar system as a whole for the condensable elements. The terms *chondritic* and *solar composition* are thus effectively synonymous. You might ask why use the CI chondritic composition for the solar system when data for the composition of the Sun is different amino acids have been identified in *Murchison* – there are only 20 biological amino acids). They are also enriched in hydrogen (present mainly in hydrated silicates) and nitrogen and somewhat poorer in Si compared to other chondrites. The composition of carbonaceous chondrites matches that of the Sun even more closely than chondrites as a whole. They are subdivided into 8 subgroups with the name of the subgroups derived from a type example: CI (*Ivuna*), CM (*Mighei*), CV (*Vigarano*) and CO (*Ornans*), CK (*Karoonda*), CR (*Renazzo*), CB (*Bencubbin*), CH (High Iron). Of these, meteorites from the CM, CV, and CO groups are the most common. CI chondrites are rare, but are nevertheless of great significance. Perhaps ironically, CI chondrites lack chondrules and CAI's. Nevertheless, they are rich in carbonaceous matter and are compositionally similar to other chondrites and hence classed with the carbonaceous chondrites. Table 10.02 lists the concentrations of the elements

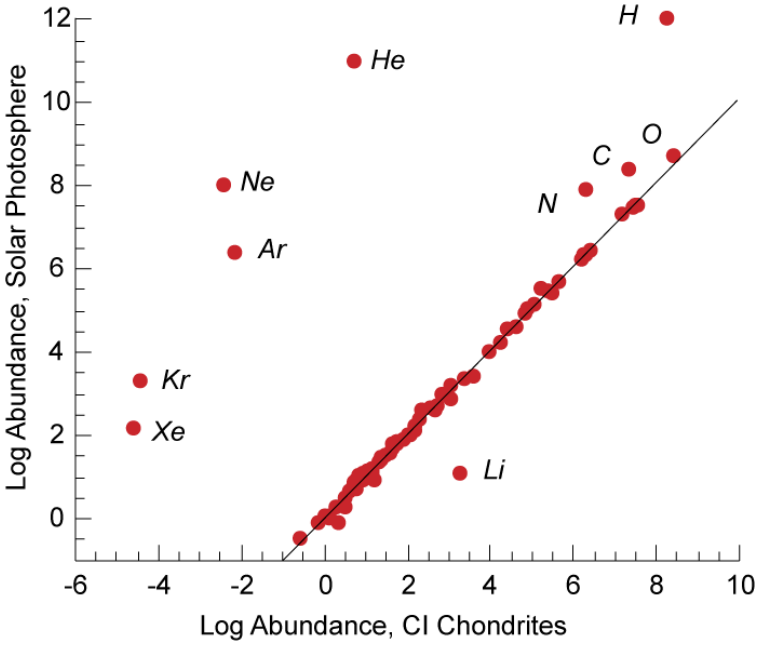

Figure 10.14. Abundances of the elements in the Sun's photosphere vs. their abundances in the carbonaceous chondrite Orgueil (CI). Abundances for most elements agree within analytical error except non-condensing elements and Li.

* These elements will never fully condense from the solar nebula, instead large fractions will remain in the gas phase. These elements are thus termed *non-condensable*. Li is depleted in the Sun compared to chondrites because, as we saw, it is consumed in nuclear reactions in the Sun.

available? The answer is that while the composition of the Sun can be determined spectrographically, this technique is not very accurate for trace elements, and, as we learned in Chapter 7, most elements are trace elements. Unfortunately, meteorites of this group are rare, likely a consequence of their fragile nature, and only one fall, *Orgueil* (which fell in the French town of that name in 1864) exists in enough quantity for complete and detailed chemical analysis.

In addition to these groups, there are two minor classes of chondrites, sometimes grouped together as "other chondrites". These include the R chondrites, of which there are only 19 known specimens. The R-chondrites are so named for the type example *Rumuruti*, which fell in Kenya in 1934. The R-chondrites are the opposite of the E-chondrites in the sense that they are highly oxidized with practically no free metal. They typically contain fewer chondrules than ordinary chondrites and many are highly brecciated, suggesting they came from near the surface of their asteroid parent body. The K group consists of just 3 specimens. They are rich in the iron sulfide, troilite, and show numerous primitive, armored chondrules and have a unique chemical and oxygen isotope composition.

In addition to metal contents and oxidation state, the other compositional differences between chondrites classes are the concentrations of *refractory* elements and the concentrations of *volatile* elements. Let's pause here to define these terms. Si, Mg, and Fe are the most abundant condensable elements in chondrites. In a hot gas of solar composition, these three elements would condense at very similar temperatures (50% of the Si, Mg, and Fe would condense between 1340 and 1311 K at 0.1 Pa). Fifty percent of Al will condense at 1650 K whereas 50% of Na will not condense until 970 K. We refer to elements that condense at higher temperature as *refractory* and elements that condense at lower tempera-

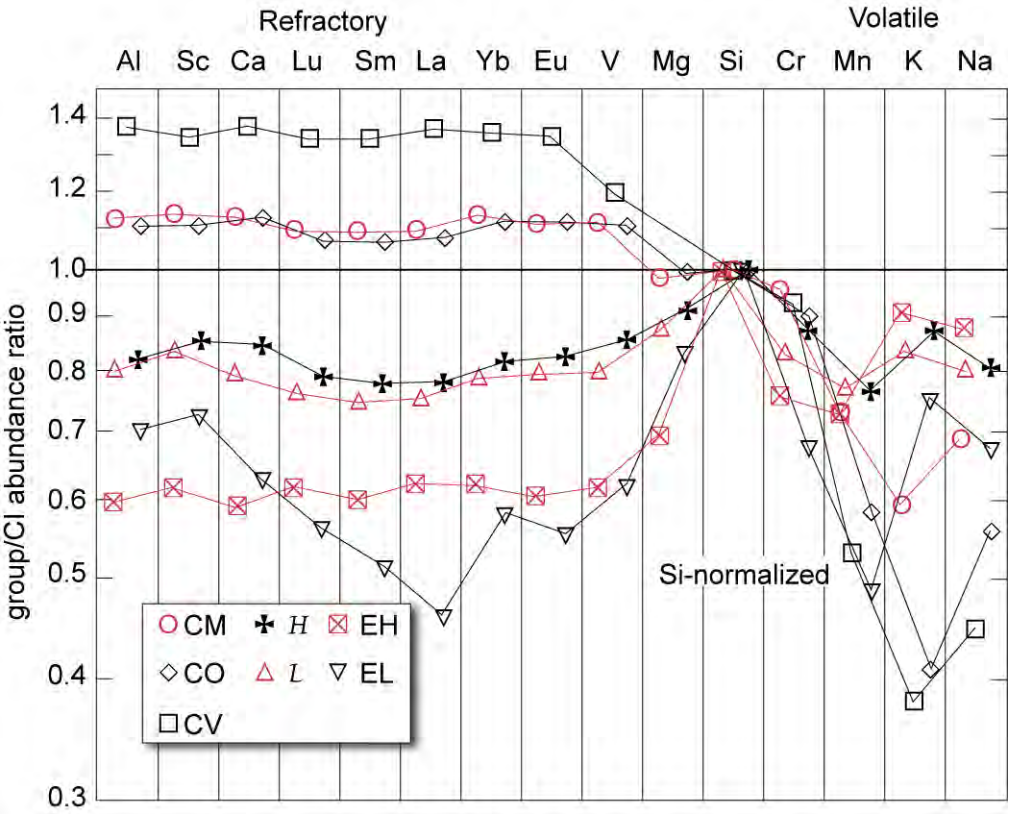

Figure 10.15. Silicon- and CI-normalized abundances of key elements in the main classes of chondrites. Elements are arranged from left to right in order of decreasing condensation temperature. Si concentration plots at 1 in each case. CI chondrites would plot as a horizontal line at 1. After Wasson and Kallemeyn, 1988.

ture as *volatile.* This classification is sometimes further refined into moderately volatile, highly refractory, etc. Figure 10.15 illustrates the compositional variation between chondrite classes for several lithophile elements, which are arranged going from most refractory (Al) and most volatile (Na). Concentrations are shown normalized both to Si and to CI chondrites. Thus Si plots at 1 for all classes, and CI chondrites would plot as a horizontal line at 1. We can see that all other chondrite groups are depleted in volatile elements compared to CI chondrites. We can also see that the other carbonaceous chondrites are enriched in refractory elements compared to CI, and ordinary and E chondrites are depleted in refractory elements compared to carbonaceous chondrites. Recalling that carbonaceous chondrites are enriched in the most volatile elements (H, C, N, etc. – not shown on this plot) compared to other chondrites, we realize that ordinary and E chondrites are depleted in both the most refractory and the most volatile elements compared to carbonaceous chondrites. An interesting feature of this diagram is that despite variations in the absolute levels of refractory elements, the ratios of refractory elements to each other remain nearly constant across all chondrite classes except EL. This is an important observation generally taken as evidence that nebular processes were generally not able to fractionate the most refractory elements.

The compositional variations among chondrites classes illustrated in Figures 10.14 and 10.15 reflect variations in conditions in the solar nebula. Nevertheless, all meteorites have undergone subsequent processing on their parent bodies. Van Schmus and Wood (1967) devised a simple way to indicate the degree of parent body processing by dividing chondrites into petrologic types 1 through 6, based on increasing degree of metamorphism and decreasing volatile content. Types 1 and 2 have experienced low

Table 10.03. Van Schmus and Wood Petrographic Classification of Chondrites

Type	1	2	3	4	5	6
	Increasing Temperature→					
	←Aqueous Alteration			Thermal Metamorphism →		
I. Olivine & pyroxene homogeneity		Greater than 5% mean deviation		Less than 5% mean deviation	Uniform	
II. Structural state of low-Ca pyroxene		Predominately monoclinic		Abundant monoclinic crystals	Orthorhombic	
III. Development of secondary feldspar		Absent		Predominately as microcrystalline aggregates		Clear, interstitial grains
IV. Igneous glass		Clear and isotropic primary glass; variable abundance		Turbid if present	Absent	
V. Metallic minerals (Max. Ni content)		Taenite absent or minor (<20%)	Kamacite and taenite present (>20%)			
VI. Average Ni of sulfide minerals		>0.5%	<0.5%			
VII. Chonrules	No chondrules	Very sharply defined chondrules		Well-defined chondrules	Chondrules rarely seen	Poorly defined chondrules
VIII. Texture of matrix	All fine-grained	Much opaque matrix	Opaque matrix	Transparent microcrystalline matrix	Recrystallized matrix	
IX. Bulk carbon content	3-5%	0.8-2.6%	0.2-1%	<0.2%		
X. Bulk water content	18-22%	2-16%	0.3-3%	1.5%		

temperature aqueous alteration while types 4-6 have experienced increasing high-temperature metamorphism. Type 3 objects have undergone the least parent body processing and are in this sense the most primitive. Table 10.03 summarizes the Van Schmus and Wood classification scheme.

The petrologic types are used together with the above groups to classify meteorites as to origin and metamorphic grade, e.g., CV3. The petrologic type is correlated to a certain degree with chondrite class. Type 1 is restricted to CI, CM, and CR chondrites and petrologic grades above 1 are not found among CI chondrites. Type 2 is restricted to CM and CR chondrites. Petrologic types 5 and 6 occur only in CK, ordinary, E, and R chondrites. Thermal metamorphism results in equilibration of the various minerals present in meteorites; consequently, petrologic types 4-6 are sometimes termed *equilibrated*, while those of low petrologic type are sometimes referred to as *unequilibrated*.

Chondrites can also be classified according to the degree of shock they have experienced. Class *S1* indicates no shock, class *S6* indicates very strong shock, with some shock melting present.

To gain a better understanding of what chondrites are and how they help us understand the processes in the solar nebula, we briefly review the principal components of chondrites in the following sections.

10.3.1.2 Chondrules

Chondrules are usually a few tenths of a mm to a few mm in diameter (Figure 10.12). Mean size varies between chondrite classes (Table 10.01), but is typically around 0.5 mm. In the least metamorphosed meteorites, they consist of mixture of crystals and glass. Most are porphyritic, with relatively large olivine or pyroxene crystals in a fine-grained or glassy matrix. Non-porphyritic chondrules can consist of cryptocrystalline material or radial pyroxene or barred olivine, all of which suggest rapid crystallization. Olivine and Ca-poor pyroxene (enstatite, hypersthene) are by far the dominant minerals, with troilite (FeS), kamacite (FeNi alloy), Ca-rich pyroxene (pigeonite, diopside), Mg-Al spinel, chromite, and feldspar being less abundant. Some rare Al-rich chondrules are compositions similar to CAI's, which are discussed below. Some chondrules contain relict mineral grains and a few contain relict CAI's. Chondrules have remnant magnetism that was acquired as they cooled through their curie point in the presence of a magnetic field, indicating the presence of such a field in the solar nebula. From the number of compound chondrules (two chondrules fused together) and those having indentations suggestive of collisions with other chondrules, the chondrule density was as high a few per m^3 at times and places in the solar nebula. While "dents" are observed in chondrules, microcraters produced by high velocity impact are absent. Many chondrules are compositionally zoned, and most chondrules contain nuclei of relict crystals. Many are rimmed with fine-grained dark secondary coatings of volatile-rich material broadly similar in composition to the chondrite matrix.

Chondrules make up nearly half the mass, on average, of primitive meteorites. Therefore, understanding their origin is critical to understanding processes in the solar nebula because nearly have the dust in the nebula, which is the raw material for terrestrial planets, was apparently processed into chondrules. The presence of glass and their spheroidal shape indicates that chondrules represent melt droplets, as has been realized for at least 100 years. How these melts formed has been more difficult to understand. The main problem is that at the low pressures that must have prevailed in the solar nebula, liquids are not stable: solids should evaporate rather than melt. Chondrules seem to have been heated quite rapidly, at rates of 10^4 K/hr or more to peak temperatures of 1650 to 1850 K and then and cooled rapidly as well, at rates of 100-1000 K/hr. In most cases, peak temperatures were maintained for only minutes and they apparently cooled completely in hours to days. These inferences are based on compositional zonation of minerals and experimental reproduction of textures. It is strengthened by other experiments that show chondrules would have evaporated if they existed in the liquid state any longer than this. Though cooling was rapid, it was considerably slower than the rate that would have resulted from radiative cooling in open space. All these observations indicate they formed very quickly, and may never have reached equilibrium.

Over the past 100 years or so, many mechanisms for chondrule formation have been proposed. These include formation through volcanism on planets or asteroids, impact melting resulting from col-

lisions of planets or planetesimals, condensation from hot nebular gas, and transitory heating of pre-existing nebular or interstellar dust. At present, there is a consensus that they formed by transitory heating of "cool" (<1000 K) nebular dust. Possibilities include collisions of small (<1 m) bodies, frictional heating of dust traveling through gas during infall, lightning, energy released by magnetic flares, or reconnection of magnetic field lines, and radiative heating resulting from high velocity outflows during the T-Tauri phase (see below) of the protosun. At present, the leading hypothesis is that most chondrules were produced in shock waves in the solar nebula. Such shock waves could have been produced by accretion shocks, bow shocks from planetesimals, infalling clumps, interactions with passing stars, or spiral density waves. The latter result from uneven distribution of mass in the nebula and resulting gravitational torques. They can be thought of as somewhat analogous to spiral arms of galaxies. Shocks produce heating because gas is accelerated in the shocks more rapidly than dust, so that the dust is heated by gas drag. Numerical modeling by Desch and Connolly (2002) has shown that shock waves can produce the quick heating and cooling that chondrules apparently experienced. Such shock wave must have been common in the inner solar system because 40% of so of the dust that ultimately formed the asteroids, and the terrestrial planets, was processed into chondrules. Some chondrules might have formed by other mechanisms: usual features of chondrules in CB chondrites suggest they may be formed in a high-energy collision between planetesimals.

10.3.1.3 Calcium-Aluminum Inclusions

Ca-Al inclusions or CAI's are sub-millimeter to centimeter-sized clasts consisting primarily of calcium- and aluminum-rich minerals. They were first described only in 1968 and were at first thought to be restricted to just the CO, CV, and CM chondrites. However, they have now been recognized in essentially all chondrite classes, except CI, although they are rare, and typically very small, in all except the carbonaceous chondrites. The principal minerals are spinel ($MgAl_2O_4$), melilite ($Ca_2Al_2SiO_7$–$Ca_2Mg_2Si_2O_7$), perovskite ($CaTiO_3$), hibonite ($CaAl_{12}O_{19}$), anorthite ($CaAl_2Si_2O_8$), and calcic pyroxene ($CaMg_2Si_2O_6$). Forsteritic olivine is also common in one subtype (forsterite, of course, is not a Ca-Al mineral *per se*, although some forsterites in CAI's are relative rich in the Ca olivine end member, monticellite). Ni-Fe alloys (taenite, kamacite, awaruite) and a wide variety of other minerals may also be present as minor or trace phases.

CAI's have attracted great interest for several reasons. First, they consist of those minerals thermodynamically predicted to condense first as hot gas of solar composition cools. Consistent with this, CAI's are remarkably poor in more volatile elements (except where they have been altered by secondary processes on parent bodies) and they are rich in refractory trace elements such as Ba, Th, Zr, Hf, Nb, Ta, Y, and the rare earths. They sometimes contain microscopic metallic nuggets, called *fremdlinge,* that consist of metals, such as Re, Os, Re, Pt, Ir, W, and Mo, which condense at temperatures even higher than the Ca-Al minerals. Second, as we shall see in a subsequent section, they are the oldest dated objects in the solar system, predating other chondritic components by several million years.

A number of different types of CAI's have been recognized. The most common type is the so-called *spinel-pyroxene inclusions*, which are typically much smaller than 1 mm in diameter (except in CV3 meteorites) and consist of small spinel grains or clumps of grains enveloped in aluminous diopside, sometimes accompanied by anorthite. *Type A* CAI's are less than 1 mm in diameter (except in CV3 meteorites) and consist primarily of melilite intergrown with hibonite, spinel, perovskite and noble metal nuggets. Most have a fluffy texture and irregular shape; more rarely they can be spherical and compact. Both the Type A and the spinel-pyroxene inclusions can be more than 1 cm in diameter in CV3 meteorites. *Type B* inclusions are typically larger, up to 1 cm in diameter, more varied in composition, and are restricted to CV3 meteorites. One subtype consists of coarse-grained melilite, calcic pyroxene, anorthite, and spinel. Another subtype consists of forsterite, melilite, calcic pyroxene, and spinel. *Type C* CAI's, which are rare, consist mostly of spinel, calcic pyroxene, and anorthite. A fifth type, the so-called *hibonite-rich CAI's*, consist of hibonite, sometimes accompanied by spinel and perovskite. A sixth type, the *hibonite-silicate spherules*, consist hibonite intergrown with aluminous pyroxene and perovskite embedded in glass of aluminous pyroxene composition. All types of CAI's are typically surrounded by

an accretionary rim several 10's of μm thick typically consisting of the same minerals as are present in the interior that appears to have resulted from high temperature gas-solid or gas-melt interaction.

Although CAI's as a whole have compositions that approximate that of the highest temperature condensate of a gas of solar composition, their compositions don't match a condensation trend exactly. Furthermore, the texture of most types of CAI's indicate that they have experienced complex histories, that include episodes of melting, evaporation, reaction with nebular gas and finally aqueous alteration and/or metamorphism on parent bodies (Grossman, 2010). However, some CAI's, notably the fluffy Type A's, do have compositions and textures suggesting they indeed high temperature condensates of nebular gas. It is possible that many other CAI's began as such condensates and they experienced subsequent episodes of transient high temperatures. Other CAI's may have formed as evaporative residues. Regardless of the details, CAI's provide evidence that some nebular dust experienced transient heating events with temperatures reaching 1700 K. This is much hotter than the nebula should have ever been at the position of the asteroid belt. For this and other reasons, there is an emerging consensus that CAI's formed close to the Sun and where subsequently cycled back out into the deeper nebula, perhaps by "X-winds, which we will discuss later in the chapter.

10.3.1.4 Amoeboidal Olivine Aggregates

Amoeboidal olivine aggregates (AOA's) are, as their name implies, aggregates of anhedral forsteritic olivine with lesser amounts of Fe-Ni metal, spinel, aluminous diopside, and rare anorthite and melilite. They are fine-grained (5-20 μm) and the aggregates have dimensions similar to those of chondrules in the same meteorite. Some contain melted CAI's. In some cases, the olivine is partially replaced by enstatite. Some have igneous textures suggesting they have been partially melted. AOA's most likely represent aggregates of grains that condensed from nebular gas at high temperature. The may well have formed in the same environment, albeit at lower temperature, as CAI's.

10.3.1.5 The Chondrite Matrix

The matrix of chondrites is dark, FeO- and volatile-rich material that is very fine-grained (typical grain size is about 1 μm). It can be quite heterogeneous, even on a 10μm scale. It also varies between meteorite classes, with an order of magnitude variation in Mg/Si, Al/Si and Na/Si. The primary constituents appear to be Fe- and Ca-poor pyroxene and olivine and amorphous material, but magnetite, Fe-metal, and a wide variety of silicates, sulfides, carbonates, and other minerals are also be present. In the most volatile-rich meteorites the olivine and pyroxene have been altered to serpentine and chlorite; in the carbonaceous chondrites, carbonaceous material is present in substantial quantities. One the whole, the composition of the matrix is complementary to that of the chondrules: whereas the latter are depleted in Fe and volatiles, the former are enriched in them. Very significantly, the matrix includes grains of SiC, graphite, diamond and other phases of anomalous isotopic composition. These "presolar grains" are of great significance and we will discuss these isotopic variations in greater detail in a subsequent section.

10.3.2 Differentiated Meteorites

The differentiated meteorites are produces of melting on asteroid parent bodies. They are igneous rocks with igneous textures, although in some cases, brecciation may be the dominant texture.

10.3.2.1 Achondrites

While all the chondrites seem reasonably closely related, the achondrites are a more varied group. The *Acapulcoites*, *Lodranites*, *Winonaites*, and *Urelites* form a group called the *primitive achondrites* because they resemble chondrites in composition and mineralogy. Beyond that they are quite diverse. Meteorites of the first 3 groups are extremely rare. They represent chondritic material that has experienced extreme metamorphism and low-degree partial melting. In a few cases, relict chondrules have been identified, providing further evidence of their primitive nature. *Urelites*, which are both more common and more diverse than the other primitive achondrites, consist of olivine, pyroxene and a few metal grains plus a percent or so carbon, present as graphite and diamond, the latter a product of shock metamor-

phism produced by impacts. Their origin is problematic; it is possible they have several origins. Some are partial melting residues like other primitive achondrites; others appear to be highly fractionated igneous rocks. *Brachinites* are also sometimes included in the primitive achondrites.

Upon heating, chondritic material will first form a metal-sulfide melt, which is much denser than the residual solid, which is mainly silicate. This metal will drain out of the matrix and ultimately form a core at the center of the body. Upon further heating, a silicate partial melt will form, into which the more incompatible elements will partition. Thus primitive achondrites are variously depleted in metal and incompatible elements relative to chondrites.

Figure 10.16 illustrates the compositional relationship between the various achondrite groups. Primitive achondrites tend to have Mn/Mg ratios similar to those of chondrites, the remaining achondrites have superchondritic Mn/Mg ratios and Fe/Mg ratios higher than primitive achondrites. This, as well as their text and mineralogy, indicates that those remaining achondrites groups originated through igneous processes. During partial melting of chondritic material, these three elements partition into the melting in the order Mn>Fe>Mg. Subsequent fractional crystallization increases the Fe/Mg ratio, but has little further effect on the Mn/Fe ratio.

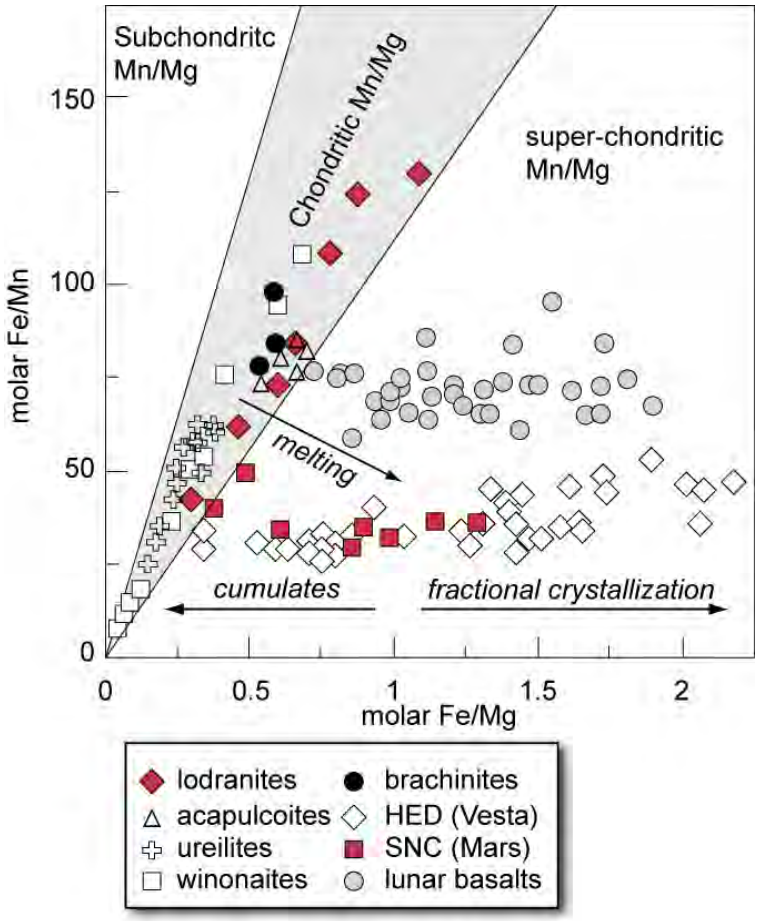

Figure 10.16. Variation in Fe/Mn and Fe/Mg ratios in achondrites and lunar basalts. Primitive achondrites are variably depleted in Fe, but have Mn/Mg ratios similar to chondrites. The HED and SNC chondrites, like lunar basalts, have superchondritic Mn/Mg ratios and higher Fe/Mg ratios than primitive achondrites as a consequence of their igneous origin. After Goodrich and Delaney (2000).

Diogenites are Ca-poor and consist principally of hypersthene (orthopyroxene), which is accompanied by minor amounts of olivine and plagioclase. They are coarse-grained and their texture suggests they formed as cumulates in a magma chamber. The Ca-rich achondrites include the *Eucrites* and *Howardites*. The eucrites resemble lunar and, to a lesser extent, terrestrial basalts, and are also called *basaltic achondrites*, and like terrestrial basalts they consist primarily of plagioclase and pyroxene. The howardites are extremely brecciated, and are a heterogeneous mixture of eucrite and diogenite material. They also contain clasts of carbonaceous chondritic material, other xenolithic inclusions, and impact melt clasts. Their brecciated character suggests they were part of the regolith, or surface, of their asteroid parent body. The howardites, eucrites, and diogenites form a group called the HED group and likely all came from a single parent body, believed to be the asteroid Vesta (Figure 10.17).

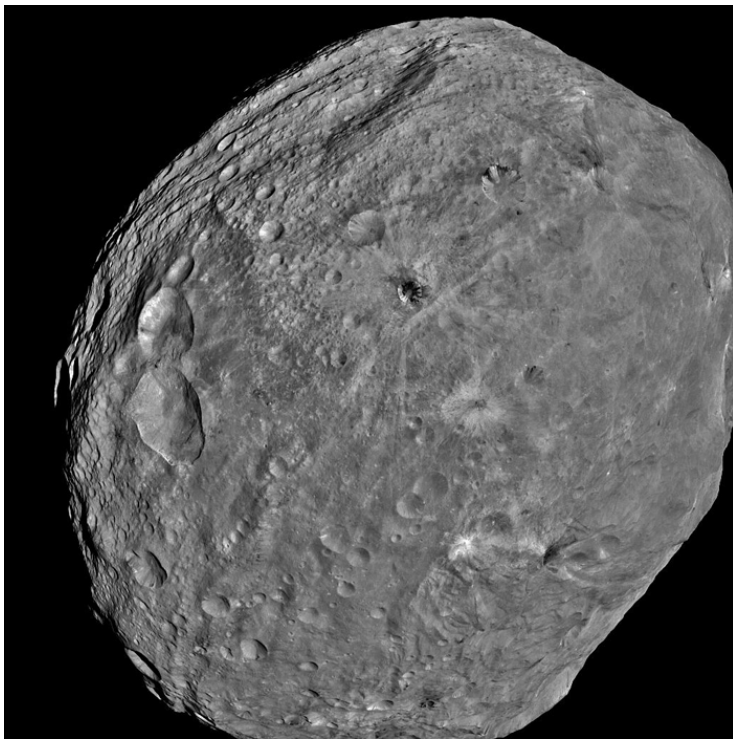

Figure 10.17. Photograph of the asteroid Vesta taken by the NASA Dawn spacecraft in 2011. Vesta, the second largest asteroid, has a smei-major orbital axis of 2.4AU, a mean diameter of 500 km and a mean density of 3420 kg/m^3. It is believed to be the parent body of the HED meteorites. NASA photo.

Two final groups are the *angrites* and the *aubrites*. The angrites (of which there are only 4 specimens, the name of the class being derived from *Angra dos Reis*) consist mostly of Al-Ti augite (Ca-rich pyroxene). They are strongly silica undersaturated and contain minerals characteristic of alkali basalts, such as nepheline and are strongly depleted in moderately volatile elements. The compositions suggest formation through partial melting under oxidizing conditions, followed by complex igneous differentiation. The aubrites are highly reduced and consist primarily of enstatite. They thus resemble enstatite chondrites, but they do not contain chondrules and they are poorer in metal and sulfide. It seems nonetheless highly likely that they formed from enstatite chondrite parent material.

A unique group of achondrites, the *SNC* meteorites (the name is derived from type meteorites *Sherogotty*, *Nakla*, and *Chassigny*) generally have much younger formation ages (0.15 – 1.5 Ga) than virtually all other meteorites. This, and certain features of their bulk compositions and trapped noble gases, led to the interpretation that these meteorites come from Mars, having been ejected by an impact event on that planet. This interpretation, initially controversial, is now the consensus view. There are 24 distinct specimens of this class (excluding pairing, that is, ones that are clearly pieces of the same rock). Finally, there are 25 meteorites of lunar origin. A handful of achondrites are unique and cannot be assigned to any class.

10.3.3.2 Irons

Iron meteorites were originally classified based largely on phase and textural relationships. Compositionally, they all consist primarily of Fe-Ni alloys with lesser amounts of (mainly Fe-Ni) sulfides. Octahedral taenite, one of the Fe-Ni alloys, is the

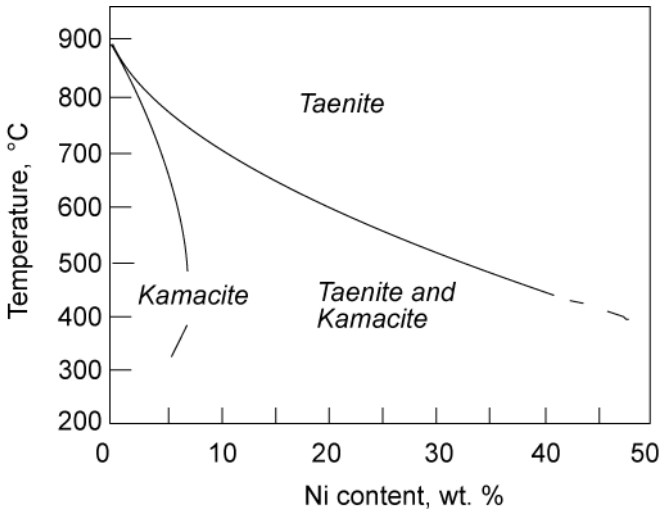

Figure 10.18. Phase diagram for iron-nickel alloy. After Wasson (1974).

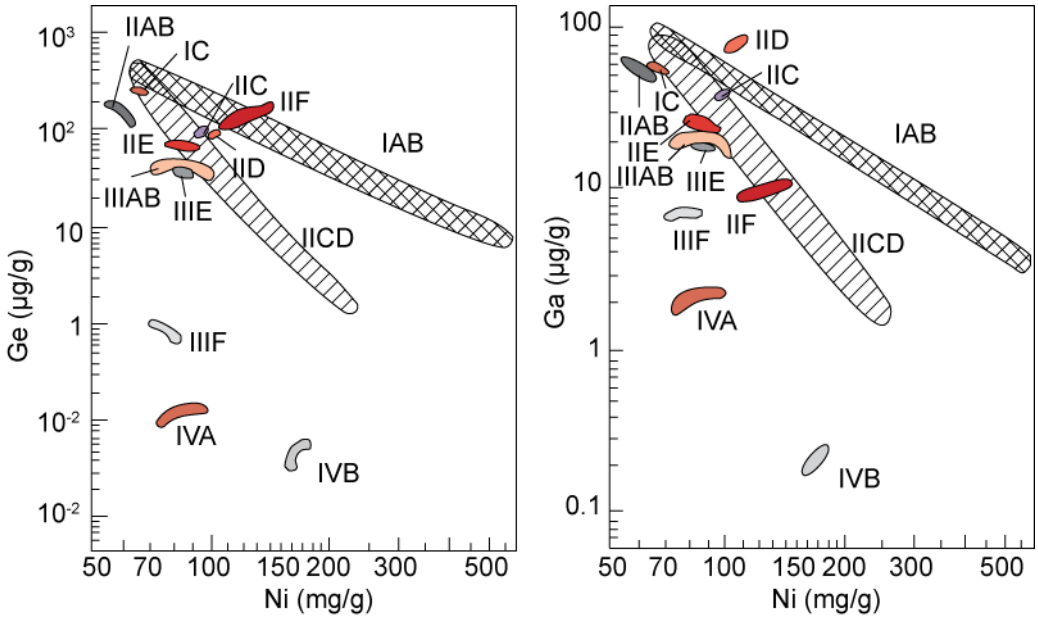

Figure 10.19. Ge-Ga and Ge-Ni plots showing location of iron meteorite groups. Points are anomalous irons. After Wasson (1985).

stable Fe-Ni metal phase at T> 900°C (Figure 10.18). At lower temperature, kamacite, a Ni-poor Fe-Ni alloy, exsolves on the crystal faces of the octahedron. If the Ni content falls below 6%, all the metal converts to kamacite at lower temperature. Thus the phases and textures of iron meteorites are related to their composition and cooling history. Iron meteorites consisting only of kamacite are named *hexahedrites*. If Ni exceeds 6%, some taenite persists and the overall pattern is octahedral (= *octahedrites*), producing what is known as a *Widmanstätten* pattern. At low Ni contents, kamacite dominates and forms large crystals (*coarse octahedrites*). At higher Ni, kamacite and crystal size diminish (*fine and medium octahedrites*). *Ataxites* are Ni-rich (>14%) iron meteorites consisting of a fine-grained intergrowth of kamacite and taenite. The 20% or so of irons with silicate inclusions form a separate class.

The current classification by Wasson is based on Ga and Ge abundances. These are named I - IV, based on decreasing Ga and Ge. It turns out that many other chemical parameters can be related to Ga and Ge concentrations. Subgroups within these classes are named A, B, etc. Figure 10.19 illustrates chemical variation among the irons.

The chemical variations within individual subclasses of irons are consistent with those produced by fractional crystallization of metal liquid. The clear implication then is that all irons from an individual subclass come from a single parent body. Perhaps some 60 parent bodies are represented by the suite of analyzed irons. There is a general consensus that iron meteorites, with a few notable exceptions, represent the cores of asteroids or *planetesimals*. Cooling rates, estimated from textures and diffusion profiles, are typically in the range of a few 10's of degrees per million years. This slow cooling is indicates the irons formed in the interior of bodies with diameters in the range of a few tens to a few hundred kilometers. A few classes of irons, most notably the IAB, may represent impact melts rather than segregated cores (Wasson et al., 1980).

10.3.3.3 Stony-Irons

The main classes of stony-irons are the *pallasites* and the *mesosiderites*. Pallasites consist of a network of Fe-Ni metal with nodules of olivine. They probably formed at the interface between molten metal and molten silicate bodies, with olivine sinking to the bottom of the silicate magma. Mesosiderites consist of an odd pairing of metal and silicate. The silicate portion is very similar diogenites – brecciated pyroxene and plagioclase, and a genetic relationship is confirmed by oxygen isotopes (discussed later).

The metal fraction seems closely related to IIIAB irons. It is possible they formed as the result of a collision of two differentiated asteroids, with liquid core of one asteroid mixing with the regolith of the other.

10.4 TIME AND THE ISOTOPIC COMPOSITION OF THE SOLAR SYSTEM

10.4.1 Meteorite Ages

10.4.1.1 Conventional Methods

Meteorite ages are generally taken to be the age of Solar System. Before we discuss meteorite ages in detail, we need to consider the question of precisely what event is being dated by radiometric chronometers. In Chapter 8, we found that radioactive clocks record the last time the isotope ratio of the daughter element, e.g., $^{87}Sr/^{86}Sr$, was homogenized. This is usually some thermal event. In the context of what we know of early solar system history, the event dated might be (1) the time solid particles were removed from a homogeneous solar nebula, (2) thermal metamorphism in meteorite parent bodies, or (3) crystallization (in the case of chondrules and achondrites), or (4) impact metamorphism of meteorites or their parent bodies. In some cases, the nature of the event being dated is unclear.

The most precise ages of meteorites have been obtained using the U-Pb chronometer (Figure 10.20). Advances in analytical techniques have remarkably improved precision over the last decade or so, to the point that ages with uncertainties of only a few 100,000 years can be obtained. However, some of the issues that traditionally plague geochronology come into focus, including lack of complete initial isotopic homogeneity and deviations from closed system behavior. In addition, new issues arise, including uncertainties in half-lives of the parents and uncertainty in, as well as variation of, the $^{238}U/^{235}U$ ratio (Amelin et al., 2009). Progress is being made in resolving these issues, but further research remains necessary.

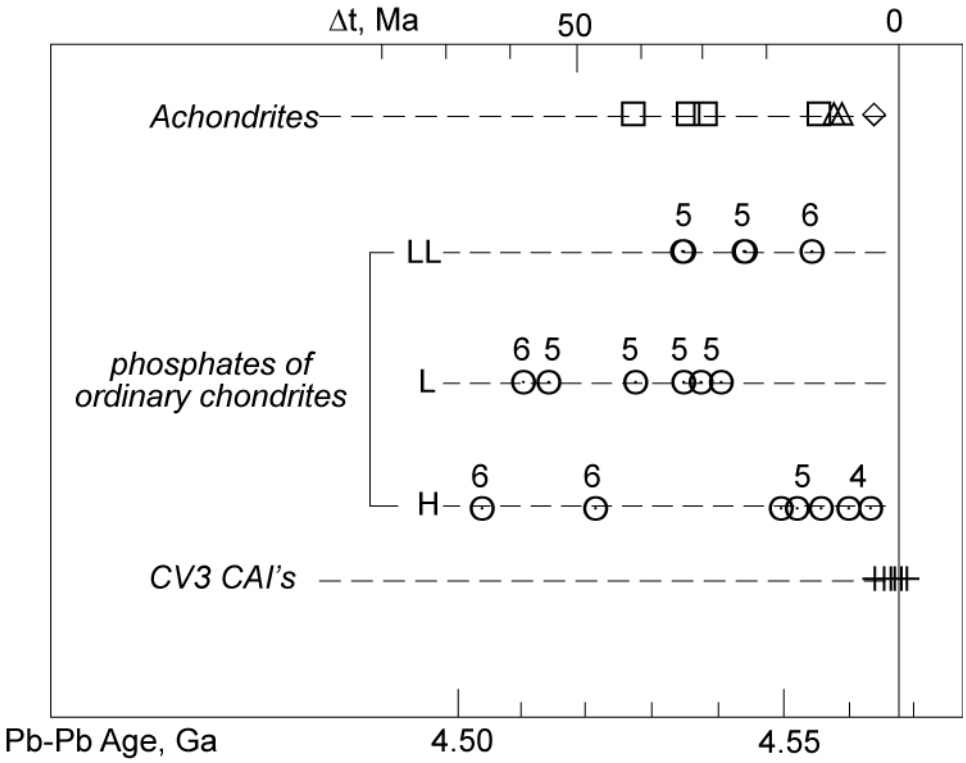

Figure 10.20. High precision Pb-Pb ages of Allende CAI's, ordinary chondrites, and achondrites. Modified from Allegre (2001).

Chapter 10: Cosmochemistry

The oldest Pb-Pb ages come from CAI's, in part because CAI's are rich in refractory elements like U and depleted in volatile elements like Pb. At present, the oldest high-precision date is 4,568.67±0.17 Ma for a CAI from the CV3 meteorite *NWA2364*[*] calculated using the "canonical" $^{238}U/^{235}U$ ratio of 137.88 (Bouvier et al., 2010). This age decreases to 4,568.22±0.17 Ma if a value of 1137.84 is used for that ratio. Bouvier et al. (2010) speculated that the $^{238}U/^{235}U$ of the CAI might be as low as 137.81, which would make the age 0.3 Ma younger. The next oldest age is a CAI from *Allende*, also CV3 meteorite, whose age, calculated using the canonical $^{238}U/^{235}U$ value, is 4567.59±0.11 Ma (Bouvier et al., 2007). Less precise ages ranging from 4567.4 to 4568.6 have been reported for other *Allende* inclusions. Amelin et al. (2009) reported a high precision Pb-Pb age of 4567.11±0.16 Ma for a CAI from the CV3 meteorite *Efremovka*. The accuracy of these dates has, however, been thrown into question by Bennecka et al.'s (2010) discovery of variable $^{238}U/^{235}U$ ratios in CAI's from Allende, which range from 137.409±0.039 and 137.885±0.009 compared to the "canonical" value of 137.88. Brennecka et al. (2010) concluded that the cause of the variability was decay of ^{247}Cm, which decays to ^{235}U with a half-life of 13.6 Ma. Amelin et al. (2010) calculated an age for one *Allende* CAI using the $^{238}U/^{235}U$ measured in that CAI (137.876) and obtained age of 4567.18±0.50 Ma. Because the $^{238}U/^{235}U$ is very close to the "canonical" value, this age falls well within error of Pb-Pb age of other CV3 CAI's. Bouvier et al. (2010) speculated that the slightly older age of *NWA2364* inclusions compared to those of *Allende* and *Efremovka* might reflect aqueous alteration of the latter after incorporation into the CV3 parent body. Chondrules in carbonaceous chondrites have slightly younger Pb-Pb ages than the CAI's, 4562.7±0.5 for *Gujba* (CB3) to 4565.5±0.5 Ga for *Allende*. The ages assume the canonical $^{238}U/^{235}U$ value. Amelin et al. (2010) found that the *Allende* whole rock and chondrules had a low $^{238}U/^{235}U$, 137.747±0.017, which implies earlier reported ages of the chondrules were too old by about 1.4 Ma.

Phosphates also have high U/Pb ratios and these were analyzed by Göpel et al. (1994) to obtain high precision ages of a variety of equilibrated (i.e., petrologic classes 4-6) ordinary chondrites, whose ages range from 4.563 to 4.502 Ga. The phosphates are thought to have formed during metamorphism, thus these ages represent the age of metamorphism of these meteorites. The oldest of these meteorites was H4 chondrite *Ste. Marguerite*. Bouvier et al. (2007) subsequently reported a Pb-Pb isochron age of 4562.7 Ma, in excellent agreement with the age determined by Göpel et al. (1994). The age of CAI's from CV3 meteeorites thus seems 3 Ma older than the oldest precise ages obtained on ordinary chondrites. No attempt has been made at high precision dating of CI chondrites, as they are too fine-grained to separate phases.

Among achondrites, the chronology of the angites is perhaps best documented. The oldest high precision Pb-Pb age is 4564.42 ± 0.12 Ma for the angrite *D'Orbigny* (Amelin, 2008). This age was calculated assuming $^{238}U/^{235}U = 137.88$. Using the measured $^{238}u/^{235}U$ for this meteorite of 137.778, the age is reduced to 4563.36±0.34 (Bouvier et al., 2011). *Angra dos Reis* has a Pb-Pb age of 4557.65 ± 0.13 Ma, and *Lewis Cliff 86010*, a coarse grained "plutonic" angrite, has an age of 4558.55 ± 0.15 Ma. Thus differentiation, cooling and crystallization of the angrite parent body apparently lasted some 6 million years. Wadhwa et al. (2009) reported an age of 4566.5±0.2 Ma for unusual basaltic achondrite, *Asuka 881394*. Bouvier et al. (2011) determined an age of 4562.89 ± 0.59 Ma for another unusual basaltic achondrite, *NWA2976*. *Ibitira*, a unique unbrecciated eucrite, has an age of 4556±6 Ma. Perhaps surprisingly, these ages are similar to those of chondrites. This suggests that the parent body of these objects formed, melted, and differentiated, and the outer parts crystallized within a very short time interval. Not all achondrites are quite so old, however. A few other high precision ages (those with quoted errors of less than 10 Ma) are available and they range from this value down to 4.529±0.005 Ga for *Nuevo Laredo* and 4.510±0.004 Ga for *Bouvante*. Thus the total range of the few high precision ages in achondrites is about 50 million years. Iron meteorites appear to be similarly old. Smoliar et al. (1996) reported a Re-Os ages of 4558±12 and 4537±8 Ma for IIIA and IIA irons, respectively; ages of other iron groups range from

[*] NWA stands for Northwest Africa. This is one of many meteorites found in the Sahara desert over the last couple of decades.

4506 to 4569 Ma, but are of lower precision and are not significantly different from the IIIA and IIA ages.

K-Ar ages are often much younger. This probably reflects Ar outgassing as a result of collisions and the ages probably date impact metamorphism.

As Figure 10.20 shows, there is little relationship between meteorite class and age. H chondrites do seem a bit older than other ordinary chondrites and Göpel et al. (1994) did find an inverse correlation between petrologic type and age (the least metamorphosed are oldest), but this does not appear to be true of chondrites in general. Furthermore, there appears to be little difference in age between chondrites and achondrites. The present state of conventional meteorite chronology may be summarized by saying that it appears the meteorite parent bodies formed around 4.567±0.001 Ga, and there is some evidence that high-temperature inclusions and chondrules in carbonaceous chondrites may have formed a few Ma earlier than other material. At least some parent bodies remained hot enough to allow metamorphism to continue for some 30 Ma after their formation. Resolving events on a finer timescale than this has proved difficult using conventional techniques. There are, however, other techniques that help to resolve events in early solar system history, and we now turn to these.

10.4.1.2 Initial Ratios

The reference 'initial' $^{87}Sr/^{86}Sr$ of the solar system is taken as 0.69897±3, based on the work of Papanastassiou and Wasserburg (1969) on basaltic achondrites (BABI: basaltic achondrite best initial). Basaltic achondrites were chosen since they have low Rb/Sr and hence the initial ratio (but not the age) is well constrained in an isochron. Subsequent high precision analyses of individual achondrites yield identical results (earlier reported low *Angra Dos Reis* have subsequently been shown to be in error). CAI's and Rb-poor chondrules from Allende have an even lower initial ratio: 0.69877±3 consistent with the idea that these formed slightly earlier than the meteorite parent bodies.

The initial $^{143}Nd/^{144}Nd$ ratio of the solar system is taken as 0.506609±8 (normalized to $^{146}Nd/^{144}Nd$ = 0.72190) based on the work on chondrites of Jacobsen and Wasserburg (1980). Achondrites seem to have slightly higher initial ratios, suggesting they formed a bit later.

The initial isotopic composition of Pb is taken from the work of Tatsumoto et al. (1973) on troilite from the Canyon Diablo iron meteorite as $^{206}Pb/^{204}Pb$: 9.307, $^{207}Pb/^{204}Pb$: 10.294, $^{208}Pb/^{204}Pb$: 29.476. These values agree with the best initial values determined from chondrites, including Allende chondrules. Subsequent work by Chen and Wasserburg (1983) confirmed these results, i.e.: 9.3066, 10.293, and 29.475 respectively.

10.4.1.3 Extinct Radionuclides

There is abundant and compelling evidence that certain short-lived nuclides once existed in meteorites. This evidence consists of anomalously high abundances of the daughter nuclides in certain meteorites and fractions of meteorites that correlate with the abundance of the parent element. The first of these to be discovered was the $^{129}I - ^{129}Xe$ decay Reynolds (1960). Since then, 18 other *extinct radionuclides* have been discovered. The most significant of these are listed in Table 10.04; a full list can be found in Dauphas and Chassidon (2011). These provide evidence of nucleosynthesis occurring shortly before the solar system

Table 10.04. Short-Lived Radionuclides in the Early Solar System

Radionuclide	Half-life Ma	Decay	Daughter	Abundance Ratio
^{10}Be	1.5	β	^{10}B	$^{10}Be/^{9}Be \sim 7.5 \times 10^{-4}$
^{26}Al	0.73	β	^{26}Mg	$^{26}Al/^{27}Al = 5.2 \times 10^{-5}$
^{36}Cl	0.301	β	$^{36}Ar/^{36}S$	$^{36}Cl/^{35}Cl \sim 17 \times 10^{-6}$
^{41}Ca	0.15	β	^{41}K	$^{41}Ca/^{40}Ca \sim 1.4 \times 10^{-8}$
^{53}Mn	3.7	β	^{53}Cr	$^{53}Mn/^{55}Mn = 6.3 \times 10^{-6}$
^{60}Fe	1.5	β	^{60}Ni	$^{60}Fe/^{56}Fe \sim 5.8 \times 10^{-8}$
^{107}Pd	9.4	β	^{107}Ag	$^{107}Pd/^{108}Pd \sim 5.9 \times 10^{-4}$
^{129}I	16	β	^{129}Xe	$^{129}I/^{127}I \sim 1.2 \times 10^{-4}$
^{146}Sm	103	α	^{142}Nd	$^{146}Sm/^{144}Sm = 0.0084$
^{182}Hf	8.9	β	^{182}W	$^{182}Hf/^{180}Hf = 9.7 \times 10^{-5}$
^{244}Pu	82	α, SF	Xe	$^{244}Pu/^{238}U \sim 0.001$
^{247}Cm	15.6	α, SF	^{235}U	$^{247}Cm/^{235}U \sim 6 \times 10^{-5}$

formed. To understand why, consider the example of ^{129}I. It decays to ^{129}Xe with a half-life of 16 Ma. Hence 16 Ma after they were created, only 50% of the original atoms of ^{129}I would remain. After 2 half-lives or 32 Ma only 25% would remain, after 4 half-lives or 64 Ma only 6.125% of the original ^{129}I would remain, etc. After 10 half lives, or 160 Ma, only $1/2^{10}$ (0.1%) of the original amount would remain. Anomalously high abundance of ^{129}Xe relative to other Xe isotopes that correlate with iodine concentration in a meteorite indicates some ^{129}I was present when the meteorite, or its parent body, formed. From this we can conclude that ^{129}I had been synthesized not more than roughly 10^8 years before the meteorite formed. This time constraint is further reduced by the identification of radiogenic ^{26}Mg, produced by the decay of ^{26}Al. That ^{26}Al is the source of the ^{26}Mg is evidenced by the correlation between ^{26}Mg and the Al/Mg ratio. The half-life of ^{26}Al is 0.73 Ma and the production ratio for $^{26}Al/^{27}Al$ in red giants is thought to be around 10^{-3} to 10^{-4}. The $^{26}Al/^{27}Al$ initial ratios in CAI's of 5×10^{-5} indicates nucleosynthesis occurred no more than a few million years before formation of these CAI's.

These short-lived 'fossil' radionuclides also provide a means of relative dating of meteorites and other bodies, because the abundance of the extinct radionuclide at the time an object formed can be deduced. Consider Figure 10.21 where $^{53}Cr/^{52}Cr$ in inclusions from *Allende* are plotted as a function of the $^{55}Mn/^{52}Cr$. Provided that (1) all inclusions formed at the same time, (2) all remained closed to Mn and Cr since that time, and (3) that ^{53}Mn was present when they formed and has since fully decayed, we can derive the following equation from the fundamental equation of radioactive decay:

$$\left(\frac{^{53}Cr}{^{52}Cr}\right) = \left(\frac{^{53}Cr}{^{52}Cr}\right)_0 + \left(\frac{^{53}Mn}{^{55}Mn}\right)_0 \left(\frac{^{55}Mn}{^{52}Cr}\right) \qquad 10.01$$

where, as usual, the subscript naught refers to the initial ratio. On a plot of $^{53}Cr/^{52}Cr$ vs. $^{55}Mn/^{52}Cr$ such as Figure 10.21, this is the equation of a line with a slope equal to the initial $^{53}Mn/^{55}Mn$ ratio, in this case 2.76×10^{-6} (note that the right hand scale expresses the $^{53}Cr/^{52}Cr$ ratio in the epsilon notation introduced in Chapter 8, or deviations in parts per thousand from a terrestrial standard, whose value is 0.1134569).

As time passes, the abundance of the radioactive nuclide will decrease, so that the initial ratio determined in diagrams such as 10.21 will be lower for younger objects. This is illustrated in Figure 11.22, which compares ^{26}Al-^{26}Mg systematics in a CAI from the CV3 meteorite *NWA2364* to those in a younger object, the eucrite *Asuka 881394*. The difference in initial $^{26}Al/^{27}Al$ indicates the latter object is some 4 million years younger than the former.

Extinct radionuclides can thus be used to establish a relative time scale of events in the early solar system. A number of factors, however, hinder this process. First, it is possible that these recently synthesized radionuclides might not have been uniformly distributed through the solar nebula. Indeed, as well shall see in a subsequent section, there is evidence of isotopic heterogeneity on the very fine scale of the matrix material of carbonaceous chondrites. Second, isotopic heterogeneity unrelated to decay of extinct radionuclides might be present in the

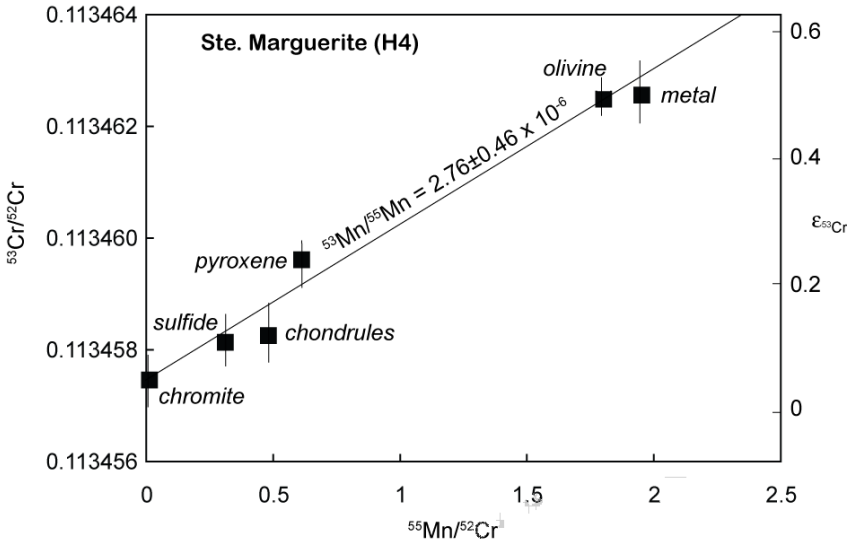

Figure 10.21. Correlation of the $^{53}Cr/^{52}Cr$ ratio with $^{55}Mn/^{52}Cr$ ratio in inclusions from the ordinary chondrite *Ste. Marguerite* (H4). Data from Trinquier et al. (2008).

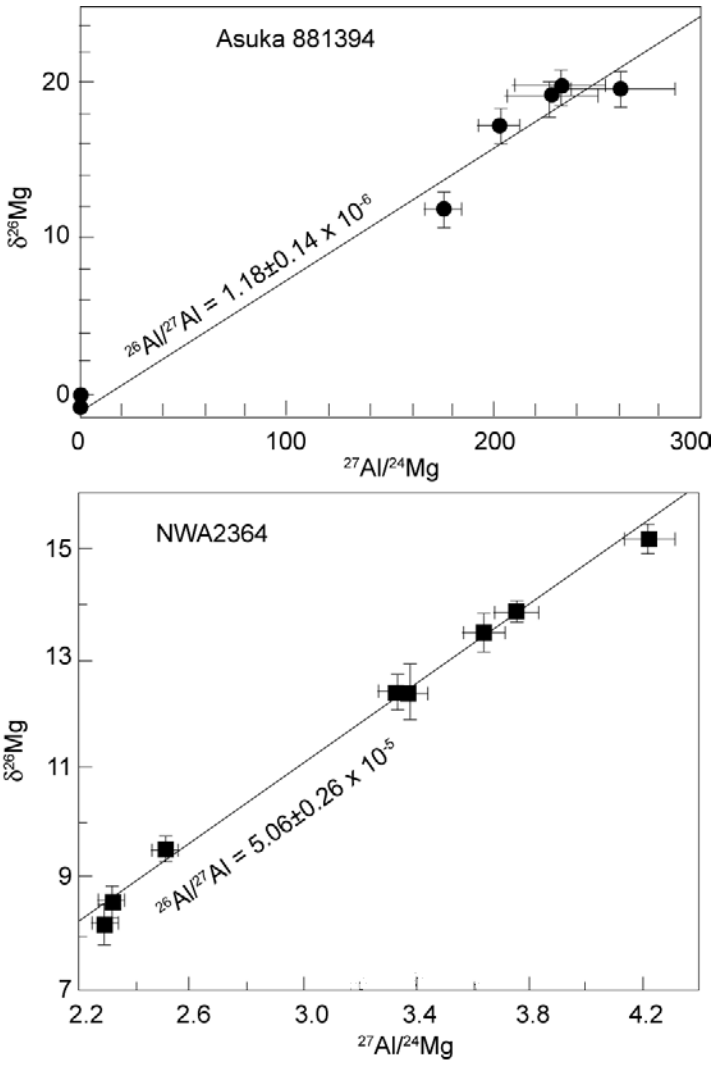

Figure 10.22. Comparison of Al-Mg isotope systematics for two different meteorites. The lower diagram shows minerals separated from a CAI in CV3 *NWA2364*, one of the oldest objects in the solar system (Bouvier and Wadhwa, 2010). The upper diagram shows plagioclase and pyroxene separates from the eucrite *Asuka 881394* (Nyquist et al., 2003). The later has an initial $^{27}Al/^{26}Al$ more than 40 times lower than *NWA2364*, implying it is some 4 million years younger.

daughter elements. Indeed, there is some evidence for this in the case of Cr, but a correction can be made by measuring an additional Cr isotope, ^{54}Cr. In the case of a light element such as Mg, mass fractionation arising from chemical or physical processes might affect the $^{26}Mg/^{24}Mg$. This too can be corrected by measuring ^{25}Mg, provided the fractionation was mass dependent. Finally, cosmic ray spallation reactions have been demonstrated in meteorites, and these can affect some of the elements of interest, but again, corrections for these effects can generally be made. In addition, there are, of course, the same issues with conventional radiogenic isotopic geochronology, such as open system behavior, etc.

Provided these can be overcome, an absolute chronology can be established by calibrating relative ages determined from extinct radionuclides with high precision Pb-Pb ages. For the earliest objects, the short-lived nuclides ^{53}Mn and ^{26}Al have proved most useful. Figure 10.23 illustrates such a time scale, anchored on objects dated by both Pb-Pb and ^{26}Al or ^{53}Mn. The chronology begins with the CAI from NWA2364. Objects such as *Lewis Hills 86010*, *St. Marguerite*, and *D'Orbigny* provide other anchors. Objects such as *Orgueil*, which has not been dated by conventional radiometric methods, can be placed on the time scale based on their apparent initial $^{26}Al/^{27}Al$ or $^{53}Mn/^{55}Mn$ ratios.

Ages, both conventional radiometric ones and those based on extinct radionuclides, can represent different things. In the case of CAI's, their age might either represent the formation, or time of aqueous alteration on the parent body. For the LL3 chondrules, this age may well represent the formation age, but some evidence suggests the chondrule event lasted for as much as 2 million years, so all chondrules need not have the same age. In other cases, such as *Ste. Marguerite*, the age may represent the age of metamorphism. In others, such as the HED parent body, it represents melting and differentiation. The angrites show a range of ages. *D'Orbigny* is a fine-grained igneous rock that probably formed near the surface of the angite parent body, which would have cooled quickly. *Lewis Cliff 86010* is a coarse-grained from the interior of the angrite parent body that would have cooled more slowly.

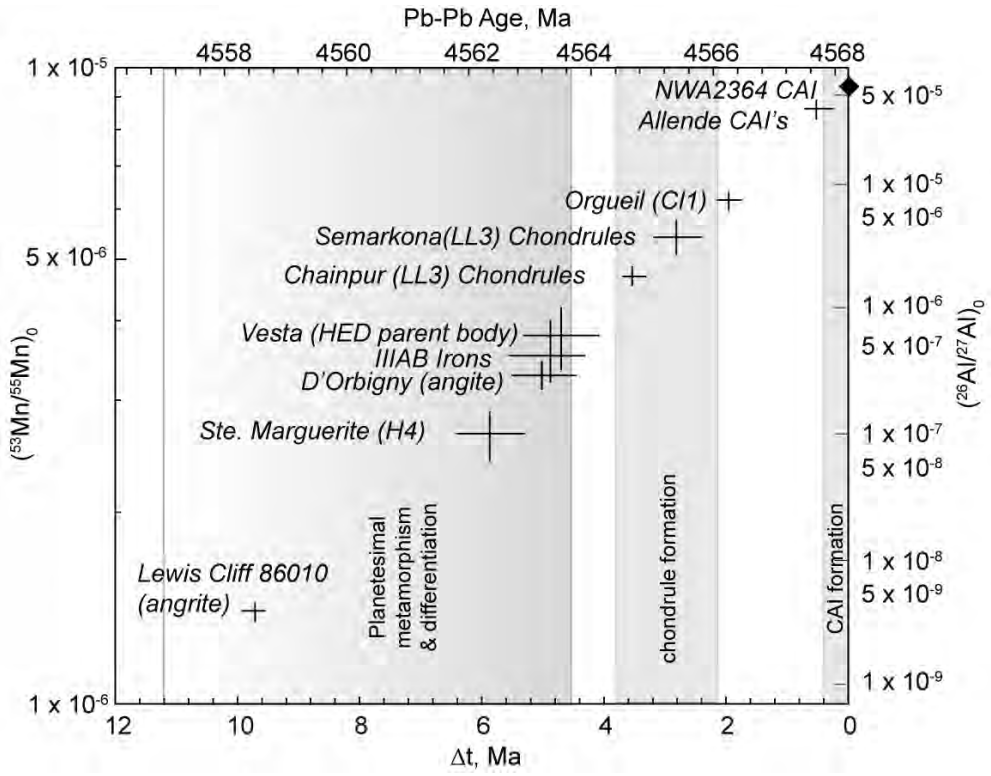

Figure 10.23. Time scale of events in the early solar system based on calibrating ^{53}Mn and ^{26}Al extinct radionuclide chronology to Pb-Pb ages. Based on data in Trinquier et al. (2008), Nyquist et al. (2009) and Bouvier and Wadhwa (2010).

As mentioned, the extinct radionuclides also provide evidence of 1 or more nucleosynthetic events shortly before, or perhaps even during, the formation of the solar system. ^{41}Ca, which decays to ^{41}K with a half-life of 150,000 yrs provides perhaps the most stringent constraint of the time of nucleosynthesis. Extinct ^{41}Ca has been identified in CAI's from several CV3 and CM2 meteorites, which had an apparent ^{41}Ca/^{40}Ca ratio of 1.4 x 10^{-8} when they formed. Isotopic variations of Ag from the decay of ^{107}Pd (half-life 6.5 Ma) in iron meteorites indicate core formation in meteorite parent bodies began, and was largely complete, within about 15 Ma of the nucleosynthesis. We'll see at the end of this chapter that the ^{182}Hf-^{182}W pair provides important constraints on timing of formation of the Earth's core.

Exactly how these nuclides were synthesized is somewhat debated. As we saw earlier in this chapter, heavy elements are synthesized mainly in red giant stars and supernovae. On a galactic scale, red giants and supernovae will be continually injecting newly synthesized elements into the interstellar medium. Those nuclides that are unstable will steadily decay away. These two competing processes will result in steady-state abundance of these nuclides in the interstellar medium. The abundances of ^{107}Pd, ^{129}I, ^{146}Sm, and ^{182}Hf listed in Table 10.04 roughly match the expected steady-state galactic abundances and hence do not require a specific synthesis event. However, the abundances of ^{10}Be, ^{26}Al, ^{36}Cl, and ^{41}Ca in the early Solar System requires synthesis of these nuclides at the time, or just before, the Solar System formed.

The conventional view is that these nuclides were synthesized in a red giant and/or a supernova in the region where the solar system formed just shortly before its formation. Some of these elements, such as ^{26}Al are most efficiently synthesized in red giants; others, such as ^{60}Fe are most efficiently synthesized in supernovae. Thus most models invoke both environments, which may or may not have been the same star at different times. Indeed, one popular hypothesis is that the formation of the solar

system was actually triggered by a supernova shock wave. Boss and Vanhala (2001) provide a good discussion of this view.

Evidence of the existence of ^{10}Be in some CAI's has led to an alternative hypothesis, namely that many of the short-lived extinct radionuclides were produced by spallation within the solar system as it was forming. As we have seen, Be is not synthesized in stars, hence the presence of ^{10}Be in CAI's and other primitive chondritic components is problematic for the red giant/supernova injection hypothesis. Another key observation is that young protostars emit X-rays. X-rays are produced by accelerating charged particles. Hence some have suggested that near the surface of the accreting protostar, magnetic reconnection events could produce flares that accelerate ions up to very high energies – essentially creating cosmic rays (e.g., Russell et al., 2001). Spallation would occur when the accelerated particles encounter dust grains – the CAI's – that happen to be close to the forming Sun (within 0.1 AU). According to this theory, some of these irradiated CAI's would have been carried back out to the vicinity of the asteroid belt by the energetic "X-winds" that are associated with these protostars.

Most workers now agree that ^{10}Be was synthesized entirely by spallation. Spallation may well have responsible for some fraction of the ^{26}Al, ^{36}Cl, and ^{41}Ca, and perhaps some of the ^{53}Mn as well. However, it cannot account for the ^{60}Fe and probably cannot account for all of the ^{26}Al, ^{36}Cl, ^{41}Ca, and ^{53}Mn. Huss et al. (2009) concluded that intermediate mass *asymptotic giant branch* (AGB) stars (a variety of red giant) and supernovae of stars with precursor masses in the range of ~20 to ~60 solar masses are the most likely sources.

10.4.2 Cosmic Ray Exposure Ages and Meteorite Parent-Bodies

As we saw in Chapter 8, cosmic rays colliding with matter in meteorites and planetary bodies produce new nuclides through spallation. The cosmic rays only penetrate to a limited depth (of the order of a meter or less: there is no cutoff, the flux falls off exponentially), so that only small bodies or the surfaces of larger bodies are exposed to cosmic rays. The rate of production of nuclides by cosmic ray bombardment can be estimated from experimental physics if the cosmic ray flux is known. Thus, assuming a more or less constant cosmic ray flux, the length of time an object has been exposed to cosmic rays, the 'exposure age', can be calculated from the amounts of cosmogenic nuclides. Exposure ages are only accurate to within about a factor of 2, due to all the assumptions that are required in estimating the rate of production of nuclides. Exposure ages for chondrites are shown in Figure 10.24; exposure ages for irons were shown in Figure 8.26. As can be seen, the ages for chondrites are considerably less than formation ages. From this we may conclude that meteorites became small bodies accessible to cosmic rays only comparatively recently. Before that, they must have been stored in larger parent bodies where they would have been protected from cosmic ray bombardment. Apparently, meteorites are continually produced by collisions of these larger bodies. Irons tend to have longer exposure ages than stones. This simply reflects their greater strength and resistance to break up.

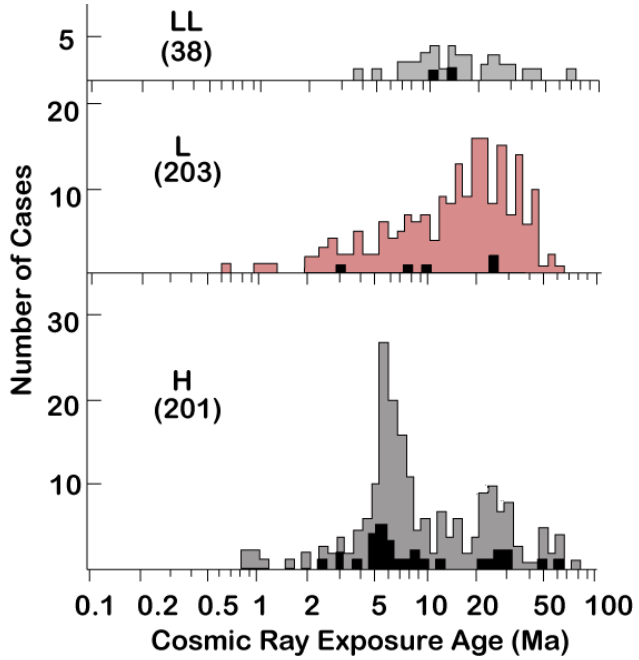

Figure 10.24. Cosmic ray exposure ages of meteorites. Filled histogram is for meteorites with regolith histories (i.e., brecciated meteorites). After Crabb and Schultz (1981).

The limited variability in composition within meteorite classes and the compositional gaps between different classes suggests all meteorites of a common class share a close genetic history. Relatively young cosmic ray exposure ages, the clustering of exposure ages of meteorite classes, extensive thermal metamorphism (reach perhaps 1000° C), evidence of melting in differentiated meteorites, and slow cooling rates of iron meteorites all indicate that meteorites were once parts of larger *parent* bodies. Meteorites from a given class may have been derived from the same parent body, though this need not always be the case. Estimates of the diameter of parent bodies of various meteorite classes range from 10 to 1000 km. There are some compositional similarities between different classes that in some cases suggest a genetic relationship between them, and possible derivation from the same parent body. For example, the aubrites and e-chondrites are both highly reduced. We saw that the silicate of mesosiderites is very similar to diogenites. Many of the pallasites seem related to the IIIAB irons and may come from the same parent body. Other pallasites seem more closely related to ordinary chondrites and to IAB irons.

Orbits for a few observed falls have been reconstructed, and these reconstructed orbits confirm the suspicion that many meteorites originate in the asteroid belt. Reflectance spectra of some asteroids can be matched to specific groups of meteorites. Based on spectroscopic studies, *Ceres*, the largest asteroid (diameter of 950 km), appears to be compositionally match the CM chondrites. *Vesta* (Figure 10.17) has a spectrum that closely matches that of the eucrites (Figure 10.24) and is considered the parent of the HED achondrite group. Recent observations from the Dawn spacecraft have confirmed this view and suggest that much of the surface of Vesta consists of material similar to howardites (the highly brecciated members of this group). Based on radar reflections, the asteroid *Psyche* suggests a Ni-Fe composition, similar to iron meteorites. The asteroid *Lutetia*, is thought to be similar in composition to e-chondrites based on spectral measurements by the European Space Agency *Rosseta* probe. S-type asteroids, which dominate the inner asteroid belt are probably the parents of the ordinary chondrites, although this remains somewhat uncertain. Other asteroids, notably those of class "M", appear to be composed of Fe-Ni metal and are analogous to iron meteorites. It is quite interesting and important that the asteroid belt appears to be compositionally zoned, with "igneous" asteroids, analogous to the differentiated meteorites, predominating in the inner part and "primitive" meteorites, analogous to carbonaceous chondrites, dominating in the outer part of the belt.

Although meteorites represent a wide range of compositions, there is no particular reason to believe that those in collections are representative sample of the compositions of Solar System bodies. The reflectance spectra of most asteroids do not match those of any of meteorite classes – suggesting they have a greater variety of compositions than represented by meteorites. Collisions among asteroids and the gravitational influence of Jupiter probably sends a more or less constant flux of asteroid fragments into orbits that will ultimately lead to collisions with the Earth.

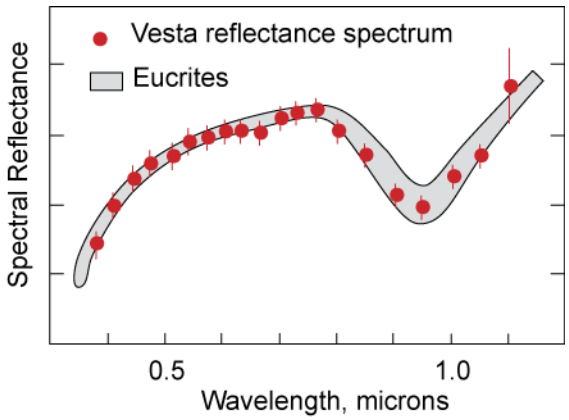

Figure 10.25. Comparison of the laboratory-determined reflectance spectrum of eucrite meteorites (basaltic achondrites) with that of the asteroid Vesta. The close match suggests that the crust of Vesta is basaltic, and similar to eucrites. After McSween (1987).

10.4.3 Isotopic Anomalies in Meteorites

10.4.3.1 Neon Alphabet Soup and Interstellar Grains in Meteorites

Since Thomson's discovery that elements could consist of more than one isotope in 1912, scientists have realized that the isotopic composition of the elements might vary in the universe. They also realized that these variations, if found, might provide clues as to how the elements came into being. As the only available extraterrestrial material, meteorites were of ob-

vious interest in this respect. However, isotopic analyses of meteorites, by Harold Urey among others, failed to reveal any differences between meteorites and terrestrial materials. This apparent isotopic homogeneity was raised as an objection to the polygenetic hypothesis of Burbidge, Burbidge, Fowler, and Hoyle (1957), since isotopic variations in space and time were an obvious prediction of this model. Within a few years of its publication, however, John Reynolds, a physicist at the University of Califonia, Berkeley, found isotopic variations in noble gases, particularly neon and xenon (Reynolds, 1960).

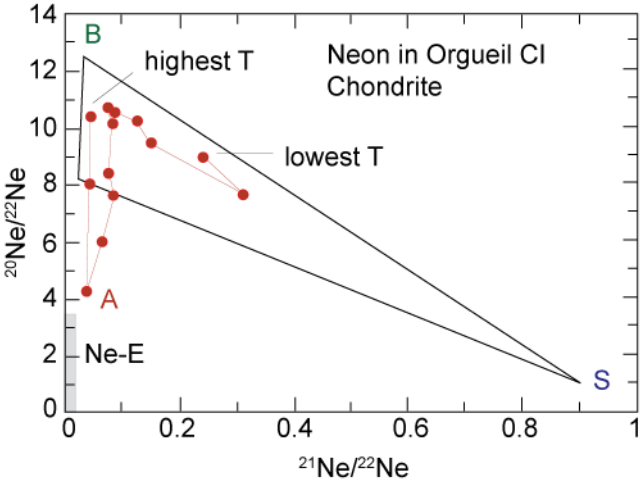

Figure 10.26. Neon isotopic compositions in a step-heating experiment on Orgueil CI chondrite, which produced the first evidence of 'pre-solar' or exotic Ne. The points connected by the line show the changing Ne isotope ratios with increasing temperature. Shaded area was the original estimate of the composition of the pure Ne-E component. Also shown are the compositions of Ne-A ('solar'), Ne-B ('planetary'), and Ne-S ('spallogenic'). After Black and Pepin (1969).

Noble gases are present in meteorites at concentrations that are often as low as 1 part in 10^{10}. Though they are fairly readily isolated and analyzed at these concentrations, their isotopic compositions are nonetheless sensitive to change due to processes such as radiogenic decay (for He, Ar, and Xe), spallation and other cosmic ray-induced nuclear processes, and solar wind implantation. In addition, mass fractionation can significantly affect the isotopic compositions of the lighter noble gases (He and Ne). Through the late 1960's, all isotopic variations in meteoritic noble gases were thought to be related to these processes. For example, Ne isotopic variations could be described as mixtures of three components, "Neon A" or planetary (similar in composition to the Earth's atmosphere), "Neon B", or solar, which differed from atmospheric due to mass fractionation, and "Neon S", or spallogenic (cosmogenic) (Figure 10.26). The isotopic variations in Xe discovered by Reynolds were nonetheless significant because they were due to the decay of ^{129}I and ^{244}Pu, which must have been only recently (on a cosmic time scale) synthesized.

In 1969, the picture became more complex when evidence of a ^{22}Ne-rich component, named "Neon E" was found in the high temperature (900-1100°C) release fractions of six carbonaceous chondrites (Black and Pepin, 1969). However, the carrier of Neon-E proved difficult to identify. Many scientists participated in an intensive search over nearly 2 decades for the carrier phase of these components. The search quickly focused on the matrix, particularly that of CM2 meteorites. But the fine-grained nature of the matrix, together with the abundance of sticky and refractory organic compounds, made work with the groundmass difficult. In the late 1980's, E. Anders and his colleagues at the University of Chicago (e.g., Tang and Anders, 1988) found that Neon-E is associated with fine-grained (<6 μm) graphite and SiC (silicon carbide) of the matrix. Ne-E actually consists of two isotopically distinct components: Ne-E(L), which was found to reside in graphite, and Ne-E(H) which resides in SiC. The $^{20}Ne/^{22}Ne$ ratio of Ne-E(H) is less than 0.01, while that of Ne-E(H) is less than 0.2.

The other key noble gas in this context is xenon. Having 9 isotopes rather than 3 and with contributions from both ^{129}I decay and fission of Pu and U, isotopic variations in Xe are bound to be more complex than those of Ne. On the other hand, its high mass minimizes mass fractionation effects. Eventually, 2 isotopically distinct components were identified: Xe-HL, so named because it shows enrichments in both the heaviest and lightest Xe isotopes (Figure 10.27), and the Xe-S component, so named because it is enriched in the s-process only isotopes ^{128}Xe and ^{130}Xe. Anders' University of Chicago group eventually identified the carrier of Xe-HL as microdiamonds and that of Xe-S as SiC.

Once these interstellar grains were isolated, it was possible to study their isotopic compositions in detail using ion microprobes‡. Very large variations in the isotopic composition of carbon and nitrogen (Figure 10.28). The SiC grains do not form a single population, but represent a number of populations of grains, each produced in a different astronomical environment. Isotopic variations in a number of other elements, including Mg, Si, Ca, Ti, Sr, Zr, Mo, Ba, Nd, Sm, and Dy.

That the first "interstellar" or "presolar" grains discovered were unusual minerals such as graphite, SiC and diamond had to do with the way they were isolated. Essentially, they were the residue after the rest of the meteorite was dissolved away. Subsequently, however, similar isotopic anomalies have been found in Si_3N_4, spinel, hibonite, a variety of metal carbides, TiO_2, Fe-Ni metal and olivine. The latter may turn out to be the most common kind of presolar grain. In the exceptionally primitive carbonaceous chondrite *Acfer*, Nagashima et al. (2004) and Nguyen and Zinner (2004) found presolar silicates were present in the groundmass at an abundance of about 30 to 40 parts per million, compared to 14 parts per million for presolar SiC.

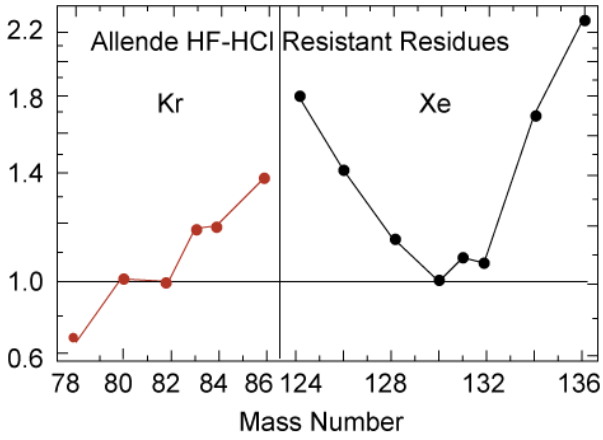

Figure 10.27. The isotopic composition of Kr and Xe of the 'Xe-HL ' component in Allende matrix. Xe-HL is characteristically enriched in both the light and heavy isotopes, while the lighter noble gases show enrichment only in the heavy isotopes. After Anders (1988).

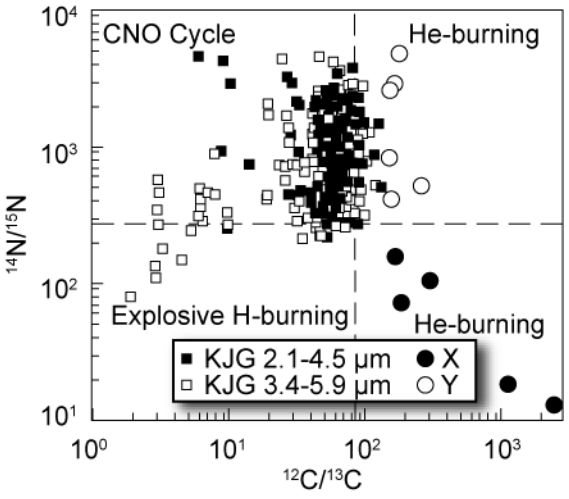

Figure 10.28. Isotopic composition of C and N in SiC from Murchison (CM2) meteorite. Dashed lines show the isotopic composition of normal solar system C and N. Populations X and Y, which are anomalous here, are anomalous in other respects as well. From Anders and Zinner (1993).

Discovery of isotopically anomalous interstellar grains has inspired theorists to attempt to explain them, and there has been considerable progress on understanding stellar and explosive nucleosynthesis in the past 2 decades as a result. However, even the very limited treatment of nucleosynthetic processes in stars earlier in this chapter is sufficient to allow us to identify the environment in which some of these grains were produced. Thus, if we examine a chart of the nuclides, we quickly see that the lightest Xe isotope, ^{124}Xe is a p-process-only nuclide, while the heaviest Xe isotopes, ^{134}Xe and ^{136}Xe, are r-process-only nuclides. The p- and r-processes occur in supernovae, thus Xe-HL, as well perhaps as the diamonds that carry it, must have been produced in supernovae. Xe-S is enriched in ^{128}Xe and ^{130}Xe, which are s-process-only isotopes. The s-process, of course, operates mainly in red giants, so we might guess the SiC was produced in red giants. Carbon and nitrogen in the SiC is, in most cases, enriched in ^{14}N and ^{13}C relative to normal solar system nitrogen and carbon. As we noted earlier in the chapter,

‡ Ion microprobes fire a narrow beam of ions (often O or Cs) at a surface. This produces ions from the surface that can be analyzed in an attached magnetic sector mass spectrometer. This is known as secondary ionization mass spectrometry or SIMS). Because the ion beam can be focused very finely (a few microns in diameter), very small areas can be analyzed.

there tends to be some net production of ^{14}N, and consumption of ^{12}C in the CNO cycle, which operates in main sequence stars, but also in the H-burning shell of red giants. As it turns out, our guess of red giants as sources of this SiC would be a good one. Theoretical studies show a close match between the observed isotopic patterns and those produced in the red giant phase (also called asymptotic giant branch) of medium-sized stars (1-3$M_\odot$). These studies show that such stars could also produce the ^{107}Pd and ^{26}Al that was present when the meteorites formed (e.g., Wasserburg et al., 1995).

10.4.3.3 Oxygen Isotope Variations

Another element commonly showing isotopic variations is O. Until 1973, O isotope variations in meteorites were thought to be simply the result of mass-dependent fractionation, as they are on Earth. But when R. Clayton of the Univ. of Chicago went to the trouble of measuring ^{17}O (0.037% of O) as well as ^{18}O and ^{16}O, he found that these variations were not consistent with simple mass-dependent fractionation. This is illustrated in Figure 10.29. On a plot of $^{17}O/^{16}O$ vs. $^{18}O/^{16}O$, almost all terrestrial materials (atmospheric ozone is a notable exception, as we learned in Chapter 9) plot on a line with a slope of 0.52 – the *Terrestrial Fractionation Line*. Lunar samples fall on this same line, but meteorites and meteoritic components do not; and some appear to plot on a line with a slope of 1. The initial interpretation was that this reflected mixing between a more or less pure ^{16}O component, such as might be created by helium burning, injected into the solar nebula by a red giant and a component of 'normal' isotopic composition. A decade later, experiments conducted by Thiemens and Heidenreich (1983) suggested a different interpretation. They found that ozone produced by a high frequency electric discharge showed "mass independent fractionation", i.e., where the ozone was equally enriched in ^{17}O and ^{18}O relative to ^{16}O. The experiment demonstrates that a slope of 1 on the $\delta^{17}O$ — $\delta^{18}O$ diagram could be produced by chemical processes. Thiemens suggested this kind of fractionation arises because non-symmetric (e.g., $^{16}O^{17}O$ or $^{18}O^{16}O$) molecules have more available energy levels than symmetric (e.g., $^{16}O^{16}O$) molecules (as we saw in Chapter 9, symmetry enters into the calculation of the partition function). Since then mass independent fractionation has been found in ozone of the Earth's atmosphere as well as in Archean sulfides and sulfates, so there is no question that it can occur in nature.

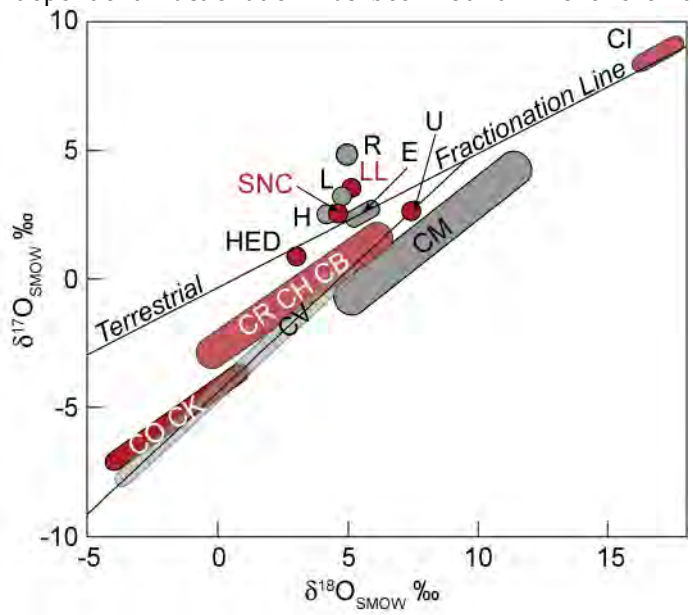

Figure 10.29. Variation of O isotope ratios in meteorites CO, CK, etc.: carbonaceous chondrites; H, L, LL: ordinary chondrites; HED: howardites, eucrites, diogenites; U: ureilites; SNC: Shergottiites, naklites, Chausigny; E: enstatite chondrites. The Earth, Moon, and aubrites have the same isotopic composition as enstatite chondrites. Modified from Clayton (2004).

A somewhat different idea was been proposed by Clayton (2002). He suggested that the anomalies arose through radiation self-shielding in the solar nebula. In his model, ultraviolet radiation from the early proto-Sun dissociated carbon monoxide, which would have been among the most abundant gases in the solar nebula. Because $C^{16}O$ rather than $C^{17}O$ or $C^{18}O$ was the dominant oxygen-bearing species, the radiation of the wavelength necessary to dissociate $C^{16}O$ would have been quickly absorbed as it traveled outward from the Sun. At greater distance from the Sun, radiation of the frequency necessary to dissociate $C^{16}O$

would have been absent, while that needed to dissociate $C^{17}O$ and $C^{18}O$ would still be available. Thus at these distances, $C^{17}O$ and $C^{18}O$ are preferentially dissociated, and equally so, making ^{17}O and ^{18}O preferentially available for reaction to form silicates and other meteorite components. Since the solar nebula would have been fairly opaque at this time, this isotopic fractionation would have occurred in the inner part of the nebula, near the forming star, and they expelled back out by the "X-wind". The implication of this is that most of the solid matter that makes up the Earth and it neighbors must have cycled through this inner region at one point. Clayton's model also predicts that the Sun itself should be poor in ^{18}O and ^{17}O compared to meteorites and the Earth – closer in composition to the CAI's. This prediction appears to have recently been confirmed based on analysis of solar wind implanted in lunar soil.

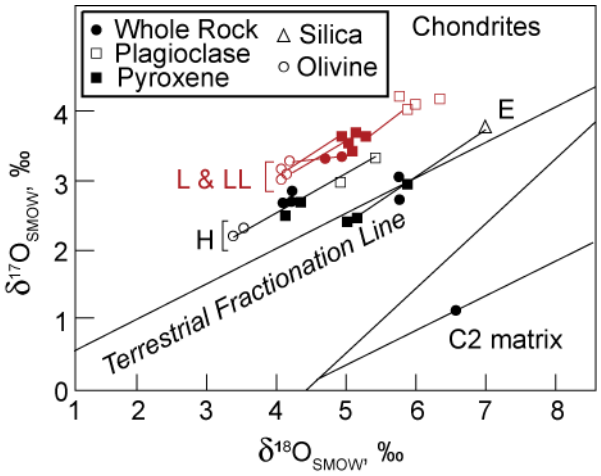

Figure 10.30. O isotope variation among minerals of various meteorite classes (Clayton et al., 1976).

As Figure 10.30 shows, while variations *between* classes are mostly mass-independent, variations *within* groups of meteorites fall along mass-dependent fractionation lines. This strongly suggests that, for the most part, different groups could not have come from the same parent body and that the different groups probably formed in different parts of the presolar nebula. There are a few exceptions: IIE irons fall on a mass-dependent fractionation line (MDFL) with H-chondrites, IVA irons plot on a MDFL with L and LL chondrites, basaltic and hypersthene achondrites plot on a MDFL with IAB irons and some stony-irons. This suggests a genetic relationship between these objects, perhaps derivation from a single a single parent body. The Moon and the Earth plot on a single MDFL, evidence of their close genetic relationship. Intriguingly, the enstatite chondrites also plot along the terrestrial fractionation line. This has led some to suggest that enstatite chondrites might be a better compositional model for the Earth than either carbonaceous or ordinary chondrites.

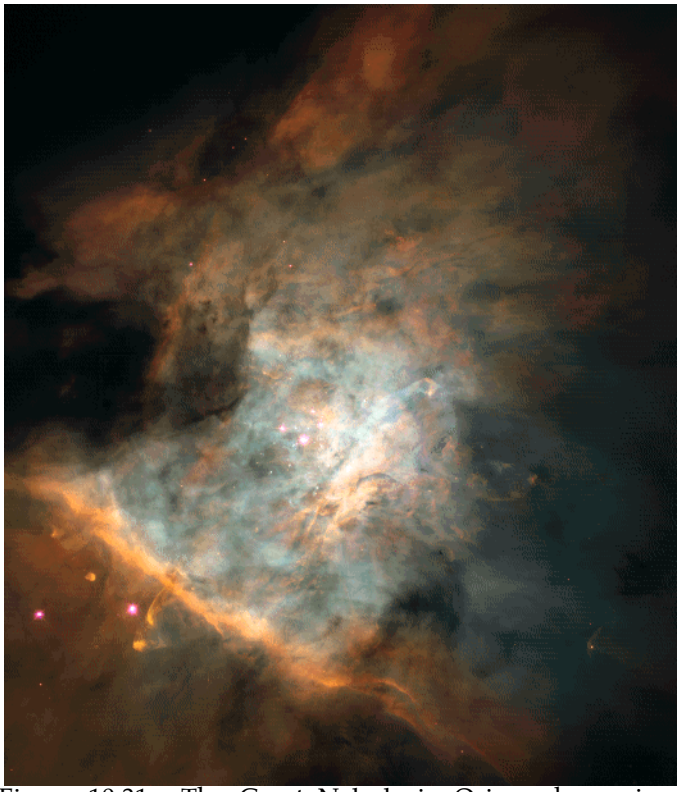

Figure 10.31. The Great Nebula in Orion, shown in a Hubble Space Telescope photograph, is cloud of gas and dust within which stars are forming. Credit: NASA.

10.5 ASTRONOMICAL AND THEORETICAL CONSTRAINTS ON SOLAR SYSTEM FORMATION

As the preceding sections show, meteorites provide some tremendous insights into the formation of our solar system. However, before we try to use these observations to draw some conclusions about how the solar system, and the Earth, formed, we need to consider several other sets of observations. The first of these is astronomical observations of star formation occur-

ring elsewhere in the universe. As it turns out, star formation is more or less an everyday event in the universe and we can watch it happening. The second is theoretical considerations of how solids condense from a hot gas of solar composition. We have seen that meteorites provide evidence for at least transient high temperatures in the early solar system. What can we expect when hot gas cools? We can use thermodynamics to find the answer. Finally, any theory of solar system formation must successfully predict the solar system as it exists. Consequently, we'll briefly review the nature of our solar system.

10.5.1 Evolution of Young Stellar Objects

Astronomical observations have established that stars form when fragments of large molecular clouds collapse, as is occurring in the Great Nebula in Orion (Fig. 10.31). Such clouds may have dimensions in excess of 10^6 AU‡ and masses greater than 10^6 $M_\odot$ (solar masses). Typically, about 1% of the mass of these clouds consists of submicron-sized dust, about 1% is gaseous molecules heavier than He, and the remainder is H_2 and He gas. Gravity will tend to make such clouds collapse upon themselves. This tendency may be resisted by thermal motion that tends to expand the cloud, rotational motion that stabilizes it against collapse, and internal pressures generated by turbulence. More recent observations reveal that magnetic fields, which couple to the ionized fraction of the gas, play a key role in stabilizing these clouds. A careful balance between the forces tending to collapse the cloud and forces tending to expand it can result in the cloud being stable indefinitely. Collapse of a part of a nebular can occur through the removal of a supporting force, magnetic fields in particular, or by an increase in an external force, such as a passing shock wave.

In addition to random density perturbations that can spontaneously collapse, shock waves could trigger cloud collapse and star formation. Once potential source of shock is supernovae. Another is the density waves which manifest themselves as the spiral arms of the galaxies. We can think of the galactic arms as being similar to a traffic jam on the galactic orbital freeway. Though traffic continues to flow through the region of the traffic jam, there is nevertheless a sort of self-perpetuating high concentration of stars in the traffic jam itself. As clouds are pulled into the arms, they are compressed by collisions with other matter in the arms, leading to collapse of the clouds and initiation of star formation.

The Taurus-Auriga cloud complex is a good example of a region in which low mass stars similar to the Sun are currently forming. The cloud is about 6×10^5 AU across, has a mass of roughly 10^4 $M_\odot$, a density of 10^2–10^3 atoms/cm^3, and a temperature around 10 K. Embedded within the cloud are clumps of gas and dust with densities 2 orders of magnitude higher than the surrounding cloud. Within some of these clumps are luminous protostars. About 100 stars with mass in the range of 0.2-3 $M_\odot$ have been formed in this cloud in the past few million years.

As the cloud collapses, it will warm adiabatically, resulting in thermal pressure that opposes collapse. Magnetic fields inherited from the larger nebula will intensify as the system contracts, and can accelerate charged particles away from the forming star. Further intensification of the magnetic field occurs as an increasing fraction of the material ionizes as temperature increases. Finally, even small amounts of net angular momentum inherited from the larger nebula will cause the system to spin at an increasing rate as it contracts. For a cloud to collapse and create an isolated star, it must rid itself of over 99% of its angular momentum in the process of collapse. Otherwise the resulting centrifugal force will break up the star before it can form. Much of what occurs during early stellar evolution reflects the interplay between these factors.

Protostellar evolution of moderate-sized stars (i.e. stars similar to the Sun) can be divided into 6 phases, labeled –I, 0, I, II, and III, based on the spectra of their electromagnetic emission (Lada and Shu, 1990; Boss, 2005). The first phase, the –I phase, is the initial collapse of a molecular cloud to form a protostellar core and nebular disk. No astronomical examples of this phase have been found, so understanding this phase depends entirely on theoretical calculations. Model calculations show that once a cloud fragment or clump becomes unstable, supersonic inward motion develops and proceeds rapidly

‡ AU stands for Astronomical Unit, which is the Earth-Sun distance or 1.49×10^8 km.

as long as the cloud remains transparent and the energy released by gravitational collapse can be radiated away. Once the cloud becomes optically dense so that energy is no longer radiated away, the collapse slows. At this point, the protostellar core has a radius of about 10 AU and a mass of perhaps only 1% the final mass of the star. When temperatures in the core reach 2000 K energy is consumed in the dissociation of hydrogen, allowing further collapse and bringing the radius down to several times that of the eventual star. For a star of about 1 solar mass, the time scale is thought to be roughly 10^6 to 10^7 years. It is longer for smaller stars and shorter for larger ones.

For subsequent phases, observations at wavelengths ranging from radio waves to X-rays provide a wealth of information on protostellar objects and their nebulae. During phase 0, the protostar is deeply embedded in its surrounding cocoon of gas and dust and cannot be directly observed. At the beginning of the phase, the mass of the protostellar core is still very much smaller than that of the infalling envelope of gas and dust. In the meantime, angular momentum progressively flattens the envelope into a rotating disk, the stellar nebula. Material from surrounding envelope continues to accrete to the disk, but mass is also transferred from the disk to the protostellar core at a slow rate.

The object L1551 IRS5 in the constellation Taurus is considered the prototypical Class I object and detailed observations of it over the last decade have provided considerable insights into this stage of stellar evolution. Observations at radio wavelengths revealed there are actually two protostars about 45 AU apart with a combined mass of about 1 $M_\odot$ (binary stars are more common that individual stars such as the Sun). The protostars are deeply embedded in circumstellar disks that have diameters of about 20 AU. Because they are optically thick, temperatures in the interior of these disks cannot be determined directly. However, surface temperatures of the disks can be determined from the infrared spectra of these objects and they range from 50 to 400 K at 1 AU and drop off exponentially with distance. Models that reproduce these surface temperatures have disk interior temperatures that range from 200 to 1500 K at 1 AU and decrease exponentially with radial distance. The highest temperatures, which are enough to vaporize silicates, are likely short-lived and persist for only for a period of perhaps 10^5 yr during which accretion rates are highest. More moderate temperatures, in the range of 200-700 K, could persist in the inner part of the disk for substantially longer than this.

A very interesting feature of L1551 IRS5 and other Class I objects is strong "bipolar flows" or jets oriented perpendicular to the circumstellar disks that extent some 1000 AU from the disks. The jets consist of gas moving outwards at velocities 200-400 km/sec. Within these jets temperatures may locally reach 100,000 K. As the material in the jets collides with the interstellar medium it creates a shock wave that in turn generate X-rays. The physics that generates these jets is incompletely understood, but magnetic fields undoubtedly play a dominant role. In one theory, the X-wind model (Shu et al., 1997; Shang et al., 2000), the bipolar outflows are the cores of a much broader outflow that emerges from the innermost part of the circumstellar disk as it interacts with the strong magnetic field of the central protostar. As Shang et al. (2000) write, "in the X-wind model, the combination of strong magnetic fields and rapid rotation of the young star-disk system acts as an 'eggbeater' to whip out part of the material from the surrounding disk while allowing the rest to sink deeper in the bowl of the gravitational potential well." The jets and associated X-wind remove both mass and angular momentum from the system (Figure 10.32). The latter is particularly important, because as material is accreted from the disk to the star, conservation of angular momentum causes the star to rotate ever faster. Shang et al. (2000) estimate that about 1/3 of the mass accreted to the disk and a larger fraction of the angular momentum is carried away by the X-wind. If this angular momentum were not lost in some way, the resulting centrifugal force would break up the star.

Phase II is represented by so-called *Classical T-Tauri Stars*, of which the star T-Tauri (now known to be a binary pair) is the type example. During this phase, a visible star begins to emerge from its cocoon of gas and dust, but it remains surrounded by its circumstellar disk (Figure 10.33). The star has a cool surface (4000 K) but luminosity several times greater than mature stars of similar mass (Figure 10.01). The luminosity is due entirely to continued accretion and gravitational collapse – fusion has not yet ignited in its interior. A T-Tauri star of one solar mass would have a diameter still several times that of the Sun. X-ray bursts from these stars suggest a more active surface than that of mature stars, likely

driven by strong stellar magnetic fields and their interaction with the accretion disk. The surrounding disk is still warm enough to give off measurable IR radiation.

Accretion to the star continues in this phase, but has dropped to rates of 10^{-6} to 10^{-8} $M_\odot$ per year. The accretion continues to drive bipolar outflows and associated X-wind (Figure 10.32). Typical mass loss rates from the flows and winds are 10^{-8} $M_\odot$ per year. These winds may be important for a number of reasons. First, the mass loss is significant comparable to the inferred accretion and infall rates, meaning there may be little or no net accretion. Secondly, The outwardly blowing gas has the potential to flings solids outward to the cooler, more distant parts of the disk. In the process, solids are lifted above disk close to the star where are exposed to the intense radiation and are heated in the process.

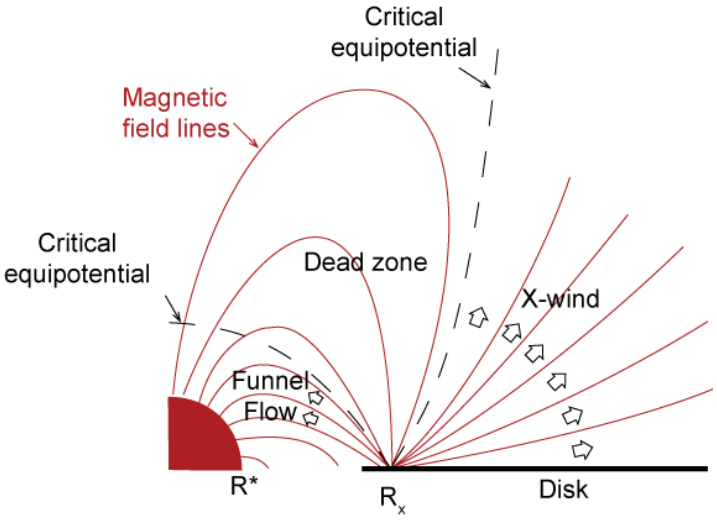

Figure 10.32. Cartoon illustrating the X-wind model. As a result of interaction with the accretion disk, the magnetic field lines of the young star truncate at radius R_x, which typically has a value of a few stellar radii. For disk material in stable orbit at R_x, two equipotential surfaces emerge from the disk, such that gravity dominates inward of the inner one and centrifugal force dominates outward of the outer one. Between these surfaces is a "dead zone" into which matter cannot freely flow. Thus matter swept off the disk surface by magnetic forces will either be pulled into the star in "funnel flow" or move away from the star as the "X-wind". After Shang et al. (2000).

Both Class I and II objects can go through occasional 'FU Orionis outbursts'. The name FU Orionis derived from a star in the Orion nebula that suddenly brightened by 6 magnitudes over 6 months in 1936. Its luminosity has been slowly decaying since then. During such an outburst, the disk outshines the central star by factors of 100–1000, and a powerful wind emerges, producing mass losses of 10^{-6} $M_\odot$ per year in the case of FU Orionis, some 4 orders of magnitude greater than in quiescent T-Tauri stars. These outbursts are thought be the result of greatly enhanced mass accretion rates, perhaps as high as 10^{-4} $M_\odot$ per year. The cause is unclear: thermal instability in the disk, changes in the structure of the disk, and the gravitations effects of a binary companion or a giant planet or protoplanet orbiting close to the star have all been suggested as causes of the enhanced mass accretion rate. The outbursts appear to last no more than a century. By the end of Phase II, the star is perhaps 2 to 6 million years old.

Phase III is represented by *Weak-Lined T-Tauri Stars*, so-called because spectral emission and absorption lines are much weaker than in classical T-Tauri stars. In addition, the excess infrared emission that characterizes classical T-Tauri stars is absent in weak-lined T-Tauri stars. The inference from these observations is that the disk has largely dissipated by this stage. Like classical T-Tauri stars, weak-lined T-Tauri stars are cooler yet more luminous than mature main sequence stars of similar mass, but less so. In other words, they are closer to the main sequence on the Hertzsprung-Russell diagram than classical T-Tauris.

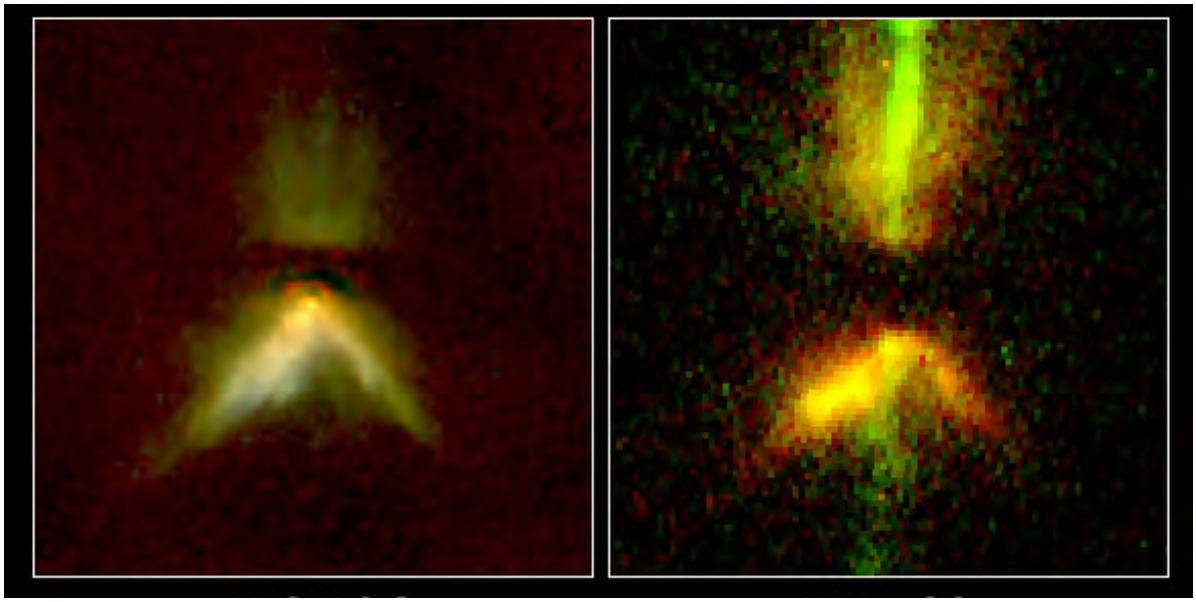

Figure 10.33. Two Hubble Space Telescope views of the T-Tauri star DG Tau B. Image on the left is taken with the Near Infrared Camera and Multi-Object Spectrometer, the image on the right is taken with the Wide Field Planetary Camera. The accretion disk is a dark horizontal band in both images. The bipolar outflows appear green in the visible image. Infrared interferometry indicates there is a gap of about 0.25 AU between the star and the inner edge of the disk, which extends out about 100 AU. Photo credit: NASA.

Weak-lined T-Tauris are particularly luminous in the X-ray part of the spectrum. These X-rays are thought to be produced in hot plasma during magnetic reconnection events above the stellar surface. The same process in the Sun produces bright solar flares, but flares of weak-lined T-Tauris are 100-1000 times more powerful. Outflows and winds subside to those of typical main sequence stars as accretion ends and the star reaches its final mass. During the weak-lined T-Tauri phase, the star contracts to its final radius and density. At the end of this process, fusion ignites in the core and the luminosity and temperature of the star settles onto the main sequence. The entire process from Phase 0 through Phase III consumes perhaps 10 million years.

10.5.2 The Condensation Sequence

In the preceding section, we saw young stellar objects and their surrounding disks are highly energetic and at least locally very hot environments. We learned earlier that chondrites contain a variety of components, chondrules, CAI's, and AOA's, that provide evidence of at least local and transient high temperatures as our solar system was born. It is thus useful to ask what the chemical effects of temperature are. For example, suppose we heated material of solar or chondritic composition to the point where everything evaporated. What would be the sequence of condensation? The theoretical condensation sequence has been calculated from thermodynamic data, largely by Larimer, Grossman, and Lewis, all of whom have worked with E. Anders at the University of Chicago (e.g., Larimer, 1967; Grossman, 1972). The condensation temperature of an element reflects its vapor pressure, its tendency to react with other elements to form compounds in the gas or solid solutions or alloys in the solid, and its abundance in the gas. Let's consider two examples of condensation sequence calculations. First, consider iron, which is a particularly simple case since it condenses as Fe metal:

$$Fe_{(g)} \rightarrow Fe_{(s)} \qquad 10.02$$

Assuming ideality, the partial pressure of iron is simply its mole fraction in the gas times the total pressure (P_T). Since hydrogen is by far the dominant element in the gas (~98%), the mole fraction can be ap-

proximated as 2 times the solar Fe/H ratio (the 2 arises from hydrogen's presence as H_2). Thus the partial pressure of Fe is written as:

$$p_{Fe} = \frac{[\text{Fe}]_\odot}{1/2[\text{H}]_\odot} P_T \qquad 10.03$$

where $[\text{Fe}]_\odot$ and $[\text{H}]_\odot$ are the solar abundances of Fe and H and P_T is total pressure. Once condensation begins, we can express the equilibrium constant for this reaction as the ratio of the partial pressure of Fe in the gas to the concentration in the solid:

$$\text{K} = \frac{p_{Fe}}{[\text{Fe}]_s} \qquad 10.04$$

where $[\text{Fe}]_s$ is the concentration in the solid and p_{Fe} is the partial pressure in the gas.

Condensation begins when the partial pressure of Fe exceeds the equilibrium vapor pressure of solid Fe. Since:

$$\Delta G = -RT \ln K \qquad (3.86)$$

the equilibrium constant can also be written as:

$$-\ln K = -\frac{\Delta H_V}{RT} + \frac{\Delta S_V}{R} \qquad 10.05$$

ΔH_V and ΔS_V are the enthalpy and entropy of vaporization. Once condensation of an element begins, its partial pressure drops by $(1 - \alpha)$ where α is the fraction condensed. Hence, equation 10.03 becomes:

$$p_{Fe} = \frac{(1-\alpha)[Fe]_\odot}{1/2[H]_\odot} P_T \qquad 10.06$$

Combining 10.04, 10.05, and 10.06, the equation describing condensation is:

$$\ln(\alpha - 1) = -\frac{\Delta H_V}{RT} + \frac{\Delta S}{R} - \ln\frac{[Fe]_\odot}{1/2[H]_\odot} - \ln P_T + \ln[Fe]_s \qquad 10.07$$

Now consider elements such as Mg and Si, which form compounds in both the gas and solid, which complicate the calculation considerably. The reaction for the condensation of forsterite is:

$$\text{Mg}_{(g)} + \text{SiO}_{(g)} + 3\text{H}_2\text{O} \rightarrow \text{Mg}_2\text{SiO}_{4(s)} + 3\text{H}_2 \qquad 10.08$$

The equilibrium constant for this reaction is:

$$\text{K} = \frac{a_{Mg_2SiO_4} p_{H_2}^3}{p_{Mg}^2 p_{SiO} p_{H_2O}^3 P_T^3} \qquad 10.09$$

The first step is to compute partial pressures of the gaseous species. For example, for SiO and H_2O above, we may write reactions:

$$2\text{H} + \text{O} \rightleftarrows \text{H}_2\text{O} \qquad \text{and} \qquad \text{Si} + \text{O} \rightleftarrows \text{SiO}$$

and calculate equilibrium constants for them from the free energies of these species, e.g.:

$$\text{K} = \frac{p_{SiO}}{p_{Si} p_O} \qquad 10.10$$

Values of K can be computed from thermodynamic data. For each element, an additional constraint is imposed by the total abundance of that element in the gas. Thus for example:

$$[\text{SiS}] + [\text{Si}] + [\text{SiO}] + [\text{SiO}_2] = [\text{Si}]_\odot - [\text{Si}]_s \qquad 10.11$$

where $[\text{Si}]_s$ is the total of silicon in condensed phases. Combining equilibrium constant equations such as 10.10 with mass balance equations such as 10.11 leads to a series of simultaneous equations. These can be solved by successive approximation using a computer. These kinds of calculations were first done by Larimer (1967) and have since been refined by many workers (e.g., Grossman, 1972, Petraev

and Wood, 1998, Ebel and Grossman, 2000, and Grossman, 2010). Values of equilibrium constants such as 10.09 can then be computed from ΔH and ΔS using equation 10.05.

Further complications arise when solid solutions form. For example, the forsterite term in 10.08 is 1 if forsterite is treated as a pure phase. If the solid solution with fayalite is considered, then the value of the activity must also be calculated. Values for activity coefficients are difficult to obtain, and ideal solid solution is generally assumed. Thus the activity of forsterite in 10.09 would be replaced by its mole fraction. Solid solution results in the condensation of an element at a higher temperature than if a pure component were the condensed phase.

Some elements, such as Au and Cu, will condense primarily either by reaction with already condensed Fe metal grains, or by condensing with Fe metal. At lower temperatures (around 670 K for P_T = 10 Pa), the Fe metal will react with H_2S gas to form FeS. Moreover, from the onset of condensation a small but increasing amount of the Fe will react with H_2O gas to form FeO that dissolves in the silicates. A marked increase in the Fe content of silicates occurs around 400-500 K.

Figure 10.34 shows 2 theoretical sequences calculated by Larimer (1967). In the 'fast cooling' sequence, matter does not react with nebular gas after it has condensed – this is effectively fractional condensation, analogous to fractional crystallization. At any given time and temperature, the solid phases are a mixture of material condensed over a range of temperature. In the 'slow cooling' or "equilibrium" sequence, condensed material continually reacts and re-equilibrates with the gas as temperature drops, so that at any time, only an assemblage in equilibrium with the gas at that temperature is present. Figure 10.35 illustrates the minerals expected at a given temperature somewhat more clearly. The condensation sequence depends critically on total pressure and H pressure; the sequence shown is for relatively low total and H pressure. At relatively high pressure, metallic Fe liquid is the first phase to condense.

In a nutshell, the sequence goes like this (Figure 10.35). The first elements to condense would be Re and the most refractory of the platinoid metals (Os, Ir, Ru), which would condense as metallic phases. Since these are extremely rare elements, they would likely form very small grains. As we noted earlier, small nuggets of such metal, called "Fremdlinge" (the German word for "strangers"), are found as inclusions in CAI's. Following this would be condensation of oxides and silicates of Ca, Al and Ti. They should be rich in refractory trace elements such as U, Th, Zr, Ba and the REE. This closely matches the

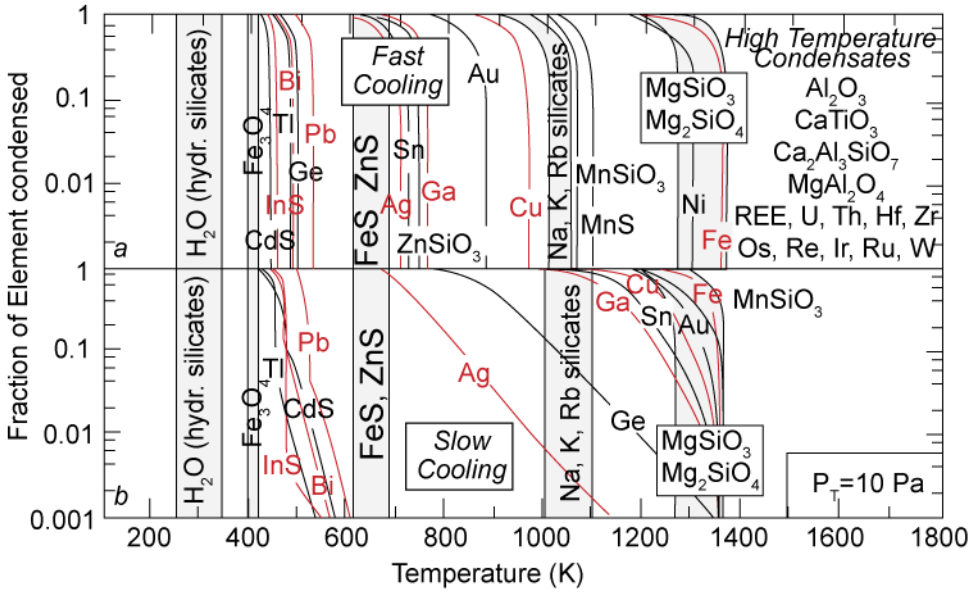

Figure 10.34. Condensation sequence of a gas with solar composition. In slow cooling, condensed solids are assumed to continually re-equilibrate with the gas. Fast cooling leads to disequilibrium and condensation of pure elements and compounds. Black lines show condensation of silicates and oxides; red lines show condensation of metals and sulfides. After Larimer (1967).

composition of the CAI's, suggesting the possibility that CAI's are high temperature condensates.

Next in the condensation sequence should come metallic Fe-Ni and compounds richer in the moderately refractory elements such as Mg and Si: olivines and pyroxenes. If the cooling takes place under equilibrium conditions the high temperature (CAI) assemblage should react to form anorthite as well, and at lower temperature when Na condenses, plagioclase. These phases are the ones that predominate in chondrules, with the important caveat that chondrules are poorer in metal than the condensation sequence would predict. Since these phases condense at temperatures similar to Fe-Ni metal, some process must have separated metal from silicates before formation of the chondrules.

The Fe should also largely react out to form more Fe-rich olivine and pyroxene. At lower temperature, S condenses and reacts with Fe to form sulfides. At even lower temperature, the Fe reacts with O to form magnetite and the silicates react with water vapor to form hydrated silicates. Sulfates, carbonates and organic compounds will also form around these temperatures.

If equilibrium conditions prevail, only the last named compounds would exist when condensation was complete, but all might exist if disequilibrium prevails. The CI chondrites seem to be very similar in composition and petrography to equilibrium condensates (down to 300 K or so), or, more accurately, accretions of equilibrium condensates. The other carbonaceous chondrites approximate to varying degrees aggregates of disequilibrium condensates. In particular, the CV and CO's chondrites contain both the highest temperature condensates (CAI's) and lowest temperature material (hydrated silicates) and much of everything expected to condense in between. CV and CO chondrites are depleted in the more volatile elements and compounds (such as water, but also the moderately volatiles such as Ga and Ge, alkalis).

10.5.3 The Solar System

The solar system consists of a central star, the Sun, and a variety of bodies that orbit it. These are somewhat arbitrarily divided into planets, asteroids, comets, Kuiper Belt objects, etc. Table 10.5 lists some data regarding the planets. The planets can be divided into three groups based on their size, density and composition. These are:

- The terrestrial planets:
  Mercury
  Venus
  Earth-Moon
  Mars
  (asteroids)
- The gas giants:
  Jupiter
  Saturn
- The outer icy planets:
  Uranus
  Neptune

Seven of the 8 planets have orbits that fall on a single plane, ±3°. The same 7 have nearly circular orbits, with eccentricities all less than 0.1. Mercury's orbit is in-

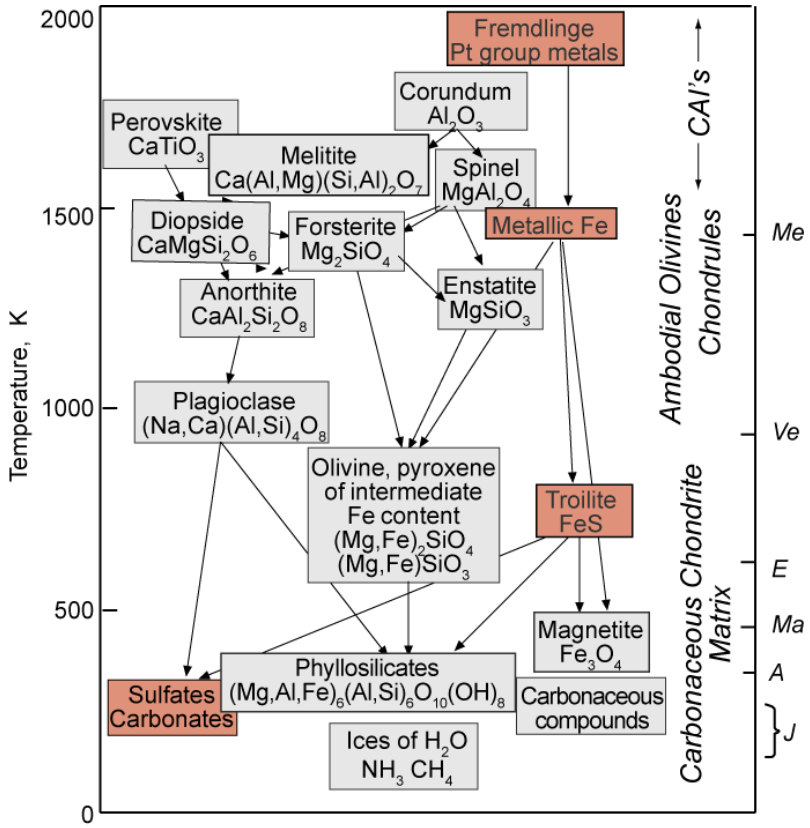

Figure 10.35. Simplified mineralogical condensation sequence.

clined some 7° with an eccentricity of 0.2. (Pluto's orbit is inclined 17° and has an eccentricity of 0.25; this highly anomalous orbit is one reason it is no longer considered a planet). Most major satellites of the planets also orbit in nearly the same plane. The Sun's equator is inclined some 7° to this plane. Thus the angular momentum vectors of major solar system objects are all rather similar, consistent with formation from a single rotating nebula. Rotational vectors of planets are generally inclined to their rotational vectors, some highly so, and Venus and Neptune have retrograde rotations (as does Pluto).

The definition of "planet" is somewhat open to debate. The asteroids have long been known to stably orbit the Sun, but are not considered planets. More than 100,000 asteroids are known and there may be millions. The largest is Ceres, discovered in 1801, which has a diameter of 950 km and a mass of 9.5×10^{20} kg. Pluto, once considered the 9th planet, is more than an order of magnitude smaller than Mercury and smaller than some of the major satellites of Jupiter, Saturn, and Neptune, and has a very anomalous orbit. It is more correctly considered a Kuiper Belt object. The Kuiper Belt, which lies between 30 to 50 AU from the Sun, is a great ring of debris, similar to the asteroid belt but of much lower density material – presumably dominated by hydrocarbons and ices of H_2O, CH_4, and NH_3 with lesser amounts of silicates, etc. This region is thought to be the place of origin for short-period comets. There are estimated to be over 70,000 Kuiper belt objects with a diameter greater than 100 km, with a total mass similar to that of the Earth. In the last several years 5 new Kuiper Belt objects have been discovered that rival Pluto in size. *Eris*, discovered in 2003, with a radius of 1200 km, is the largest of these and is larger than Pluto. It has an elliptical orbit with semi-major axis of 68 AU, and has a moon of its own: *Dysnomia*. Sedna, also discovered in 2003, is the most distant. It has a mass, density, and radius in between those of Pluto and Chiron and a highly elliptical orbit with a semi-major axis of 937 AU. Sedna is distinctly red in color, possibly due to a surface composed of hydrocarbon sludge.

Finally, the Oort Cloud is a region from 50,000 to 100,000 AU where long-period comets are thought to originate. Comets appear to be low-density icy dust balls. Based on spectral analysis of ejecta from Comet Tempel 1 produced by NASA's Deep Impact mission, they appear to consist principally of water ice, HCN, a variety of hydrocarbons including polycyclic aromatic hydrocarbons, amorphous carbon,

Table 10.05. Data Regarding the Sun, the Planets, and Their Major Satellites

	Mass (kg)	radial distance (AU)	radius (km)	density (g/cc)	1 atm density (g/cc)	Principal atmospheric components
Sun	1.99×10^{30}		6.96×10^{5}	1.4		
Mercury	3.35×10^{23}	0.39	2.44×10^{3}	5.42	5.3	—
Venus	4.87×10^{24}	0.72	6.05×10^{3}	5.24	3.95	CO_2, N_2, Ar
Earth	5.98×10^{24}	1.0	6.38×10^{3}	5.52	4.03	N_2, O_2, Ar
Moon	7.35×10^{22}		1.74×10^{3}	3.3	3.4	—
Mars	6.42×10^{23}	1.6	3.39×10^{3}	3.93	3.7	CO_2, N_2, Ar
asteroids	4×10^{21}	2.8	$\leq10^{3}$		3.4-3.9†	
Jupiter	1.90×10^{27}	5.2	6.99×10^{4}	1.31		H, He
Io	8.63×10^{22}		1.82×10^{3}	3.42		—
Europa	4.71×10^{22}		1.55×10^{3}	3.03		—
Ganymede	1.51×10^{23}		2.63×10^{3}	1.98		—
Callisto	1.06×10^{23}		2.40×10^{3}	1.83		—
Saturn	5.69×10^{26}	9.6	5.95×10^{4}	0.69		H, He
Titan	1.38×10^{23}		2.58×10^{3}	1.88		N_2, CH_4
Uranus	8.73×10^{25}	19.1	2.54×10^{4}	1.30		H, He, CH_4
Neptune	1.03×10^{26}	30.8	2.13×10^{4}	1.76		H, He, CH_4
Triton	2.14×10^{22} (?)		1.35×10^{3}	2.08		—

†*Densities of anhydrous chondrites*

silicates, including olivine and pyroxene, spinel, carbonates, and hydrated silicates. While most comets are quite small, a few km to 10's of km in diameter, it is estimated that the total mass of the Oort cloud is between 5 and 100 Earth masses (M_E).

The terrestrial planets all consist of silicate mantles surrounding Fe-Ni metal cores and thin atmospheres that are highly depleted in H and He compared to the Sun. The gas giants Jupiter and Saturn are much more similar in composition to the Sun. The atmosphere of Jupiter is 81% H and 18% He by mass (compared to 71% and 28%, respectively, for the Sun), with CH_4 and NH_3 making up much of the rest. Saturn's atmosphere consists of 88% H and 11% He. The He depletion of both these atmospheres relative to the solar composition reflects a concentration of He in the interior. On the whole, the H/He ratio of Jupiter is close to the solar value. Elements heavier than He are about 5 times enriched in Jupiter compared to the Sun. The H/He ratio of Saturn as a whole is about a factor of 3 lower than the solar one and elements heavier than He are roughly 15 times enriched compared to the Sun. The nature of these planets' interiors is not entirely certain. Jupiter probably has a core consisting of liquid or solid metal and silicates with a mass roughly 15 times that of the Earth. Saturn probably has a similar core with a mass 100 times that of the Earth. Surrounding the core are layers of liquid metallic H and ordinary liquid H, both containing dissolved He. The icy planets consist of outer gaseous shells composed of H and He in roughly solar ratio with a few percent CH_4 surrounding mantles consisting of liquid H_2O, CH_4, H_2S, NH_3, H, and He and finally liquid silicate-metal cores. Elements heavier than He are about 300 times enriched in Neptune and Uranus compared to the Sun. In a gross way, this compositional pattern is consistent with a radial decrease in nebular temperature: the terrestrial planets are strongly depleted in the highly volatile elements (e.g., H, He, N, C) and somewhat depleted in moderately volatile elements (e.g., K, Pb). From what can be judged from reflectance spectra, the asteroids also fit this pattern: the inner asteroids (sunward of 2.7 AU) are predominantly igneous and compositionally similar to the achondrites, which are highly depleted in volatile and moderately volatile elements. The outer asteroids (beyond 3.4 AU) are richer in volatile elements and appear to be similar to carbonaceous chondrites.

The planet that we know the most about (other than Earth) is Mars. Observations on Mars and its composition come from (1) a variety of space craft orbiting Mars (as of 2011 there were 3 active) making spectroscopic measurements, (2) a variety of landers equipped with instruments capable of analyzing rocks and soil (to date there have been 6 successful landers), and (3) the SNC meteorites (of which there are 4 falls and 22 finds). This has enabled the achievement of a vague understanding of the composition and history of Mars. Comparing the volatile inventory of Mars with that of Earth, Mars at first appears depleted in volatile elements. It has a much smaller atmosphere than the Earth (surface pressures are 0.006 atm). Like Venus, the Martian atmosphere is dominated by CO_2, with N_2 as the second most abundant component. However, it is now clear from orbiter and surface observations that significant amounts of liquid water existed on the Martian surface during at least its first billion years or so and there is evidence of some small ephemeral stream at present. To attain the necessary temperatures, Mars would mast have had CO_2 pressures at its surface of 5 to 10 atm. This early atmosphere has been lost, a consequence of several factors, including lower gravity and the lack of a geomagnetic field that serves to prevent erosion of the atmosphere by the solar wind. Thus the depletion of highly volatile elements on Mars may be partly a secondary feature. Nevertheless, Dreibus and Wänke (1987) estimated the water content of the Martian mantle to be an order of magnitude or so lower than that of the Earth. It is possible that Mars lost a larger fraction of the highly volatile elements during accretion than did the Earth.

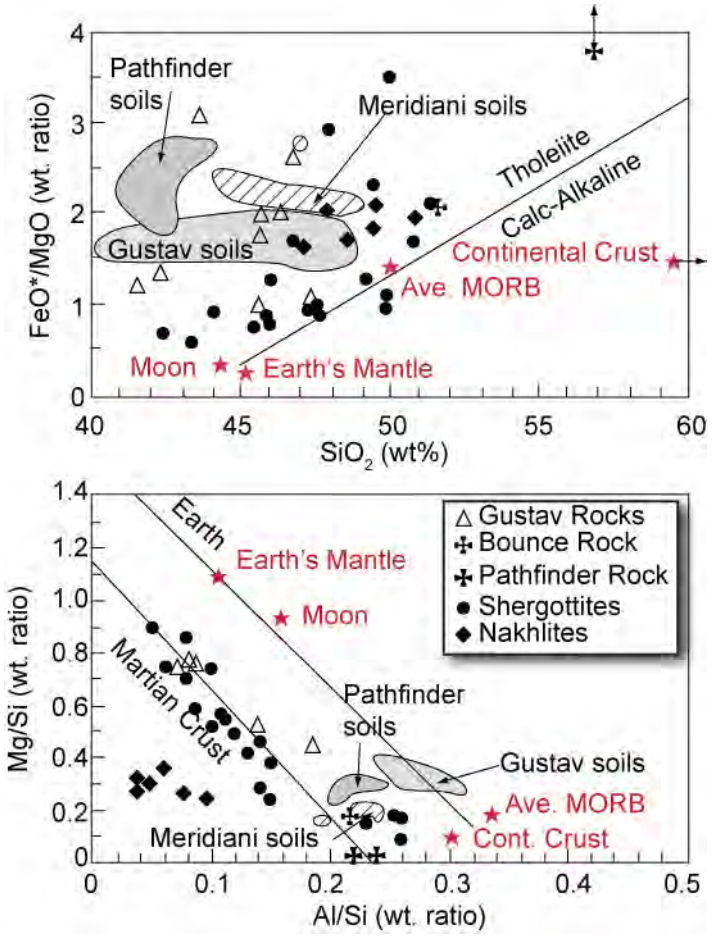

Figure 10.36. Major element chemistry of Martian meteorites and rocks and soils analyzed by NASA Martian landers. Mars appears to have a lower Al/Si ratio and a higher Fe/Mg ratio than the Earth. Modified from McSween et al. (2009).

Like the Earth, Mars has an iron core, but it appears to comprise a smaller fraction of planetary mass than Earth's. The Martian core has a diameter of 1400-1700 km and is about 15-20% of the mass of the planet. By comparison, the Earth's core is 32% of the mass of the planet. The smaller core appears to translate in to a more iron-rich Martian crust and mantle and is likely due to accretion of Mars under more oxidizing conditions than the Earth, resulting in a lower $Fe_{metal}/Fe_{silicate}$ ratio. Both SNC meteorites and lavas analyzed by the NASA rovers are richer in Fe than comparable terrestrial basalts (Figure 10.36). Surface rocks on Mars are dominantly tholeiitic basalts formed by extensive partial melting; more differentiated rocks such as andesites and granites are uncommon or absent.

There is evidence that Mars in richer in moderately volatile elements than the Earth. Analyses of both Martian soil and the composition of SNC meteorites suggest a K/U ratio about 19,000, whereas this ratio is about 13,800 in the Earth. The significance of this ratio is that U is a highly refractory element while K is a moderately volatile one. Sr-Nd isotope systematics of SNC meteorites appear to define an array shifted to higher $^{87}Sr/^{86}Sr$ ratios compared with that of the Earth, implying Mars has a Rb/Sr ratio of about 0.07 compared to 0.03 for the Earth (Taylor, 1992). Pb isotope ratios of these meteorites indicate a $^{238}U/^{204}Pb$ ratio of about 5 for Mars, compared with the terrestrial value of ~8.5. These ratios are consistent with the higher K/U of Mars, since Rb and Pb are both moderately volatile elements while Sr is a refractory one. Thus Martian moderately volatile/refractory element ratios appear to be systematically higher than terrestrial ratios.

The comparison of Venus with the Earth is particularly interesting, although we know considerably less about Venus than Mars. What we do know is based on gamma ray spectroscopy and analyses of the Venetian atmosphere by spacecraft. Although the two planets are of similar size, the Venetian atmosphere is almost 100 times more massive than that of the Earth. Whereas the Venus's atmosphere is dominated by CO_2, that of the Earth is dominated by N_2 and O_2. However, the differences in both atmospheric mass and the abundance of CO_2 may reflect the difference in geological and, particularly, biological processes, on the two planets. Both planets appear to have similar relative abundances of carbon and nitrogen (Prinn and Fegley, 1989). In the case of the Earth, however, most of the surficial

carbon is locked up in carbonates and organic carbon in rocks. This is in part due to biological activity, as is the presence of O_2 in the terrestrial atmosphere. There are, however, other differences that are more fundamental. The Venetian atmosphere is richer in noble gases than is the terrestrial one. Furthermore, the $^{40}Ar/^{36}Ar$ ratio of the Venetian atmosphere is about 1.15, whereas that of Earth is about 300. Since ^{40}Ar is produced by radioactive decay, it is related to the planetary K/Ar ratio. The terrestrial $^{40}Ar/^{36}Ar$ is high because the Earth captured relatively little primordial Ar; most of the Ar in the terrestrial atmosphere has been produced by decay of ^{40}K. Apparently, Venus captured much more primordial Ar and has a much lower K/Ar ratio than the Earth.

Although the Earth is depleted in noble gases relative to Venus, it appears to be richer in H_2O (Prinn and Fegley, 1989). Furthermore, the Earth and Venus appear to have similar K/U ratios, implying similar depletions in the moderately volatile elements (Taylor, 1991).

Thus in detail, we find the compositional differences between planets cannot simply be explained by radially decreasing temperature. The noble gas-rich nature of Venus is just one example. Another example is Mercury. Considering its density, Mercury appears to be much richer in iron than the other terrestrial planets, which is difficult to explain as simply a temperature effect since Fe condenses a the same temperature as Mg silicates (Fig 10.33 and 10.34). In the outer Solar System, we find that although Uranus and Neptune are further from the Sun, they are poorer in H and He than Saturn and Jupiter.

10.5.4 Other Solar Systems

As of 2011, 716 confirmed planets had been discovered orbiting other stars and several thousand more were suspected but not yet confirmed. Multiple planets occur in about 15% of the cases and as many as 5 planets have been found orbiting a single star. For stars having Fe/H ratios comparable to or greater than that of the Sun, planets have been found in about 15% of stars. The first extrasolar planets, or "exoplanets" to be discovered were found by detecting the "wobble" or their stars spectroscopically: an orbiting planet exerts a gravitational pull on the star and the resulting velocity changes produces a Doppler shift in the light emitted by the star. To date, most exoplanets have been discovered by this method, which is most likely to detect large planets orbiting near the star. Subsequently, a variety of space telescopes have detected planets by direct imaging, infrared imaging, and occultation (dimming of the light of the star as a planet transits in front of it). The most promising mission is NASA's Kepler Space telescope, which uses the transit method to detect candidate planets and has detected 33 confirmed planets and thousands of candidates in its first two years, including two planets comparable in size to the Earth and Venus. Nevertheless, the range of sizes and orbital radii of known planets represents a highly skewed sample of all exoplanets. Consequently, at this point we can draw only a few conclusions from the discovery of exoplanets. First, they are not rare; second, unlike our own solar system, large planets can be present quite near the star. Thus planets and solar systems may be a normal consequence of star formation, but the distribution of planents in our solar system is not necessarily typical. Finally, planets are generally substantially smaller than their central stars; they are not merely undersized companions. This latter observation suggests planets form in a fundamentally different way than stars and isolated brown dwarfs.

10.6 BUILDING A HABITABLE SOLAR SYSTEM

We have now examined star and solar system formation from several perspectives: observations about the planets of own solar system, observations conditions in the early solar system derived from meteorites, observations about stars presently forming elsewhere in the galaxy, and attempts to reproduce processes and conditions, in both laboratory or mathematical and computer simulations. Let's first review how these observations constrain the process of formation of *our* solar system 4.56 billion years ago, and then try to deduce what actually happened back then.

10.6.1 Summary of Observations

The planets in our solar system show a very strong compositional zonation. The 4 inner planets are strongly depleted in volatile elements, with some suggestion of increasing depletion inward. The two

giant planets have compositions close to that of the Sun, indicating they formed from a nebula that had experienced little chemical fractionation. The outer icy planets appear slightly depleted in the most volatile elements (H and He), but are much more volatile-rich that the terrestrial planets.

Chondrites can be viewed as mixtures of 4 principal components: CAI's, chondrules, amoeboid olivine aggregates (AOA's), and matrix. The CAI's consist of highly refractory material, very similar in composition to what we would expect if chondritic dust were heated to the point where 95% of it evaporated, or, conversely, the first 5% of a gas of chondritic composition condensed. In either case, minimum *sustained* temperatures of ~1700 K are required (assuming pressures of around 10 Pa). AOA's appear to have condensed from a gas at only slightly lower temperatures. Chondrules also provide evidence of high temperatures but in these cases, peak temperatures must have been of short duration. Finally, chondritic groundmass material includes a variety of materials of which the most significant is presolar grains – ejecta of red giants and supernova. The grains have escaped nebular processing. While most such grains (e.g., graphite, SiC, diamond) are inherently refractory and hence would not necessarily be destroyed by high temperatures, these grains retain significant quantities of noble gases, suggesting they never experienced substantial heating.

Variations in the chemical composition of chondrites clearly indicate chemical inhomogeneities within the solar nebula. Much of this is clearly related to volatility, implying significant variation in temperature in space and/or time in the nebula. Other variations relate to oxygen fugacity. Since H_2 is the principal reductant and it dominates the gas, while O constitutes a significant fraction of condensed matter, variation in oxygen fugacity most likely reflects variation in the ratio of gas to dust. In addition, there must have been significant variations in the metal/silicate ratio within the nebula to explain chondritic variations.

Planetesimals that were the parent bodies of achondrites and irons underwent sufficient heating to melt and differentiate. The oldest achondrites are do not appear to be significantly younger than many chondrites. Thus planetesimals formed, melted, and differentiated within a few million years, at most, of the formation of chondrites.

We can also draw a number of conclusions from the isotopic compositions of meteorites. First, the isotopic composition of most elements in most meteorites and meteorite components is uniform. This contrasts to the isotopic heterogeneity of presolar solar grains preserved in some chondrites. From this we may conclude that, at least at radii less than or equal to that of the asteroid belt, the solar nebula was well mixed and extensively processed. Some isotopic variation is indicative of the presence of short-lived radionuclides when the solar system formed. Most were most likely produced in red giants or supernovae and injected into the molecular cloud that ultimately formed the Solar System during or very shortly before its collapse. Other radionuclides, ^{10}Be in particular, were likely produced by spallation, perhaps by from energetic particles produced by the young Sun itself. Decay of these radionuclides, as well as conventional dating, suggests the time scale for nebular processing and planet formation was a few million to a few tens of millions of years.

10.6.2 Formation of Chondrite Components

Chondrites are a mix of materials formed under different conditions in different environments. With some understanding of the star-forming process, we can begin to discern what these environments were, as illustrated in Figure 10.37.

As we found in section 10.4.1m CAI's were the first formed solids in our solar system. They represent material that condensed at temperatures of 1700 K or so. Many were subsequently reheated and subjected to partial melting and evaporative loss. The ages of such "processed" CAI are indistinguishable from apparently "primary" CAI's, suggests the period of their formation was short, perhaps 50,000 years. They likely formed within 1 AU of the Sun as it transitioned from a Class I to Class II young stellar object.

Initial ^{26}Al/^{27}Al Al in at least some amoeboid olivine aggregates are as high as in CAI's, suggesting they formed around the same time. They condensed from somewhat cooler nebular gas (~1400 K) than the CAI's.

Pb-Pb and extinct radionuclide dating indicates that chondrules formed 1-2 million years later than CAI's (and CB chondrules may have formed 4 to 6 million years later than CAI's) when the Sun had evolved to become a classical T-Tauri (class II) or weak-lined T-Tauri (class III) star. Heating experienced by chondrules was even more transient, lasting minutes to hours. This kind of transient thermal event matches well that expected for shock waves within the solar nebula (Desch and Connolly, 2002). The rapid cooling experienced by chondrules suggests ambient temperatures were low, perhaps 300 K. Overall, the conditions are consistent with those expected in the asteroid belt. Since chondrules make up much of the mass of primitive meteorites, we can infer that a very significant fraction of the solid matter in the inner solar system was processed in this way.

Finally, the chondrite matrix represents material that condensed over a range of temperatures, including quite low ones, possibly at a variety of radial distances or at a variety of times as the nebula cooled. In addition, solid grains in the matrix reacted with nebular gas at low temperature. Subsequent reactions occurred on the parent bodies between components that condensed over a range of temperature. The matrix also contains presolar grains that were incorporated into chondrites without significant processing in the solar nebula.

The compositional variation between chondrites classes can be partly explained by varying the proportion of these components. Variation in radial distance from the Sun and in vertical distance above

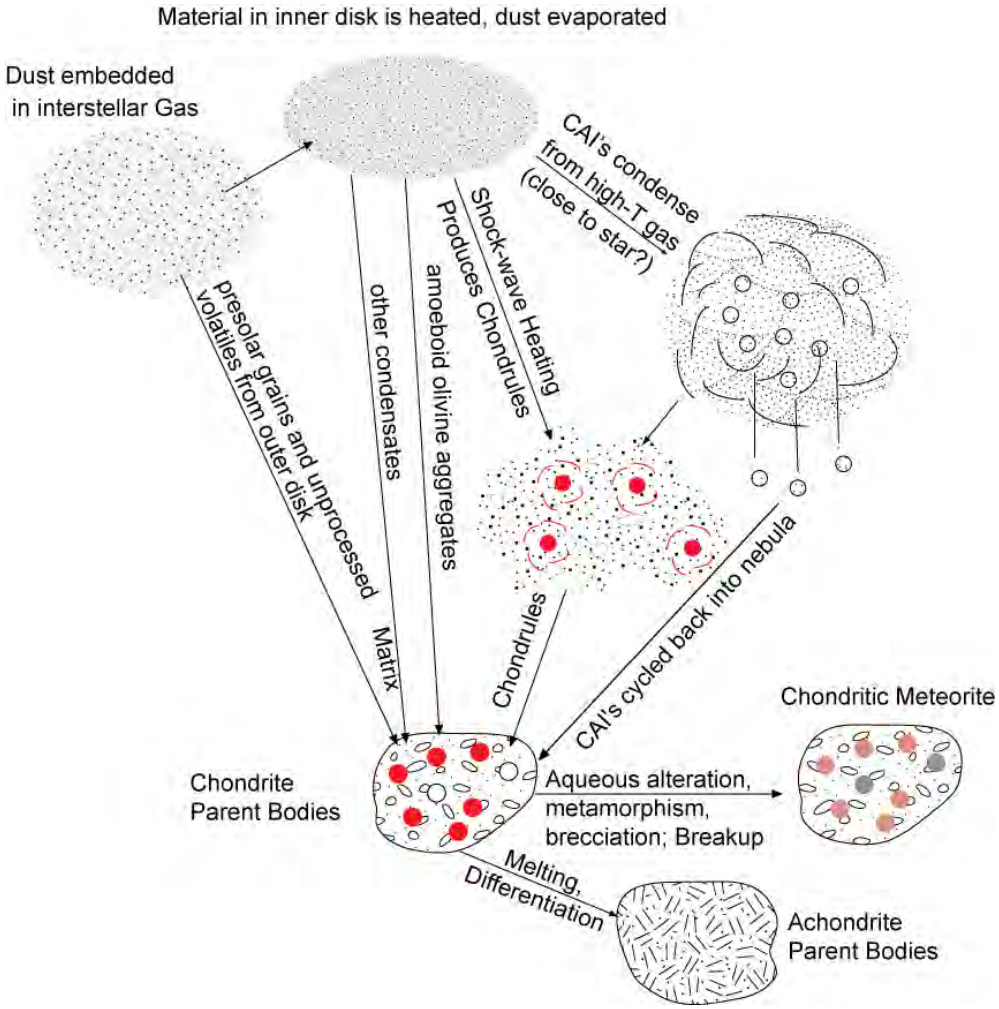

Figure 10.37. Cartoon illustrating the processes involved in the formation of chondrites and their components. Modified from McSween (1987).

or below the central plane helps to explain some of the remaining compositional variation. Gravity within the disk would tend to concentrate the dust component near the central plane of the disk; the gas to disk ratio would have increased vertically above and below the disk. This variation effectively controls the ratio of H to O, and therefore the oxygen fugacity. More oxidized components formed near the central plane, more reduced components formed some distance above or below it. Gravity, magnetic fields, gas drag, and other forces produced sorting between metal and non-metal grains, further enhancing compositional variation.

10.6.3 Formation of the Planets

Unlike star formation, there are few astronomical observations to guide theories of planet formation, possible planets have been imaged in very young stars still surrounded by nebular disks (e.g., Legrange et al., 2010). Hence current ideas on how the planet formed rest solely on theoretical modeling and observations of the present solar system: meteorites and the planets themselves.

Terrestrial planet formation can be divided into three stages: (1) dust condenses out of the hot nebular disk; (2) dust grains grow by accretion from micron-sized particles to planetesimals and protoplanets; (3) protoplanets grow into planets via long-term, long-distance, cumulative gravitational interactions.

As we saw earlier, observed surface temperatures of nebular disks imply that interior temperatures in the inner parts of these disks are hot enough to vaporize much of the dust. On time scales of a perhaps 10^5 years or so, the inner disk cooled to the point where the silicates and iron recondensed, but temperatures remained warm enough so that ices of water, methane, ammonia, etc. could not condense. At greater distances, the orbit of Jupiter and outward, the disk remained cool enough so that silicates and iron were never vaporized. More volatile compounds such as water might have been vaporized but they recondensed long before the nebula dissipated. The radial distance beyond which ice condenses, ~160 K at prevailing pressures, from the nebula is known as the "snowline". The snowline would have migrated inward as the nebula cooled.

In the inner solar system, the condensed dust comprised only about 0.5% of the mass of the nebula; in the outer solar system, the dust included ices and comprised 2% of the mass. Gravity caused the dust to quickly settle to the mid-plane of the nebula, so that it concentration there would be much higher (as we noted, the dust to gas ratio controlled oxygen fugacity – the mid-plane would have had higher oxygen fugacity). Van der Waals and electrostatic forces caused the dust grains to stick together and aggregate into "dust balls" (just the way dust in a house aggregates to form "dust bunnies"). In the inner solar system many of these dust balls were melted to form chondrules, probably by gas drag during shockwaves. Turbulence in the gas may have also concentrated the dust in eddies. Dust accumulation would have proceeded more rapidly in the outer, cooler parts of the solar system beyond "snow line". Nebular evolution models generally place the snow line between the asteroid belt and the orbit of Jupiter. Much of the water and other ices probably condensed on pre-existing dust particles. This has two effects: first, it enhances the overall concentration of solids, and second, it greatly increases the tendency of grains to stick to each other.

This process produces millimeter- to centimeter-sized particles, the size of CAI's and chondrules. How these particles grow into kilometer-sized blocks, where gravity begins to play a role, is less certain. One possibility is that gravitational instabilities develop in the dust and km-sized blocks develop by gravitational attraction. It seems likely, however, that gas turbulence would be sufficient to prevent this. What is clear is that the transition from dust to km-sized bodies must have happened quickly or the dust would have been swept into the growing Sun. Because of the thermal motion of gas molecules, the gas rotates more slowly than the velocity necessary to keep solid bodies in stable orbit: the Keplerian velocity. Thus gas drag slows the particles embedded within it, and they spiral inward toward the Sun. The effect is negligible for micron-sized dust and bodies of a km or more, but it is quite significant for meter-sized blocks, which will spiral into the Sun from the Earth's orbit in 100 yrs. Thus growth through this stage must be fast if any solids are to form planets. Further evidence of rapid formation of planetesimals comes from Hf-W ages of some iron meteorites suggesting they formed only

~1 Ma after formation of CAI's. Thus at least some planetesimals must have accreted, melted, and differentiated into silicate and iron parts very quickly, perhaps during, or even before, the time of chondrule formation.

Two mechanisms for rapid growth of planetesimals have been recently proposed. In the first, transient high pressure regions in the disk concentrate meter-sized boulders, and this concentration of solids then affects flow of the gas so to capture solids drifting inward. Computer simulations suggest this process leads to gravitationally bound "clumps" that collapse to form planetesimals on times scales of a few orbital periods, i.e., a few years to a few decades (Johansen et al., (2007). The second mechanism is concentration of particles in low vorticity (i.e., slowly rotating) eddies within the disk. Simulations show that particles can become sufficiently concentrated in these eddies to become gravitationally bound and eventually contract to form ~100 km size planetesimals (Chambers, 2010). This process could form planetesimals in a few thousand years beyond the snow line, but might require a few million years inside it.

Early formed planetesimals larger than 1 km would have been heated by decay of ^{26}Al such that interior temperatures would have reached 1500 K within ~500,000 years and thus would have undergone metal-silicate differentiation. Such bodies are the likely parent bodies of the achondritic and iron meteorites. Collisions between planetesimals would in some cases lead to growth of ever large bodies. But collisions would also have destroyed some planetesimals, with the debris replenishing the nebular dust, from which a new generation of planetesimals could grow. Later-formed planetesimals might have avoided melting and differentiation: these are likely the parent bodies of the chondritic meteorites.

Once planetesimals have formed, gravity becomes important and bodies grow by collision. This process is termed "*oligarchic growth*" because it ends with a relatively few large objects. It has been extensively modeled with computer simulations and is comparatively well understood. Because larger bodies have larger effective cross-sections (their gravity pulls in other bodies from a wider area), the largest bodies grow fastest. The larger bodies also tend to acquire the most regular orbits, which leads to gravitational focusing and further enhancement of growth rates. This leads to very rapid growth in the early stages. As a relatively few large objects become dominant growth slows somewhat. Models suggest that bodies the size of the Moon (0.01 M_E or Earth masses) or Mars (0.1 M_E) could have formed in the inner solar system within 10^5 to 10^7 years. The Hf-W system may provide a tighter constraint on this stage. Hf-W data on SNC meteorites suggest that Mars had formed and differentiated into a silicate mantle and iron core about 2 million years after CAI formation (Dauphas and Chassidon, 2011). However, the HED parent body (Vesta) and the angite parent body, both of which are considerably smaller than Mars, apparently formed and differentiated later. Thus planetary growth may have proceeded at different rates in different parts of the solar nebula.

Once Mars-sized bodies have formed, only a few large bodies are present within any planet-forming zone, and collisions between them become infrequent. Consequently, growth slows dramatically. Indeed, simulations suggest it might have required an additional 10^8 years for bodies the size of the Earth or Venus to form (Wetherill, 1990; Wetherill and Stuart, 1993; Chambers and Wetherill, 1998). Another feature of the late stages of accretion is that the collisions involve very large bodies and are consequently catastrophic. The energy released in these collisions leads to extensive melting. As we shall see below, this fits very well with the evidence that we have for the origin of the Earth and the Moon.

There is somewhat more uncertainty as to how the giant planets formed. There are essentially two classes of theories. The first and best established is that of *core accretion*. It proposes that rocky, icy cores of giant planets accreted in a process very similar to that described above, albeit enhanced by the presence of ice beyond the snow line. Once these cores reached mass of 10 Earth masses, they would have had sufficient gravity to capture gas from the solar nebula and eventually become gas giants. This theory nicely explains why the gas giants have enhanced concentrations of condensable elements compared to the Sun. On the other hand, simulations assuming a "minimum mass nebula" take much too long to form giant planets in this way – 10^8 years or more. As we saw, it appears that nebular disks dissipate within at most 10 Ma – the gas giants must have captured their gas shrouds within this time.

The "minimum mass nebula" has just enough mass to produce the planets observed, which is the mass of the planets plus the non-condensable fraction missing from them and is about 0.01 $M_\odot$. However, in simulations involving more massive nebulae, >0.1 $M_\odot$, gas giants do form in this way within 10 Ma. The other theory, a relative newcomer, is gas instability (Boss, 1997). It posits that a density perturbation in the disk could cause a clump of gas to become massive enough to be self-gravitating. Once that happens, the clump could collapse into a planet on times scales of 10^3 yrs. These density perturbations occur in simulations with nebular masses significantly greater than the minimum mass. One criticism of this model is that it fails to explain why the giant planets are depleted in H and He, and does not readily explain why these planets have rocky cores. Either way, it appears planet formation is an inefficient process, with perhaps 90% the original nebular mass either being swept into the Sun or lost to space. However, very massive nebulas, containing a solar mass or more and which were once popular among theorists, have fallen out of favor.

Within 10^7 years, the nebula cleared. This resulted from a variety of factors. While the planets were forming, gas and dust were steadily spiraling into the central star. Small bodies that were not swept up by the forming planets would have been flung, through gravitational interaction with the planets, into the central star or out to interstellar space. In the outer solar system, the giant planets swept up large amounts of gas. As the Sun became hotter and more luminous, the nebula would have dissipated through "photoevaporation". (This term is a bit of a misnomer, since most of the nebula is gas to begin with, it does not evaporate in the conventional sense. By it does absorb radiational energy, which is converted to kinetic energy through collisions. The fast moving gas molecules then escape to interstellar space.) Finally, the enhanced solar winds of the T-Tauri stage would have helped to drive out remaining gas and dust. As a result, the nebula clears mostly from the inside out. However, nearby large stars could also erode the nebula from the outside in through photoevaporation. This is observed to occur in the Orion nebula. The nebula must have cleared of gas before the inner terrestrial planets were able to accumulate their full share of volatile elements, perhaps because the inner solar system cleared before it cooled enough for these elements to condense. It may have cleared before the ice giants, Uranus and Neptune, were able to capture their full compliment of gas.

In many solar systems, giant gas planets have orbits smaller than that of Mercury. It is highly unlikely that gas giants could form so close to their central star, rather, astronomers believe they must have migrated inward from where they formed. How and how fast the nebular disk clears may affect giant planet migration. Where outer disks are short-lived due to erosion, as in Orion, migration may be minimal, leaving giant planets in the out part of the their solar systems. Long-lived outer disks (as in the Taurus star-forming region) should allow significant giant planet migration and lead to the observed "hot Jupiters" observed to orbit other stars (Boss, 2005). Presumably, our solar system is an example of the former, in which the giant planets presently orbit close to where they formed. Even minor inward migration, however, could have had consequences for orbits of other planets and planetesimals. Giant planet migration is one possible explanation for the 'late heavy bombardment' discussed in the next section.

10.6.4 Chemistry and History of the Moon

Before we consider the formation of the Earth specifically, there is one more set of observations we need to consider: observations about the Moon. The Moon is of interest for several reasons. First, it is the only solar system body, other than the Earth, that we have returned samples from and has been explored by men. From this exploration we have found that much of the earliest history of the Moon is preserved, giving us unique insights into the early planetary history. In contrast, no trace remains of the earliest period of Earth history (some SNC meteorites date to 4.5 Ga, implying that evidence of early Martian history might be preserved on its surface, but we have yet to explore and sample those parts of Mars). Second, the Moon is closely associated with the Earth, not only physically, but chemically as well. Lunar oxygen isotope compositions fall on the terrestrial fractionation line, implying the Moon and Earth share the same O isotopic composition. The Moon is nearly unique in this respect: with the exception of E-chondrites, all analyzed meteoritic material, including the SNC meteorites, falls off this

line. This strongly implies that the Moon and the Earth are closely related. As we shall see, the Moon holds important clues to the earliest part of Earth's history.

10.6.4.1 Geology and History of the Moon

The Moon can be divided into three geologic provinces: the highlands – mountainous regions apparently consisting largely of anorthosite, the uplands – areas of mild relief covered by a blanket of ejecta from the large impacts, and the Mare – the large craters filled with basaltic lavas. Much of the surface of the Moon is covered with fine debris of impacts, called the regolith, consisting of rock and mineral fragments, glass, and some meteorite particles. For the most part, it seems to be locally derived; thus the regolith in the Mare differs from that of the highlands, although large impacts would have showered debris over large regions. Basalt from the Mare encompasses a variety of magma types, including both incompatible-element rich and incompatible-element poor types and both quartz-normative and olivine normative tholeiites. Highland rocks include anorthosite (nearly monomineralic calcic plagioclase), anorthositic gabbro (plagioclase and pyroxene with lesser amounts of olivine), dunite, and K-rich basalts. The highlands are extremely brecciated; most of these rock types have been found only as clasts in breccias. Table 10.06 shows some representative compositions of lunar rocks, and Figure 10.38 shows rare earth patterns of

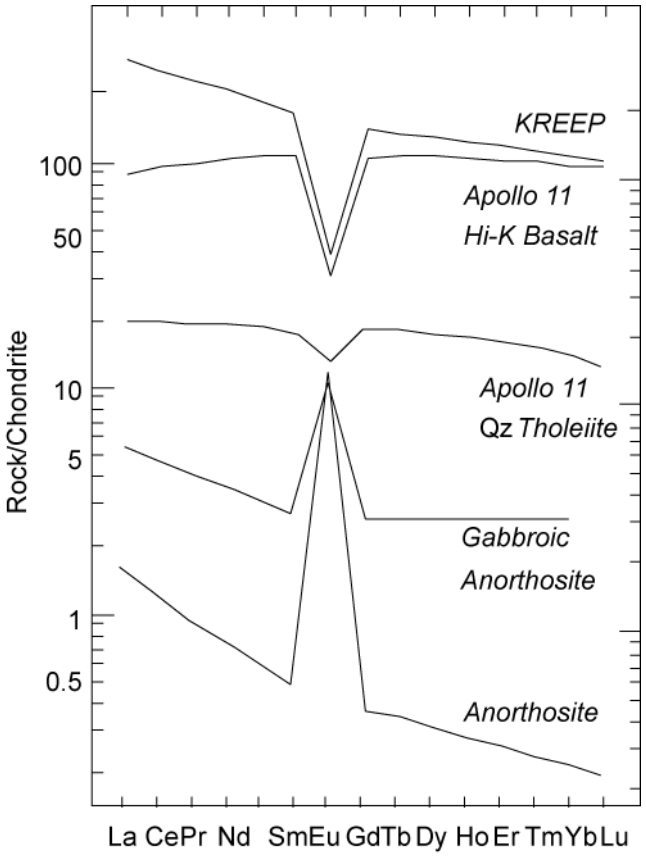

Figure 10.38. Rare earth patterns of representative lunar rocks. From Taylor (1975).

Table 10.06. Representative Compositions of Lunar Rocks

	Highland Anorthosite	Highland Anorth. Gabbro	Mare Qz. Tholeiite	Low-K Mare Basalt	Fra Mauro KREEP
SiO_2	44.3	44.5	46.1	40.5	48.0
TiO_2	0.06	0.39	3.35	10.5	2.1
Al_2O_3	35.1	26.0	9.95	10.4	17.6
FeO	0.67	5.77	20.7	18.5	10.9
MnO	—	—	0.28	0.28	—
MgO	0.80	8.05	8.1	7.0	8.7
CaO	18.7	14.9	10.9	11.6	10.7
Na_2O	0.8	0.25	0.26	0.41	0.7
K_2O	—	—	0.07	0.10	0.54
P_2O_5	—	—	0.08	0.11	—
Cr_2O_3	0.02	0.06	0.46	0.25	0.18
Total	100.5	99.9	100.3	99.7	99.4

the same rock types.

Most of the lunar Mare are thought to have been created by large impacts between 4.2 and 3.8 Ga. Subsequently, the Mare were flooded by basalt to a depth of 5 to 10 km. These were partial melts generated at 100 or so km depth. The flooding occurred over an extensive time: 3.9 to 3.1 Ga. Mare flooding was the last major lunar geologic event. Subsequent to that time, the only activity has been continual bombardment by meteorites and asteroids, which continued to produce minor disruption of the surface and build up of the regolith, and rare volcanism.

Figure 10.39 illustrates the highlights of lunar history. The oldest lunar rocks are nearly as old as meteorites. These are clasts of anorthositic highland rocks found in breccias. This suggests lunar differentiation began about 4.5 billion years ago. But most highland rocks have ages between 3.9 and 4.0 Ga. For the most part, these ages are interpreted as (and sometimes can be shown to be) the time of impact metamorphism. Apparently the Moon suffered very heavy bombardment by meteorites and asteroids as late as 3.9 Ga. The clustering of ages around this time gives rise to the idea of a 'late heavy bombardment' of the Moon.

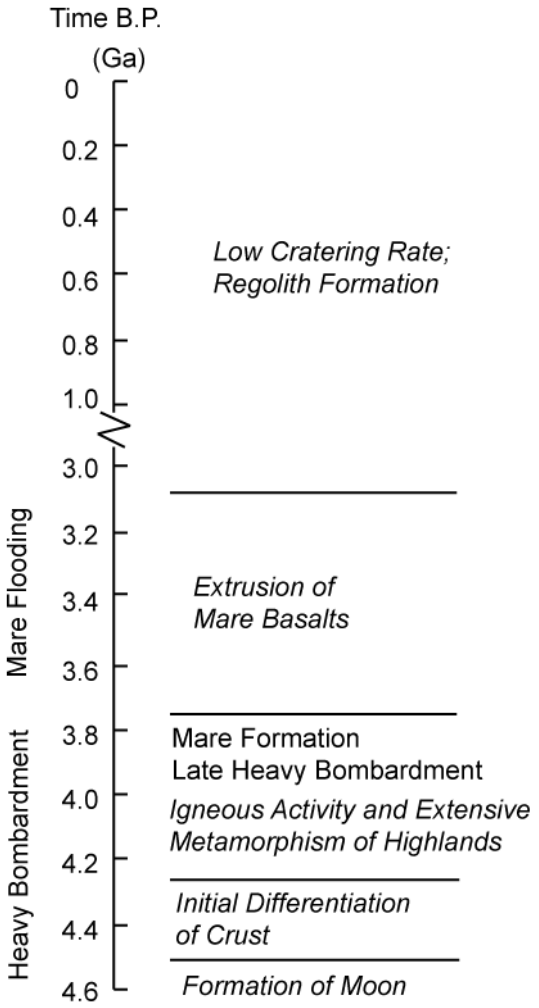

Figure 10.39. Highlights of lunar chronology

One of the more important conclusions derived from study of the Moon is that it underwent very extensive melting just after its formation, perhaps forming a magma ocean 100 km or more deep. The anorthosite of the highlands is thought to have originated by plagioclase flotation in the magma ocean, i.e., anorthosite 'icebergs' forming the lunar crust. The lunar crust seems to have been largely in place within 100 to 200 Ma after the Moon's formation. Fractional crystallization of this magma ocean and floatation of plagioclase accounts for the general Eu depletion (Figure 10.38) observed in basalts derived from the lunar mantle. A particularly incompatible-element enriched basalt, called KREEP (K-REE-P: potassium, rare earth element and phosphorus enriched) is thought to be derived from a part of the mantle that was the last part of the magma ocean to crystallize and was consequently strongly enriched in incompatible elements.

10.6.4.1 Composition of the Moon

Table 10.07 compares the composition of the Earth and the Moon. There are several notable differences. First, the Moon is depleted in moderately volatile elements (Na, K) compared to the Earth. Second, although the silicate part of the Moon (mantle + crust) is richer in iron than the silicate Earth, the bulk lunar composition is poorer in iron that the terrestrial one. The latter reflects the small size of the lunar core, which has a diameter of only 340±90 km, representing only about 2% of the mass of the planet. The lunar depletion in Fe compared to the Earth extends to all siderophile and chalcophile elements as well. The Moon is also much more depleted in the volatile elements as well. In the words of Newsom and Taylor (1989), it is "bone dry"*. Conversely, the Moon is enriched the refractory litho-

* Recently discovered water locked-up in the regolith at the south lunar pole has probably been added by meteorite impacts rather than being intrinsic to the Moon.

phile elements, having nearly twice the Al and Ca as the Earth. Despite these compositional differences, the similarity of terrestrial and lunar oxygen isotope composition strongly suggests they formed from the same part of the solar nebula.

10.6.5 The Giant Impact Hypothesis and Formation of the Earth and the Moon

The Earth and the Moon are physically closely associated, so one might suspect their origins are related. As we saw, there is evidence that the Moon was extensive melted very early in its history. We saw that numerical simulations of planetary growth within the solar nebula predict collisions between very large bodies in the final stages of accretion. We also have seen that the Moon and the Earth share an identical and unique oxygen isotopic composition. In addition, the Earth-Moon system has an anomalously large amount of angular momentum compared to the other planets and most of this angular momentum resides in the Moon. Finally, the Earth's rotational axis is tilted 23° with respect to its orbital plane. These observations led Hartmann and Davis (1975) to propose that the Earth collided with a very large body in the final stages of its accretion. A substantial fraction, perhaps 2%, of the mass of the two bodies was blasted into orbit around the Earth, with much of this debris later coalescing to form the Moon. This idea has become known as the *Giant Impact Hypothesis* and is now widely accepted (even if some of the details are still debated). The energy released in this impact would have been sufficient to melt the entire mantle of the Earth and to vaporize some of it, though this depends on how efficiently the impact energy is dissipated.

Detailed models of the impact have been produced (e.g., Newsom and Taylor, 1989). The model can be best summarized as follows. During the latest stages of accretion, the Earth was struck at low angle, and relatively low velocity (5 km/s) by a body slightly larger than Mars. The impactor, called *Theia* by some, presumably shared the depletion in highly and moderately volatile elements that characterizes the terrestrial planets. Metallic cores had already formed in both the Earth and the impactor. The collision completely disrupted the impactor and partially disrupted the Earth's mantle, with much of the resulting debris having gone into orbit around the Earth. Most of the disrupted core of the impactor quickly (a matter of hours) accreted to the Earth and the silicate material in orbit more slowly coalesces to form Moon. About 85% of the material forming the Moon is derived from the impactor, the remainder from the Earth's mantle. A small core then segregated from the largely molten Moon. Most of the core of the impactor quickly sank through the disrupted mantle of the Earth to coalesce with the existing terrestrial core. The depletion of siderophile elements in the Moon is thus a result of its formation from the silicate portions of the impactor and Earth, in which the siderophile were already depleted by core formation. The volatile element depletion of the Moon is a consequence of the evaporation of these elements during impact.

Table 10.07. Comparison of the Compositions of the Earth and Moon

	Bulk Earth	Bulk Moon	Silicate Earth	Silicate Moon
SiO_2	30.38	43.4	45.0	44.4
TiO_2	0.14	0.3	0.201	0.31
Al_2O_3	3.00	6.0	4.45	6.14
FeO	5.43	10.7	8.05	10.9
MgO	25.52	32	37.8	32.7
CaO	2.40	4.5	3.55	4.6
Na_2O	0.24	0.09	0.36	0.09
K_2O	0.02	0.01	0.029	0.01
Fe	28.43	2.166		
Ni	1.75	0.134		
S	1.62			
core%	32.5%	2.3%		
mantle%	67.5%	97.7%		

Terrestrial composition from McDonough and Sun (1995), assuming the light element in the core is S. Lunar composition from Taylor (1992).

10.6.6 Tungsten Isotopes and the Age of the Earth

If the Giant Impact Hypothesis is correct, then the impact marks the time of final segregation of the metal and silicate in the Earth (and the Moon) as well as the completion (or nearly so) of accretion of the Earth. If we can date this event, we can determine the age of the Earth. Looking at Table 10.04, we see that the ^{182}Hf-^{182}W decay pair

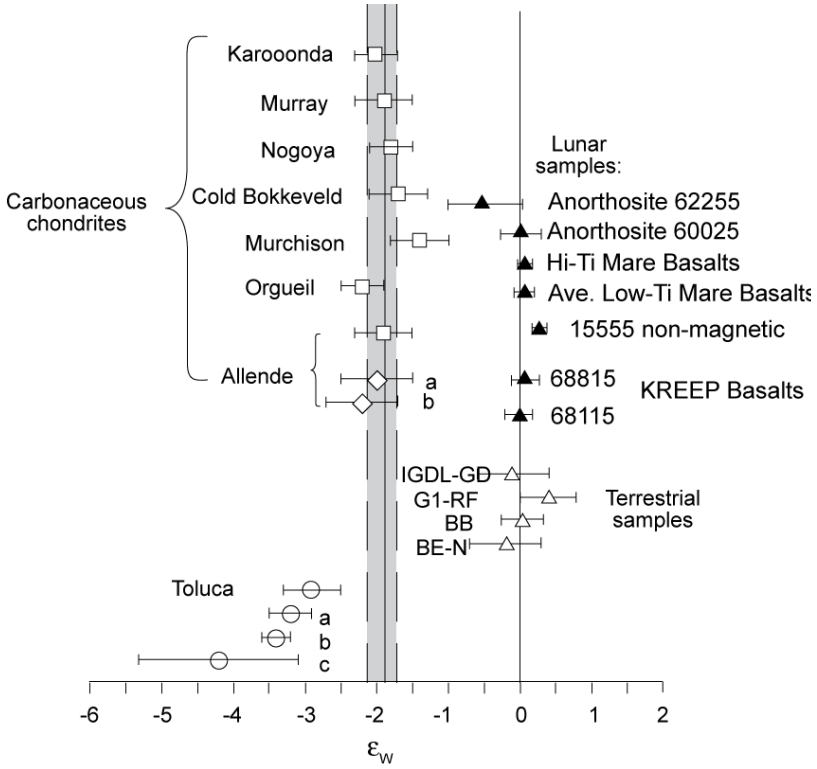

Figure 10.40. W isotope ratios measured in meteorites and terrestrial and lunar materials. Data from Kleine et al. (2002), Yin et al (2002), Touboul et al (2007, 2009).

is just the ticket: Hf is lithophile and should be concentrated in the mantle while W is siderophile and should be concentrated in the core. Furthermore, the half-life of ^{182}Hf is 9 Ma, just right for examining events in the first few 10's of millions of years in the solar system. Furthermore, both are highly refractory elements, while has the advantage the one can reasonably assume that bodies such as the Earth should have an approximately chondritic Hf/W ratio. Over the last dozen years this system has provided very interesting insights into the early history of Mars, the Moon, and the Earth. Among other things, the story of Hf-W illustrates the importance of the fundamental dictum in science that results need to be independently replicated before they be accepted.

Because the variations in $^{182}W/^{183}W$ ratio are quite small, they are generally presented and discussed in the same ε notation used for Nd and Hf isotope ratios (Chapter 8). However; ε_W is the deviation in parts per 10,000 *from a terrestrial tungsten standard*, and $f_{Hf/W}$ is the fractional deviation of the Hf/W ratio from the chondritic value. Assuming that the silicate Earth has a uniform W isotope composition identical to that of the standard (an assumption supported by the observation that all terrestrial samples analyzed thus far have this composition), then the silicate Earth has ε_W of 0 by definition. The basic question can posed this way: if the $^{182}W/^{183}W$ ratio in the silicate Earth is higher than in chondrites, it would mean that much of the Earth's tungsten had been sequestered in the Earth's core before ^{182}Hf had entirely decayed. Since the half-life of ^{182}Hf is 9 Ma and using our rule of thumb that a radioactive nuclide is fully decayed in 5 to 10 half-lives, this would mean the core must have formed within 45 to 90 million years of the time chondritic meteorites formed. If on the other hand, the $^{182}W/^{183}W$ ratio in the silicate Earth was the same as in chondrites, which never underwent silicate-metal fractionation, this would mean that at least 45 to 90 million years must have elapsed (enough time for ^{182}Hf to fully decay) between the formation of chondrites and the formation of the Earth's core.

'Anomalous' W isotopic compositions were first found in the IA iron *Toluca* by Harper et al. (1991). They found the $^{182}W/^{183}W$ ratio in the meteorite was 2.5 epsilon units lower (and subsequently revised to 3.9 epsilon units lower) than terrestrial W. Lee and Halliday (1995) reported W isotope ratios for 2 carbonaceous chondrites (*Allende* and *Murchison*), two additional iron meteorites, and a lunar basalt. They found the iron meteorites showed depletions in ^{182}W similar to that observed in *Toluca*. The chondrites, however, had ε_w values that were analytically indistinguishable from "terrestrial" W, as was the lunar basalt. Based on this similarity of isotopic compositions of chondritic and terrestrial W, Lee and

Halliday (1995) concluded that the minimum time required for formation of the Earth's core was 62 million years. Subsequently, Yin et al. (2002) and Kleine et al., (2002) reported W isotope ratios in carbonaceous chondrites that were 1.9 to 2.6 epsilon units lower than the terrestrial standard (Figure 10.40). In the same issue of the journal *Nature*, reported similarly low ε_W (i.e., -2) for 7. Furthermore, Kleine et al. (2002) analyzed a variety of terrestrial materials and found they all had identical W isotopic compositions, what are some 2 epsilon units different from that of the chondrites (Figure 10.40). It thus appears that the original measurements of Lee and Halliday (1995) were wrong. The measurement error most likely relates to what was at the time an entirely new kind of instrument, namely the multi-collector ICP-MS. Touboul et al. (2007) showed that the Moon has and isotopically homogeneous W isotopic composition that is identical to that of the silicate Earth – about 2 epsilon units higher than chondrites. This episode illustrates why science places such importance on *independent replication* of observations (Chapter 1).

What the high $^{182}W/^{183}W$ of the silicate Earth relative to chondrites implies for the timing of formation of the Earth's core depends on how the core formed. In the simplest model, where the core segregates instantaneously from homogeneously accreted metal and silicate, the ^{182}W excess of Earth's mantle of ε_W= +1.9 relative to chondrites and a Hf/W ratio of 17 for the bulk silicate Earth indicates this happened ~30 Ma after the solar system (time of CAI formation). This model is unlikely, however, since we know that metal cores segregated from even relatively small planetary embryos only a few million years after the start of the solar system. Large planets such as the Earth form by collisions between and accretion of these already differentiated planetary embryos. Thus most studies have considered continuous core formation models. In such models, there is no single ''age" for core formation and the reported ages rather correspond to either the mean time of core formation (formation of 63% of the core or the time of the Moon-forming impact), which most likely determines the termination of the major stage of Earth's accretion and the last time the core and mantle could equilibrate. In continuous formation models, W isotopic evolution will depend on the degree to which tungsten in the silicate and metal parts of colliding bodies equilibrate. Thus tungsten isotope systematics have been variously interpreted as implying core formation ages anywhere from 30 Myr to >100 Myr after CAI formation. However, the identical $^{182}W/^{184}W$ ratios of the Moon and silicate Earth, despite the two bodies having different Hf/W ratios, indicate that the Moon-forming giant impact occurred after extinction of ^{182}Hf, or more than 60 Ma after CAI formation. The minimum age of the Moon is constrained by Sm-Nd ages of the lunar anorthositic crust. This age is 4.456±0.040 Ga, or about 100 Ma after the beginning of the solar system. Touboul et al. (2007) thus estimate an age for the Moon of 62 +90/-10 Ma after the start of the solar system (Figure 10.41).

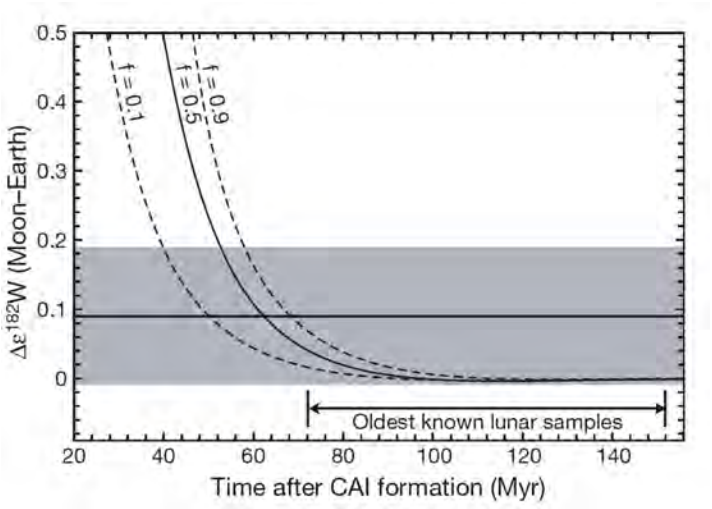

Figure 10.41. Difference between ε_W of Earth and Moon (Δ) versus the age the giant impact (and presumably final core formation in the Earth). *f* is the relative difference in Hf/W ratios between the silcate part of the Earth and the silicate part of the Moon (i.e., $(Hf/W_{Moon}-Hf/W_{Earth}/Hf/W_{Earth})$. The grey area shows the best value of $\Delta\varepsilon_W$ (0.09±0.10). The Hf/W ratio of the Earth's mantle is estimated at 18 and that of the Moon is 26.5, corresponding to an f of 0.47 (solid line). After Touboul et al. (2007).

We will see in the following chapter that the Earth has a composition that is different from that of the Sun and of chondrites, particularly with respect to volatile and moderately volatile elements. This distinctive composition

reflects its formation in the warm inner region of the solar nebula, but perhaps also the cataclysmic events in the final stages of its formation. The final energetic cataclysm, the giant impact, may be partly responsible for the volatile-poor nature of the Earth as well as the Moon.

References and Suggestions for Further Reading

Allegre, C. J., Condensed matter astrophysics: constraints and questions on the early development of the Solar System, *Phil. Trans R. Soc. Lond.*, A359: 2137-2155, 2001.

Amelin, Y., U-Pb ages of angrites, *Geochim. Cosmochim. Acta*, 72: 221-232, doi: 10.1016/j.gca.2007.09.034, 2008.

Amelin, Y., A. Kaltenbach, T. Iizuka, C. H. Stirling, T. R. Ireland, M. Petaev and S. B. Jacobsen, U–Pb chronology of the Solar System's oldest solids with variable $^{238}U/^{235}U$, *Earth Planet. Sci. Lett.*, 300: 343-350, doi: 10.1016/j.epsl.2010.10.015, 2010.

Amelin, Y., J. Connelly, R. E. Zartman, J. H. Chen, C. Göpel and L. A. Neymark, Modern U–Pb chronometry of meteorites: Advancing to higher time resolution reveals new problems, *Geochim. Cosmochim. Acta*, 73: 5212-5223, doi: 10.1016/j.gca.2009.01.040, 2009.

Anders, E. and E. Zinner. 1993. Interstellar grains in primitive meteorites: diamond, silicon carbide, and graphite. *Meteoritics*. 28: 490-514.

Anders, E., 1988. Circumstellar material in meteorites: noble gases, carbon and nitrogen, in *Meteorites and the Early Solar System*, ed. by J. F. Kerridge and M. S. Matthews. Tuscon: Univ. of Arizona Press

Boss, A. P., Giant planet formation by gravitational instability, *Science*, 276:1836-1839, 1997.

Boss, A. P. The solar nebula, *in* A. M. Davis (ed.), *Meteorites, Comets and Planets*, 63-82, Amsterdam, Elsevier, 2005a.

Boss, A. P., Evolution of the solar nebula. VII. Formation and survival of protoplanets formed by disk instability, *Astrophys. J.*, 629: 535-548, 2005.

Boss, A. P. and H. A. T. Vanhala, Injection of newly synthesized elements into the protosolar cloud, *Phil Trans R Soc Lond*, 359: 2005-2017, 2001.

Bouvier, A. and M. Wadhwa, The age of the Solar System redefined by the oldest Pb-Pb age of a meteoritic inclusion, *Nature Geosci.*, 3: 637-641, doi: 10.1038/ngeo941, 2010.

Bouvier, A., J. Blichert-Toft, F. Moynier, J. D. Vervoort and F. Albarede, Pb–Pb dating constraints on the accretion and cooling history of chondrites, *Geochim. Cosmochim. Acta*, 71: 1583-1604, doi: 10.1016/j.gca.2006.12.005, 2007.

Bouvier, A., L. J. Spivak-Birndorf, G. A. Brennecka and M. Wadhwa, New constraints on early Solar System chronology from Al–Mg and U–Pb isotope systematics in the unique basaltic achondrite Northwest Africa 2976, *Geochim. Cosmochim. Acta,* 75: 5310-5323, doi: 10.1016/j.gca.2011.06.033, 2011.

Brennecka, G. A., S. Weyer, M. Wadhwa, P. E. Janney, J. Zipfel and A. D. Anbar, 238U/235U Variations in Meteorites: Extant ^{247}Cm and Implications for Pb-Pb Dating, *Science*, 327: 449-451, doi: 10.1126/science.1180871, 2010.

Burbidge, E. M., G. R. Burbidge, W. A. Fowler, and F. Hoyle. 1957. Synthesis of the elements in stars, *Rev. Mod. Phys.*, 29: 547-650.

Chambers, J. E., Planetesimal formation by turbulent concentration, *Icarus*, 208: 505-517, doi: 10.1016/j.icarus.2010.03.004, 2010.

Chen, J. H. and G. J. Wasserburg. 1983. The least radiogenic Pb in iron meteorites. *Fourteenth Lunar and Planetary Science Conference, Abstracts*, Part I, Lunar & Planet Sci. Inst., Houston, pp. 103-104.

Clayton, R. N., Self-shielding in the solar nebula, *Nature*, 415: 860-861, 2002.

Clayton, R. N., N. Onuma, and T. K. Mayeda. 1976. A classification of meteorites based on oxygen isotopes, *Earth. Planet. Sci. Lett.*, 30: 10-18.

Cowley, C. R. 1995. *Cosmochemistry*. Cambridge: Cambridge University Press.

Crabb, J., and L. Schultz. 1981. Cosmic-ray exposure ages of the ordinary chondrites and their significance for parent body stratigraphy, *Geochim. Cosmochim. Acta*, 45: 2151-2160.

Dauphas, N. and Chaussidon, M., 2011. A perspective from extinct radionuclides on a young stellar object: the Sun and its accretion disk. *Ann. Rev. Earth Planet. Sci.*, 39, 351-386.

Davis, A. M (ed)., *Meteorites, Comets and Planets, Treatise on Geochemistry* vol 1, 737 pp., Amsterdam, Elsevier 2005.

Desch, S.J., and H.C. Connolly, A model of the thermal processing of particles in solar nebula shocks: Application to the cooling rates of chondrules, *Meteorit. Planet. Sci.*, *37*, 183-207, 2002.

Ebel, D. S. and L. Grossman, Condensation in dust-enriched systems, *Geochim. Cosmochim. Acta*, 64: 339-366, doi: 10.1016/s0016-7037(99)00284-7, 2000.

Goodrich, C. A. and J. S. Delaney, Fe/Mg–Fe/Mn relations of meteorites and primary heterogeneity of primitive achondrite parent bodies, *Geochim. Cosmochim. Acta*, 64: 149-160, doi: 10.1016/s0016-7037(99)00107-6, 2000.

Göpel, C., G. Manhès and C. Allègre, U-Pb systematics of phosphates from equilibrated ordinary chondrites, Earth Planet. Sci. Lett., 121: 153-171, 1994.

Grossman, L., 1972. Condensation in the primitive solar nebula, *Geochim. Cosmochim. Acta*, 36: 597-619.

Grossman, L., Vapor-condensed phase processes in the early solar system, *Meteorit. Planet. Sci.*, 45: 7-20, doi: 10.1111/j.1945-5100.2009.01010.x, 2010.

Hartmann, W. K. and D. R. Davis. 1975. Satellite-sized planetesimals and lunar origin. *Icarus*. 24: 504-515.

Harper, C. L., J. Volkening, K. G. Heumann, C.-Y. Shih and H. Wiesmann. 1991. ^{182}Hf-^{182}W: New cosmochronometric constraints on terrestrial accretion, core formation, the astrophysical site of the r-process, and the origina of the solar system. *Lunar Planet Sci. Conf Absts*. 22: 515-516.

Huss, G. R., B. S. Meyer, G. Srinivasan, J. N. Goswami and S. Sahijpal, Stellar sources of the short-lived radionuclides in the early solar system, *Geochim. Cosmochim. Acta*, 73: 4922-4945, doi: 10.1016/j.gca.2009.01.039, 2009.

Jacobsen, S. B. and C. L. Harper. 1996. Accretion and early differentiation history of the Earth based on extinct radionuclides. **In** *Earth Processes: Reading the Isotope Code, Vol. 95*, S. R. Hart and A. Basu. ed., pp. 47-74. Washington: AGU.

Jacobsen, S. and G. J. Wasserburg. Sm-Nd isotopic evolution of chondrites, *Earth Planet. Sci. Lett.*, 50, 139-155, 1980.

Johansen, A., J. S. Oishi, M.-M. M. Low, H. Klahr, T. Henning and A. Youdin, Rapid planetesimal formation in turbulent circumstellar disks, *Nature*, 448: 1022-1025, doi: 10.1038/nature06086, 2007.

Kerridge, J. F., and M. S. Matthews (editors). *Meteorites and the Early Solar System*, Univ. of Arizona Press, Tucson, 1269pp., 1988.

Kleine, T., C. Münker, K. Mezger and H. Palme, Rapid accretion and early core formation on asteroids and the terrestrial planets from Hf-W chronometry, *Nature*, 418:952-954, 2002.

Lada, C. J. and F. H. Shu, The formation of Sun-like stars, *Science*, 248:564-572, 1990.

Larimer, J. W., 1967. Chemical fractionations in meteorites — I: condensation of the elements, *Geochim. Cosmochim. Acta*, 31, 1215-1238.

Lee, D. C. and A. N. Halliday. 1995. Hafnium-tungsten chronometry and the timing of terrestrial core formation. *Nature*. 378: 771-774.

Lee, D. C. and A. N. Halliday. Hf-W evidence for early differentiation of Mars and the Eucrite parent body. *Lunar Planet. Sci. Conf. Absts*. 28: 79, 1998.

Lee, T., D. A. Papanastassiou and G. J. Wasserburg. Demonstration of ^{26}Mg excess in Allende and evidence for ^{26}Al, *Geophys. Res. Lett.*, 3: 41-44, 1976.

Lagrange, A.-M., Bonnefoy, M., Chauvin, G., Apai, D., Ehrenreich, D., Boccaletti, A., Gratadour, D., Rouan, D., Mouillet, D., Lacour, S., Kasper, M., 2010. A Giant Planet Imaged in the Disk of the Young Star β Pictoris. Science 329, 57-59.

McDonough, W. F. and S.-S. Sun. 1995. The composition of the Earth. *Chem. Geol.* 120: 223-253.

McSween, H. Y., Jr., *Meteorites and their Planet Bodies*, New York: Cambridge University Press, 1987.

McSween, H. Y. and Huss, G. R., *Cosmochemistry*. New York: Cambridge University Press, 2010.

McSween, H. Y., G. J. Taylor and M. B. Wyatt, Elemental Composition of the Martian Crust, *Science*, 324: 736-739, doi: 10.1126/science.1165871, 2009.

Nagashima, K., A.N. Krot, and H. Yurimoto, Stardust silicates from primitive meteorites, *Nature*, *428*, 921-924, 2004.

Newsom, H. E. and J. H. Jones (editors). 1990. *Origin of the Earth*, Oxford: Oxford Univ. Press.

Newsom, H. E. and S. R. Taylor, Geochemical implications of the formation of the Moon by a single giant impact. *Nature*. 338: 29-34, 1989.

Nguyen, A. N. and E. Zinner, Discovery of ancient silicate stardust in a meteorite, *Science*, 303: 1496-1499, 2004.

Palme, H. and A. Jones, Solar System Abundances of the Elements, in A. M. Davis (ed.), *Meteorites, Comets, and Planets*, 41-62, Elsevier, Amsterdam 2005.

Papanastassiou, D. A., and G. J. Wasserburg. 1969. Initial strontium isotopic abundances and the resolution of small time differences in the formation of planetary objects. *Earth Planet. Sci. Lett.*, 5: 361-376.

Petaev, M. I. and J. A. Wood, The condensation with partial isolation (CWPI) model of condensation in the solar nebula, *Meteorit. Planet. Sci.*, 33: 1123-1137, doi: 10.1111/j.1945-5100.1998.tb01717.x, 1998.

Prinn, R. G. and B. Fegley. 1989. Solar nebula chemistry: origin of planetary, satellite and cometary volatiles. in *Origin and Evolution of Planetary and Satellite Atmospheres,* ed. S. K. Atreya, J. B. Pollack and M. S. Mathews. Tuscon: Univ. of Arizona Press.

Reynolds, J. R., Isotopic composition of xenon from enstatite chondrites, Zeitshrift für Naturforschung, 15a: 1112-1114, 1960.

Rubin, A. E. 1995. Petrological evidence for collisional heating of chondritic asteroids. *Icarus*. 113: 156-167.

Russell, S. S., M. Gounelle and R. Hutchinson, Origin of short-lived radionuclides, *Phil Trans R Soc Lond*, 359: 1991-2004, 2001.

Shang, H., F. H. Shu, T. Lee and A. E. Glassgold, Protostellar winds and chondritic meteorites, *Space Sci. Rev.*, 92:153-176, 2000.

Shu, F. H., H. Shang, A. E. Glassgold and T. Lee, X-rays and fluctuating X-winds from protostars, *Science*, 277:1475-1479, 1997.

Smoliar, M. I., R. J. Walker and J. W. Morgan, Re-Os Ages of Group IIA, IIIA, IVA, and IVB Iron Meteorites, Science, 271: 1099-1102, doi: 10.1126/science.271.5252.1099, 1996.

Sugiura, N. and A. N. Krot, 26Al-26Mg systematics of Ca-Al-rich inclusions, amoeboid olivine aggregates, and chondrules from the ungrouped carbonaceous chondrite Acfer 094, *Meteorit. Planet. Sci.*, 42: 1183-1195, doi: 10.1111/j.1945-5100.2007.tb00568.x, 2007.

Swindle, T. D. and F. Podosek.1989. Iodine-Xenon Dating. in *Meteorites and the Early Solar System,* ed. 1093-1113. Tuscon: Univ. of Arizona Press.

Taylor, S. R. 1991. Accretion in the inner nebula: the relationship between terrestrial planetary compositions and meteorites. *Meteoritics*. 26: 267-277.

Tang, M. and E. Anders. 1988. Isotopic anomalies of Ne, Xe, and C in meteorites. II. Interstellar diamond and SiC: Carriers of exotic noble gases, *Geochim. Cosmochim. Acta*, 52, 1235-1244, 1988.

Tatsumoto, M., R. J. Knight, and C. J. Allègre. 1973. Time differences in the formation of meteorites determined from the ratio of lead-207 to lead-206, *Science*, 180: 1279-1283.

Taylor, S. R. 1975. *Lunar Science: A Post-Apollo View*. *Pergamon Press*, New York, 372 pp.

Taylor, S. R. 1992. *Solar System Evolution: A New Perspective*. Cambridge: Cambridge University Press.

Thiemens, M. H., and J. E. Heidenreich. 1983. The mass independent fractionation of oxygen — A novel isotopic effect and its cosmochemical implications, *Science*, 219: 1073-1075.

Van Schmus, W. R., and J. A Wood. 1967. A chemical petrologic classification for the chondritic meteorites. *Geochim. Cosmochim. Acta*, 31: 747-765.

Wadhwa, M., Y. Amelin, O. Bogdanovski, A. Shukolyukov, G. W. Lugmair and P. Janney, Ancient relative and absolute ages for a basaltic meteorite: Implications for timescales of planetesimal accretion and differentiation, *Geochim. Cosmochim. Acta*, 73: 5189-5201, doi: 10.1016/j.gca.2009.04.043, 2009.

Wasserburg, G. J., M. Busso, R. Gallino and C. M. Raiteri. 1994. Asymptotic giant branch stars as a source of short-lived radioactive nuclei in the solar nebula. *Astrophys. J.* 424: 412-428.

Wasson, J. T., *Meteorites*, Springer-Verlag, Berlin, 316 pp., 1974.

Wasson, J. T., *Meteorites: Their Record of Early Solar System History*, New York: W. H. Freeman, 1985.
Wasson, J. T. and G. W. Kallemeyn, Compositions of chondrites, *Phil Trans R Soc Lond*, A 325:535-544, 1988.
Wetherill, G. W. 1990. Formation of the Earth, *Ann. Rev. Earth Planet. Sci.*, 18: 205-256.
Wetherill, G. W. and G. R. Stewart. 1993. Formation of planetary embryos: effects of fragmentation, low relative velocity, and independent variation of eccentricity and inclination. *Icarus*. 106: 190-209.
Wood, J. A.. 1988. Chondritic meteorites and the solar nebula, *Ann. Rev. Earth Planet. Sci.*, 16, 53-72.
Yin, Q., S. B. Jacobsen, Y. K., J. Blichert-Toft, P. Télouk and F. Albarède, 2002. A short timescale for terrestrial planet formation from Hf-W chronometry of meteorites, *Nature*, 418:949-951.

Problems

1. On the part of the chart of the nuclides below, identify the mode of origin (S, R, or P process) of the stable isotopes of W, Re, Os, and Ir by writing S, R or P in the box for each (remember some nuclides can be created by more than one process). Identify those isotopes you feel should be most abundant and those least abundant. On the chart below, mass numbers are given for only the stable isotopes. As a start, assume the S-process path starts at ^{181}Ta. Assume the unstable isotopes will decay before capturing a neutron during the S-process.

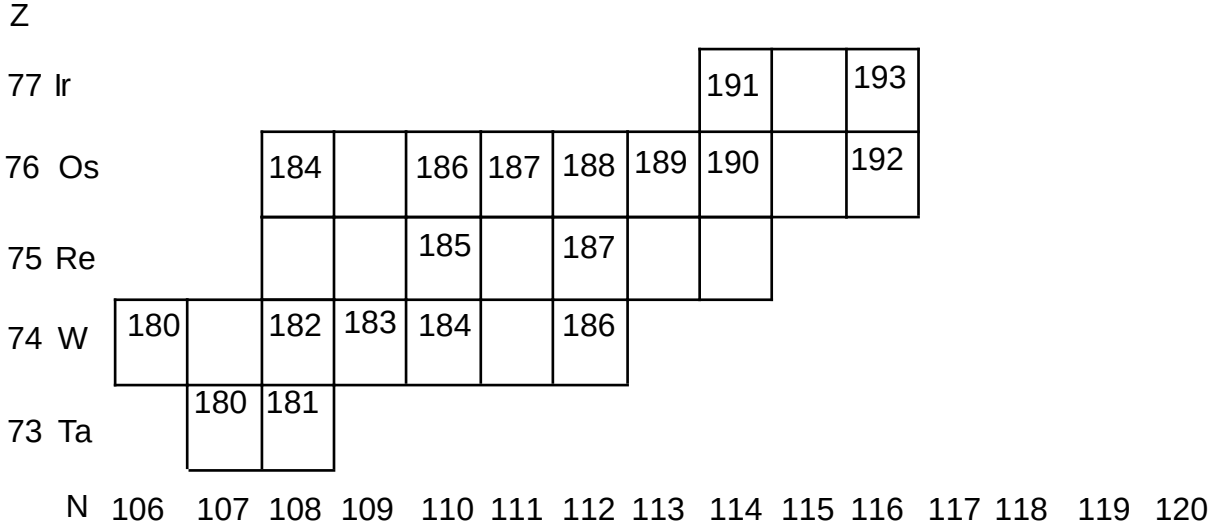

2. One calcium-aluminum inclusion in the Allende meteorite has δ^{26}Mg values which imply a ^{26}Al/^{27}Al ratio of 0.46×10^{-4} at the time of it's formation. A second inclusion apparently formed with a ^{26}Al/^{27}Al ratio of 1.1×10^{-4}. The half-life of ^{26}Al is 7.2×10^{5} years. Assuming both these inclusions formed from the same cloud of dust and gas and that the ^{26}Al/^{27}Al ratio in this cloud was uniform, what is the time interval between formation of the two inclusions?

3. Assuming that the oxygen in CV chondrites are a mixture of oxygen having an oxygen isotope composition lying on the terrestrial fractionation line in Figure 10.28 and pure ^{16}O, how much ^{16}O would have to be added to oxygen lying on the terrestrial fractionation line to reproduce their oxygen isotopic composition?

4. Using the partition coefficients in Table 7.5, estimate the fraction of plagioclase that would have to fractionally crystallize from a lunar magma ocean to produce the Eu anomaly of KREEP shown in Figure 10.32. Hint: concern yourself only with the Eu/Sm ratio.

5. Make a plot of the log of the fraction of Os condensed from a gas of "solar" composition as a function of temperature (e.g., a plot similar to Figure 10.33). Assume a total pressure of 10^{-4} atm, ΔH^o_v of 738 kJ/mol, ΔS^o_v of 139 J/mol, and the solar system abundances in Table 10.2. Assume the solid is pure Os metal. (*HINT: about 50% will be condensed at 1737 K.*)